4. SEA ICE AND SNOW MEASUREMENTS

Oguz Demir[1], Jari Haapala[2], Mario Hoppmann[3], Stefan Hendricks[3], Nikolay Kolabutin[4], Nathan Kurz[5], Ruibo Lei[6], Ilkka Matero[3], Marcel Nicolaus[3], Marc Oggier[7], Ian Raphael[10], Julia Regnery[3], Martin Schiller[3], Egor Shimanschuk[4], Gunnar Spreen[8] and David Wagner[9]

(not onboard) Don Perovich[10]

[1]EDU.OSU
[2]FI.FMI
[3]DE.AWI
[4]RU.AARI
[5]GOV.NASA
[6]CN.PRIC
[7]EDU.UAF
[8]DE.UNI-Bremen
[9]CH.WSL
[10]EDU.DARTMOUTH

Grant-No. AWI_PS122_00

A comprehensive summary of the sea ice and snow measurements during all 5 cruise legs can be found in Nicolaus et al., 2022.

References

Nicolaus, M, Perovich, DK, Spreen, G, Granskog, MA, Albedyll, LV, Angelopoulos, M, Anhaus, P, Arndt, S, Belter, HJ, Bessonov, V, Birnbaum, G, Brauchle, J, Calmer, R, Cardellach, E, Cheng, B, Clemens-Sewall, D, Dadic, R, Damm, E, de Boer, G, Demir, O, Dethloff, K, Divine, DV, Fong, AA, Fons, S, Frey, MM, Fuchs, N, Gabarró, C, Gerland, S, Goessling, HF, Gradinger, R, Haapala, J, Haas, C, Hamilton, J, Hannula, H-R, Hendricks, S, Herber, A, Heuzé, C, Hoppmann, M, Høyland, KV, Huntemann, M, Hutchings, JK, Hwang, B, Itkin, P, Jacobi, H-W, Jaggi, M, Jutila, A, Kaleschke, L, Katlein, C, Kolabutin, N, Krampe, D, Kristensen, SS, Krumpen, T, Kurtz, N, Lampert, A, Lange, BA, Lei, R, Light, B, Linhardt, F, Liston, GE, Loose, B, Macfarlane, AR, Mahmud, M, Matero, IO, Maus, S, Morgenstern, A, Naderpour, R, Nandan, V, Niubom, A, Oggier, M, Oppelt, N, Pätzold, F, Perron, C, Petrovsky, T, Pirazzini, R, Polashenski, C, Rabe, B, Raphael, IA, Regnery, J, Rex, M, Ricker, R, Riemann-Campe, K, Rinke, A, Rohde, J, Salganik, E, Scharien, RK, Schiller, M, Schneebeli, M, Semmling, M, Shimanchuk, E, Shupe, MD, Smith, MM, Smolyanitsky, V, Sokolov, V, Stanton, T, Stroeve, J, Thielke, L, Timofeeva, A, Tonboe, RT, Tavri, A, Tsamados, M, Wagner, DN, Watkins, D, Webster, M, Wendisch, M. 2022. Overview of the MOSAiC expedition: Snow and sea ice. *Elementa: Science of the Anthropocene* 10(1). DOI: https://doi.org/10.1525/elementa.2021.000046

4.1 Supporting observations

Marcel Nicolaus[1], Jari Haapala[2], Oguz Demir[3], Mario Hoppmann[1], Stefan Hendricks[1], Nikolay Kolabutin[4], Nathan Kurz[5], Ruibo Lei[6], Ilkka Matero[3], Marc Oggier[7], Ian Raphael[10], Julia Regnery[3], Martin Schiller[1], Egor Shimanschuk[4], Gunnar Spreen[8] and David Wagner[9]

[1]DE.AWI
[2]FI.FMI
[3]EDU.OSU
[4]RU.AARI
[5]GOV.NASA
[6]CN.PRIC
[7]EDU.UAF
[8]DE.UNI-Bremen
[9]CH.WSL
[10]EDU.DARTMOUTH

Objectives

In order to support the main tasks of the team ICE work of MOSAiC, several additional observations and activities started and will be continued during the following legs. Their common aim is to document the general snow and ice conditions and to support data interpretation afterwards. Also, most mapping activities of single measurements, installations, and operations on the ice were organized and documented in this task. In particular these activities include regular time laps photos of the surrounding of the vessel with a panorama camera and standardized sea ice observations from the bridge.

Work at sea

The panorama camera (Panomax) was mounted above the crow's nest since departure in Tromsø, Norway, in September 2019. The camera worked without interruptions intervals. Each photo consists of 15680x2048 pixels. The recording of a single panorama took, depending on light conditions, up to 18 minutes. Therefore, the recording interval was set constant at 20 minutes (72 photos per day). Photographs were also taken during darkness.

Ice observations are done hourly from the bridge of RV Polarstern while the vessel was moving through ice. During the drift, observations were taken daily measurements. The aim of these observations is to describe the surrounding conditions over a 10-minute period within a radius of 1.5 nautical miles around the vessel. The list of conditions that are recorded is comprehensive, and includes for example ice concentration, floe size, fraction of ridged ice, ice thickness. In addition, several parameters describing the weather conditions and macrofauna present are also included as part of the procedure. Due to the subjective nature of the observations, new observers were initially paired with people with more experience in order to ensure consistency throughout the MOSAiC drift.

Data Management

All data are handled, documented, archived and published following the MOSAiC data policy (see APPENDIX). Final data products will be stored at the PANGAEA data repository (World Data Center PANGAEA Data Publisher for Earth & Environmental Science (www.pangaea.de)).

4.2 Snow

David Wagner[1], Ian Raphael[2]

(not onboard:) Stefanie Arndt[3], Ruzica Dadic[1], Polona Itkin[4], Matthias Jaggi[1], Glen Liston[5], Amy Macfarlane[1], Chris Polashenski[2], Martin Schneebeli[1]

[1]CH.WSL
[2]EDU.DARTMOUTH
[3]DE.AWI
[4]NO.UIT
[5]EDU.CSU

Objectives

The overarching goal of the snow measurements is to characterize this spatially variable and changeable porous medium in support of all MOSAiC inquiries from ATMOS, BGC and ECO. These include snow-focused activities as well as support for measurements and models from other tasks. The dataset will, for example, support investigations into (1) thermal conductivity of snow on sea ice and thermal transfer across the ice-atmosphere boundary; (2) surface albedo and radiative transfer at the ice surface and into the upper ocean; (3) retrievals of ice thickness from sea ice altimetry methods; (4) calculating freshwater budgets; (5) investigation of other remote signatures.

A special challenge compared to other field campaigns is the long duration of the measurements at one site. This requires a more careful management of undisturbed snow located at the sites than in short-term campaigns. Interactions between structures (containers, tents) and ice coring (flooding) must be carefully considered in the sampling design. Since disturbance of snow greatly alters microstructure and internal snow properties, particularly thermal properties, snow disturbance by foot and snowmobile traffic must be localized. As the snow surface closer to ship will be likely affected by black carbon and therefore have a different albedo, a “clean site” at a sufficient distance is necessary for the optical measurements. The extended duration of the experiment will require a shift in mentality from the typical effort in a short-term experiment to spread impacts out spatially, to an approach which involves fixed disturbed areas that are used to access relatively undisturbed areas.

Work at sea

Conducted snow work can be distributed in the following sub-tasks:

1. Snow pits
2. Snow sampling
3. Terrestrial Laser Scanning (TLS) of the snow surface
4. Snow lab work

Snow pits

We established 4 main snow measurement and sampling sites, these are three plots of originally roughly 200 x 200 m named as Snow1, Snow2 and Snow3 as well as along the RS transect line/Northern Transect (Figure 4.2.1). However, compared to the date of establishment, the plots were shifted several hundred meters relative to the ship due to ice dynamics and they were partially compressed horizontally due to ridge formation, that means they shrank. The reason for establishing so many snow measurement sites was that we needed several ice types as underground but we also needed backup-area for the case of drifting away of the plots and/or ridge and lead formation within - which was proven to be the right choice after experiencing so many major ice deformation events.

In total, we dug 75 snow pits, of which 15 were A-Pits,18 B-Pits and 39 C-Pits. For the conducted types of measurements for each snow pit type see Table 4.2.1. For a list of dug snow pits related to DSHIP device operation IDs see Table 4.2.2. In the following, a short overview of established snow plots and A-Pit sites is given.

- Snow1: this is the mainly used plot, and was the first we established. It is within the CO and close to the former RS site as well as close to MET city. Here we started four A pits, of which 3 we maintained until handover with Leg 2. One of these is on SYI close to MET City, one is on a frozen melt pond and one is on lead just frozen in beginning of November 2019.
- Snow2: the second plot we established, former out of the CO but due to ice movements after the storm in mid of November it is, like Snow1, now about 500 m further south-west. There, we dug in total 2 A-Pits on frozen melt ponds.
- Snow3: The plot furthest away from the ship, now about 1-1.4 km south of *Polarstern*. Here we dug and maintain one A-Pit, on a frozen lead.
- RS/Northern Transect: Weekly (Thursdays) measurements with Cb-Pits: SnowMicroPen (SMP), Snow-Water Equivalent (SWE) and at some locations salinity sampling.

The A-Pits at each location, were dug, if possible at all, 2-weekly. In addition, and if possible, we dug B-Pits in the weeks between the A pits as well as before and after drifting and blowing snow events.

We also dug one A-Pit at the FYI Coring/Dark site where we wanted to continue to measure, but eventually the pit and the flags were consumed by a ridge.

Each Monday, Cc-Pits were conducted at the FYI and the SYI coring site each.

Once after a wind event, we also conducted several simple Ca-Pits (SMP) along the former ROV road which we planned to continue, however due to major ice deformation and drifting, it was not possible at all to conduct further measurements.

The many ice events were in general a major issue for snow measurements, as sometimes it did not allow us to continue the work at a specific site. Also the safety and time constraints made it more difficult to fulfil the plan.

Apart from that, we experienced well working snow pit devices including SMP and NIR, even at temperatures down to -30 °C.

Snow Sampling

Each week, at an A-Pit location, we conducted several sampling tasks. Due to time, personnel and weather/ice constraints we could not fulfil all requests as listed. Furthermore, some sampling was requested only for e.g. 2-weekly, monthly ore only after snowfall. However, we took snow samples for the following purposes

- Black Carbon (AWI/Daniela Krampe)
- Halocarbons (BGC/Katarina Abrahamsson)
- Ice Nucleating Particles (INPs) (Jessie Creamean)
- Iodide (Uni Grenoble/Hans-Werner Jacobi)
- 18-O (BGC/Dorothea Bauch)
- Major Ions (AWI Glaciology/Maria Hörhold)
- Major Ions, Bromide, INPs, 34S (SO4), Salinity, S-Isotopes (BAS/Markus Frey)
- Major Organic Compounds (PSI/Julia Schmale)
- Methane (BGC/Josefa Verdugo)
- Microplastics (AWI/SLF)
- Salinity (ICE/Gunnar Spreen)
- Sugars (TROPOS)

Beryllium sampling (contact: David Kadko) has been conducted by the BGC group by Dorothea Bauch.

In addition to the snow sampling at the snow surface and in the snow profile, part of the snow task was also to empty the rocket traps at MET city for BAS/Markus Frey. These three traps were mounted on a small mast at three different heights to collect blowing snow. Thus, they only had to be emptied after a blowing snow event. However, they did not work properly in the beginning as we found always a lot of surface hoar on its openings preventing blowing snow flowing into the cylinders of the traps. Later during leg 1, we were able to empty the traps into vials two times containing a significant amount of snow.

Samples which not already had a label have been labelled (or pre-labelled) by us and for each sample the corresponding snow pit and location within the profile has been documented.

After sampling, the bags and vials were stored either in the -20°C freezer in the F-Deck or in the -20° AWI sea ice physics freezer at the bow - either in prepared boxes by the institutes who conducted the sampling requests or in one of our own brought styrofoam boxes.

Terrestrial LiDAR Surveys (TLS)

We used terrestrial LiDAR to map snow cover on the floe at a scale of ~800x800m, and with a vertical precision of ~1cm and horizontal resolution of ~5cm. The TLS campaign focuses on

snow surface morphology through time, especially redistribution and accumulation due to storm events. The TLS data is additionally useful for site selection for snow measurements and sampling, as well as small scale ice deformation.

To face working temperatures of below -15 °C we installed the brought heater cover which worked well keeping the scanner working properly over the whole measuring period. We conducted LiDAR surveys weekly at two sites, depending on weather and ice conditions. Each scan position captures a scan area with an approximately 300m radius around the scanner. In order to cover the entire scan area, and to eliminate shadows from ridges, etc., we scanned at 7-9 scan positions in each scan area. We then registered all of the scans into one contiguous scan image using fixed reference points. These reference points are reflectors of a known size and shape that we installed at various points throughout the scan areas. Ideally these points should remain constant throughout the year, allowing us to easily compare weekly scans. Of course, due to ice deformation, many of the points have shifted or been destroyed. Of the 35+ installed points, 20 are intact. We are hopeful that scans can be compared using some combination of the remaining points and other registration methods.

Snow Lab

Part of the snow lab was

- Processing snow taken with the Micro-Computer Tomograph (CT) sample holder in the field
- Processing snow out of whole snow blocks taken in the field
- Snow casting with Diethylphthalate (DEP)
- Salinity measurements

Most of the lab work was conducted in the freezer lab container (T = -15 °C) at the aft, which we shared with a colleague who processed ice cores inside. Only the work for which temperatures > 0 °C are required were conducted in the dry lab 3 and the wet lab 2 (salinity measurements, sample labeling, refilling DEP, rinsing of salinity samplers).

If the samples were taken with the micro-CT sample holder in the field, we directly scanned them with the micro-CT which was also installed in the freezer lab container. The CT was running without major problems over leg 1 though sometimes we experienced missing stacks in the scans. This is probably an image reconstruction problem on which we work on to solve it. If the snow was too fragile to sample it directly in the field, we took whole blocks, which we cut out with a saw, into the lab. There we cut out directly the microCT sample or/and we casted the snow with Diethylphthalate (DEP) by means of a heated casting box.

Expected results

Although Leg 1 required more logistical work than was planned, most of the work planned could be conducted.

Key devices for measurements of snow on the ground such as SMP, NIR, micro-CT and TLS all worked without major issues even at experienced temperatures down to -30 °C. Thus, we can already expect a unique dataset of snow on central arctic sea ice for leg 1.

A major constraint was the limited availability of TLS, which hindered the full implementation of a stratigraphy-based directed sampling. However, a broad coverage of different stratigraphic sequences could be achieved.

We would also like to highlight the first tomographic measurements of snow on sea ice, which provides unprecedented insight into the geometry of the snow.

Data management

All data are handled, documented, archived and published following the MOSAiC data policy (see APPENDIX). All device operations were logged in the AWI sensorweb portal and all sensor raw data files are stored in platform section of MCS. Final geophysical parameters will be made available via the workspace section of MCS. Final data products will be stored at the PANGAEA data repository (World Data Center PANGAEA Data Publisher for Earth & Environmental Science (www.pangaea.de)).

Tab.4.2.1: Overview on all measured parameters for the three defined snow pit types.

Type A: Parent snow pit Every other week	Type B: Children snow pit Weeks between Type A	Type C: SnowMicroPen Sub-Types: Ca, Cb, Cc Daily
Complete sampling of physical, chemical and microbiological properties	"quick pit"	Super quick measurements
All Type B measurements MicroCT Density (volumetric, dielectric) Temperature Snow wetness (Denoth probe) Salinity Sampling/Casting of snow/ice interface for MicroCT Sampling BC at surface Sampling (BC profile, impurities) Pictures for airborne structure from motion (SfM)	SnowMicroPen (SMP) NIR photography (SSA) SWE (ETH tube) Overview photos	Ca: SnowMicroPen (SMP) Cb: Transect SMP SWE Salinity Cc: Coring SMP Temperature Salinity Density (volumetric)

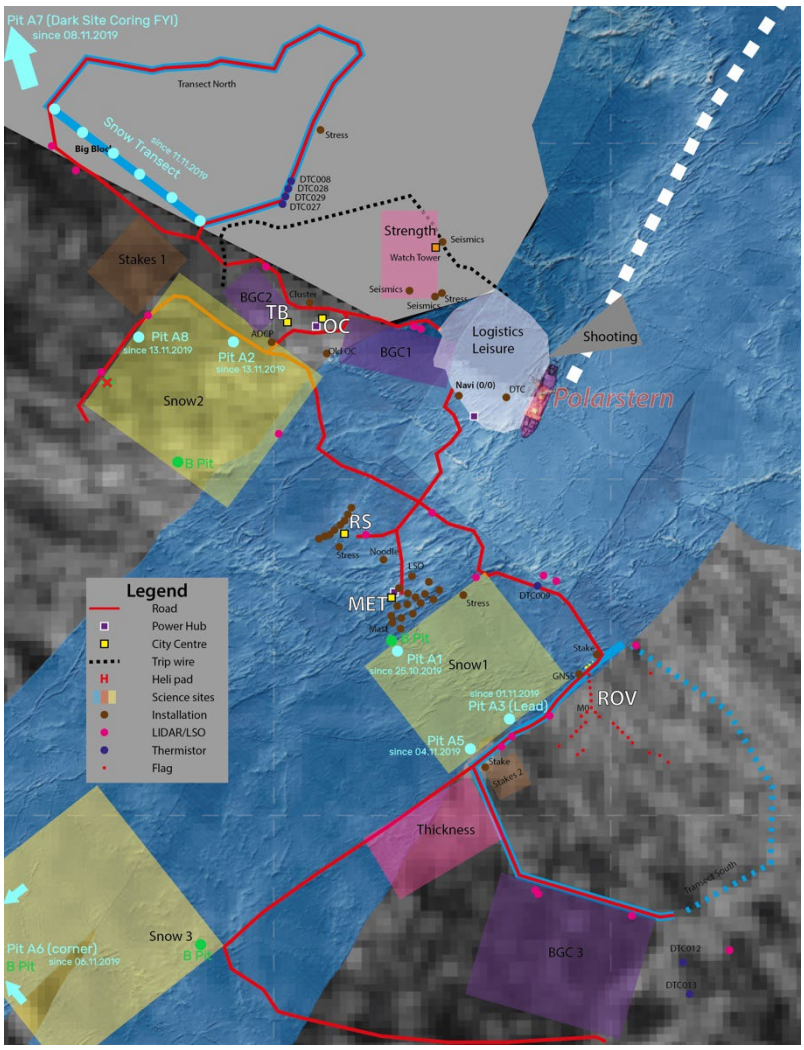

Fig.4.2.1: Floe map (state 11.12.2019) with locations of the maintained snow pits and the date first dug.

Tab.4.2.2: Overview for device operations of snowpits

Date	Device Operation ID	Pit location	Plot location	Pit Type	Samples Taken
25.10.2019	PS122/1_4-10	A1	Snow1	A	ION, PLA, BCA, BAB, BAS profile
28.10.2019	PS122/1_5-5	A1	Snow1	A	INP, PLA, ORG, ION, BAB, BAS profile, BAS surface, CAR
31.10.2019	PS122/1_5-28	A4	Transect North	Cb	
31.10.2019	PS122/1_5-102	-	Transect North	Cb	
01.11.2019	PS122/1_5-35	A3	Snow1	A	
04.11.2019	PS122/1_6-5	A4	RS city	A	BCA, ORG

04.11.2019	PS122/1_6-6	A5	Snow1	A	CAR, ION, BAS profile, BC profile
06.11.2019	PS122/1_6-29	-	ROV Road	Ca	
06.11.2019	PS122/1_6-65	-	ROV Road	Ca	
06.11.2019	PS122/1_6-66	-	ROV road	Ca	
06.11.2019	PS122/1_6-67	A3	Snow1	Ca	
06.11.2019	PS122/1_6-68	-	Snow1	Ca	
06.11.2019	PS122/1_6-69	-	Snow1/Transect	Ca	
06.11.2019	PS122/1_6-70	-	Snow1	Ca	
06.11.2019	PS122/1_6-30	A6	Snow3	A	INP
07.11.2019	PS122/1_6-41	Transect North	Transect North	Cb	
07.11.2019	PS122/1_6-42	Transect North	Transect North	Cb	
07.11.2019	PS122/1_6-43	Transect North	Transect North	Cb	
07.11.2019	PS122/1_6-44	Transect North	Transect North	Cb	
07.11.2019	PS122/1_6-47	Transect North	Transect North	Cb	
07.11.2019	PS122/1_6-46	Transect North	Transect North	Cb	
07.11.2019	PS122/1_6-45	Transect North	Transect North	Cb	
08.11.2019	PS122/1_6-75	A7	Dark site Coring	B	
11.11.2019	PS122/1_7-5	A7	Dark site Coring	Cc	
11.11.2019	PS122/1_7-8	-	Dark site Coring	Cc	
11.11.2019	PS122/1_7-12	A3	Snow1	A	INP, ORG, BAB, BAS surface, BAS profile, PLA, ION, IDA, BCA, CAR
13.11.2019	PS122/1_7-32	A1	Snow1	B	
13.11.2019	PS122/1_7-33	A1	Snow1	B	

13.11.2019	PS122/1_7-34	A2	Snow2	B	
13.11.2019	PS122/1_7-35	A8	Snow2	B	
13.11.2019	PS122/1_7-36	-	Snow2	B	
13.11.2019	PS122/1_7-129	(A6)	Snow3	B	
13.11.2019	PS122/1_7-37	A6	Snow3	B	
13.11.2019	PS122/1_7-38	-	Snow3	B	
14.11.2019	PS122/1_7-68	Transect North	Transect North	Cb	
14.11.2019	PS122/1_7-69	Transect North	Transect North	Cb	
14.11.2019	PS122/1_7-71	Transect North	Transect North	Cb	
14.11.2019	PS122/1_7-70	Transect North	Transect North	Cb	
14.11.2019	PS122/1_7-73	Transect North	Transect North	Cb	
14.11.2019	PS122/1_7-72	Transect North	Transect North	Cb	
15.11.2019	PS122/1_7-87	A5	Snow1	A	
15.11.2019	PS122/1_7-88	A2	Snow2	A	BC profile
18.11.2019	PS122/1_8-1	A7	Dark site Coring	Cc	
20.11.2019	PS122/1_8-27	-	Snow2	B	
20.11.2019	PS122/1_8-29	-	Snow2	B	
20.11.2019	PS122/1_8-28	-	Snow2	B	
20.11.2019	PS122/1_8-30	-	BGC1	B	
20.11.2019	PS122/1_8-31	A2	Snow2	B	
20.11.2019	PS122/1_8-32	-	Ocean city	B	
21.11.2019	PS122/1_8-68	Transect North	Transect North	Cb	

21.11.2019	PS122/1_8-69	Transect North	Transect North	Cb	
21.11.2019	PS122/1_8-70	Transect North	Transect North	Cb	
22.11.2019	PS122/1_8-78	A8	Snow2	A	PLA
22.11.2019	PS122/1_8-79	A7	Dark site Coring	A	INP, ORG, BAB, BAS profile, SUG, ION, BCA
25.11.2019	PS122/1_9-3	A7	Dark site Coring	Cc	
25.11.2019	PS122/1_9-10	-	Dark site Coring	Cc	
26.11.2019	PS122/1_9-23	A1	Snow1	B	BAS Rocket Trap emptying
26.11.2019	PS122/1_9-25	A5	Snow1	B	
28.11.2019	PS122/1_9-71	Transect North	Transect North	Cb	
28.11.2019	PS122/1_9-111	Transect North	Transect North	Cb	
28.11.2019	PS122/1_9-72	Transect North	Transect North	Cb	
28.11.2019	PS122/1_9-73	Transect North	Transect North	Cb	
28.11.2019	PS122/1_9-74	Transect North	Transect North	Cb	
29.11.2019	PS122/1_9-107	A6	Snow3	Block	
29.11.2019	PS122/1_9-108	A5	Snow1	Block	
29.11.2019	PS122/1_9-109	A3	Snow1	Block	
29.11.2019	PS122/1_9-110	A1	Snow1	Block	
02.12.2019	PS122/1_10-18	A7	Dark site Coring	Cc	
02.12.2019	PS122/1_10-11	-	Dark site Coring	Cc	
02.12.2019	PS122/1_10-5	A5	Snow1	A	CAR, ION, BAS profile, INP, ORG, BCA, BAB, PLA
05.12.2019	PS122/1_10-50	Transect North	Transect North	Cb	

05.12.2019	PS122/1_10-58	Transect North	Transect North	Cb	
06.12.2019	PS122/1_10-70	A2	Snow2	A	
06.12.2019	PS122/1_10-71	A3	Snow1	A	
06.12.2019	PS122/1_10-72	A6	Snow3	A	
11.12.2019	PS122/1_11-23	A1	Snow1	B	BAS Rocket Traps, INP, BAS profile, ION, BCA, SUG, IDA, BAB

References

No references

4.3 IMB-buoys and stakes

Ruibo Lei[1], Mario Hoppmann[2], Ian Raphael[3],
(not on board:) Don Perovich[3], Bin Cheng[4]

[1]CN.PRIC
[2]DE.AWI
[3]EDU.DARTMOUTH
[4]FI.FMI

Objectives

Sea ice outflow from the Central Arctic to the Greenland Sea via the Transpolar Drift Stream (TDS) plays a significant role in the long-term changes of Arctic sea ice. Numerous sea ice mass balance buoys (IMBs) have been deployed in the Central Arctic, with the bulk of the measurements obtained from late spring to early winter along the TDS (Perovich et al., 2014). Nevertheless measurements encompassing an entire ice growth season are rare (e.g., Lei et al., 2018). The loss of Arctic summer sea ice increases the solar energy absorbed by the ocean and enhancing the oceanic heat flux under the ice available into winter. The quantification of this feedback within the TDS region, however, remains unresolved because of the lack of observations compared with other regions, e.g., the Beaufort Gyre. As the thinning of Arctic sea ice, more snow over the ice would be metamorphosed into ice and give contributions to the mass balance of sea ice because of the potential negative freeboard.

At the MOSAiC Central Observatory (CO), three types of IMBs, including the Snow and Ice Mass Balance Array (SIMBA), the CRREL Seasonal IMB (SIMB), and the Digital Thermistor Chain (DTC), have been deployed to measure snow and sea ice mass balance. In addition, 80 hot-wire thickness stakes have been deployed in six typical areas to measure snow and ice thicknesses. The aims for the deployments of IMBs and thickness stakes are to obtain the annual cycle of snow and sea ice mass balance, to identify the importance of the various processes that affect the seasonal evolution of ice mass balance, and to characterize the role of summer heat storage in the upper ocean and snow over the ice on sea ice mass balance. Important changes in the seasonal evolution of an ice cover can be detected, such as surface flooding, snow ice formation, melt onset, melt pond formation and -refreezing, as well as internal melt and -refreezing.

By combined the deployments at the L and M sites, we can then explore the point to point difference of the accumulation and melt of snow, as well as the growth and decay of sea ice

within the MOSAiC Distributed Network (DN) region. The influence of initial snow and ice thicknesses on the seasonality of snow and ice mass balance can be characterized. By comparing with the historic data (e.g., Perovich et al., 2014 and Lei et al., 2018), we can obtain the interannual variations of sea ice mass balance from the Central Arctic to the Fram Strait, and its responses to the changes in atmospheric circulation.

Work at sea

Deployment of SIMBA buoys

We deploy three Snow and Ice Mass Balance Array (SIMBA) buoys at the MOSAiC CO. The SIMBA measures the air–snow-ice–ocean temperature profile at a high vertical resolution of 0.02 m (Jackson et al., 2013). There is a pulsing heating energy given to each sensor daily. Using the measurements of the vertical temperature profile of air-snow-ice-ocean and the measurements of temperatures before and after the pulsing heating, we can obtain the interfaces among air, snow, sea ice and ocean, sequentially the mass balance of snow and sea ice. In total, we deployed 16 SIMBA buoys during the Leg 1 over the whole MOSAiC DN. By the end of Leg 1, we lost three SIMBA at the M sites because of the sea ice dynamic processes, and there are still 13 SIMBA buoys working well.

At the MOSAiC CO, we deployed the SIMBA buoys at the second-year and first-year coring sites on 29 October, and at the site to the southwest with distance of about 2 km from the *Polarstern* on 2 November. The measurements at the coring site can be combined with the core-based measurement, and then we can obtain the detail thermodynamic process of sea ice and snow. The initial ice thicknesses at two coring sites are 82 and 40 cm, respectively. The deployment to the SW direction was combined with the deployment of ice stress buoy.

The deployment information of the SIMBA buoy from the *Akademik Fedorov* can be referenced to the cruise report of Leg 1a. Table 4.3.1 gives the deployment information for the buoys deployed at the CO.

Tab.4.3.1 Deployment information of SIMBA buoys at the CO

Deployment time	Buoy num. /short name	H_i (m)	H_s (m)	Sensor at snow surface	Description of the deployment site
29 Oct. 00:45	PRIC 09-01 /2019T62	0.82	0.16	40	Second-year ice coring site
29 Oct. 1:45	PRIC 09-05 /2019T66	0.40	0.10	41	First-year ice coring site
2 Nov. 1:44	FMI 05-06 /2019T56	0.44	0.14	35	Combined with the deployment of one ice stress buoy

Deployment of SIMB

One Seasonal Ice Mass balance Buoy (SIMB) was deployed at the Met City of CO on 21 October 2019. Thus, there were four SIMB deployed during the Leg 1, with three at the L sites. The SIMB measures (a) the elevations of the snow (or ice) surface and the ice base using acoustic sounders, (b) vertical temperature profile from ~1.0 m above the initial snow surface to ~2.0 m below the initial ice bottom using a thermistor string with an interval of 0.1 m.

The deployment information of the SIMB4 at the Met City as following:

Dship short name: 2019I4,

IMEI number: 300434063382860,

Install date: 21 Oct.19,

Turned on time (UTC): 00:25,

Install Lat/Lon: 84.986ºN, 132.710ºE.

Deployment of DTC network

In total, 23 DTC buoys have been deployed at the CO (Figure 4.3.1), covering near all the types of ice. Similar with the SIMBA buoy, the DTC has the ability to record air, snow, ice and ocean temperatures and record the temperature rise after a period of active heating. In addition, there is one acoustic sounder using to measure the snow depth for each DTC buoy. The DTC is powered by regular lead batteries and controlled by an affordable, commercially available microcontroller, the units will send their temperature and heating profiles in fixed intervals (e.g. 1 h) or on request to a central receiving unit on the ship via a direct communication link. As shown in Table 4.3.2, the deployment sites include:

- Dark site: 3 units,
- Transect line at the front of *Polarstern* bow: 3 units,
- Stakes along the ROV road: 3 units,
- Stakes 2: 2 units,
- Remote sensing site 1.0: 5 units,
- Remote sensing site 2.0: 2 units,
- Transect North: 4 units,
- Stress panes: 1 units.

However, several DTC buoys have been destroyed by ice deformation. By the end of Leg 1, ten units are still alive.

Tab.4.3.2 Deployment information of DTC at the CO

Buoy DSHIP number	Buoy number	Deployment date	Deployment site	Ice thickness /cm	Snow depth /cm	Status by the end of Leg 1
DTC01_256	RS034	8 Nov	Dark site, FYI area	45	10	unclear
DTC02_256	RS033	8 Nov	Dark site, FYI area	68	10	unclear
DTC03_256	RS035	10 Nov	Transect *Polarstern* bow	47	9	dead
DTC04_256	RS037	10 Nov	Transect *Polarstern* bow	51	4	dead
DTC05_256	RS012	11 Nov	Stakes (close to ROV)	62	5	alive
DTC06_256	RS013	11 Nov	Stakes (close to ROV)	65	11	alive
DTC07_256	RS031	12 Nov	Stakes 2 (Southern Transect Loop)	116	15	dead
DTC11_416	RS001	5 Nov	Transect close to the remote sensing site, North	195	8.4	dead
DTC12_416	RS002	5 Nov	Transect close to the remote sensing site, middle	60	7	dead
DTC13_416	RS004	5 Nov	Transect close to the remote sensing site, South	57	12	dead
DTC14_416	RS003	7 Nov	Remote sensing site between the KuKa radar and the L-scatterometer	55	11	dead

DTC15_416	RS009	7 Nov	Remote sensing site, other side of the L-scatterometer	193	12	alive
DTC16_416	RS010	7 Nov	Stress panes close to ship	165	16	alive
DTC17_416	RS005	8 Nov	Dark site, SYI area	167	18	dead
DTC18_416	RS006	10 Nov	Transect *Polarstern* bow	230	26	dead
DTC19_416	RS007	11 Nov	Stakes (close to ROV)	132	14	dead
DTC20_416	RS008	22 Nov	Transect North	63	13	alive
DTC21_416	RS032	12 Nov	Stakes 2 (Southern Transect Loop)	61	10	dead
DTC22_416	RS022	8 Dec	Remote Sensing site 2, behind the L-band scatterometer	71	11	alive
DTC23_416	RS023	10 Dec	Remote Sensing site 2, at the end of road behind the X-band scatterometer	154	18	alive
DTC31_512	RS027	22 Nov	Transect North	309	48	alive
DTC32_512	RS029	22 Nov	Transect North	205	28	alive
DTC33_512	RS028	22 Nov	Transect North	61	15	alive

Fig.4.3.1 Preparation of thermistor chains as part of the DTC network (left) and deployment of one unit in the field (right).

Deployment and measurement of ice thickness stakes

The 'Stakes' sites consist of many hot-wire thickness gauges (used to measure ice thickness), each paired with an ablation stake (used to measure ice surface and snow height). The stakes are installed as transects or grids, and are used to measure ice mass balance and its spatial and temporal variability. They provide a cost effective alternative to IMBs like the SIMB, SIMBA, and thermistor chain buoys, allowing us to measure mass balance at much higher spatial resolution.

We installed six stakes sites with a total of eighty individual stakes in order to capture the floe's diverse ice types, as well as take advantage of collocated measurements, e.g. the Transect, ROV, and MET observations. Several stakes sites have been partially or fully destroyed by ice deformation. We reestablished or moved most of the affected sites, and at the end of Leg 1 we had five operational sites with sixty individual stakes. The deployment information of the stake site are:

- Stakes1: 8 stakes in FYI
- Stakes2: (Presumed dead)
- Stakes3: 15 stakes crossing a small ridge, in otherwise undeformed SYI
- Bow Stakes: 17 stakes in diverse area of undeformed, deformed, ponded SYI

- MET Stakes: 9 stakes crossing from ridged SYI to ponded SYI (partially intact)
- ROV Stakes: (Presumed dead)

Measurement of snow-temperature profilers

We additionally built and deployed twenty-eight snow-temperature profilers, distributed across three of the stakes sites. The profilers have five thermistors that were arranged in two different patterns depending on the snow depth. In shallow snowpack, we arranged the thermistors in horizontal fans to measure snow-ice interface temperature. In deeper snowpack, we arranged the thermistors in vertical arrays to measure the temperature profile from ice surface to snow surface. Ten of the profilers also have ultrasonic snow-pingers, providing snow surface height.

Preliminary (expected) results

The measurements of stakes and IMBs can provide the seasonal evolution of sea ice and snow mass balance for the diverse ice types. Based on the incoming data in combination with high-resolution electromagnetic thickness surveys, a 3D temperature and thermal property map of the ice floe and the surrounding atmosphere and ocean is generated at the MOSAiC CO, which is then used to calculate sea ice thickness and snow depth in the covered area. Complementing regular sea ice thickness and snow depth surveys by other methods, this information is expected to be very valuable for many studies during MOSAiC.

The deployment of SIMBA in the DN region covers the scale of 50 km × 50 km (Figure 4.3.2). Thus, the thermodynamic process of snow and sea ice measured by the SIMBA buoy was highly representative. As shown in Figure 4.3.3, the vertical temperature gradient through the snow was much higher than that within air and water.

The ice with different initial thickness have a large change in the ice growth rate. For example, at the coring site of second-year ice, the ice thickness increased from 0.82 to 0.98 m from 29 Oct. to 3 Dec., with the average ice growth rate of 0.0046 m d-1; while at the coring site of first-year ice, it increased from 0.40 to 0.70 m during the same period, with the average ice growth rate of 0.0086 m d -1. At the M1 and M6, for the ice with the initial ice thickness larger than 1.7 m in mid Oct., the vertical cooling front only expanded to the bottom of ice cover by 3 Dec., where the onset of ice basal growth has not yet started.

Fig.4.3.2 The locations of SIMBA buoys at 12:00 3 December 2019.

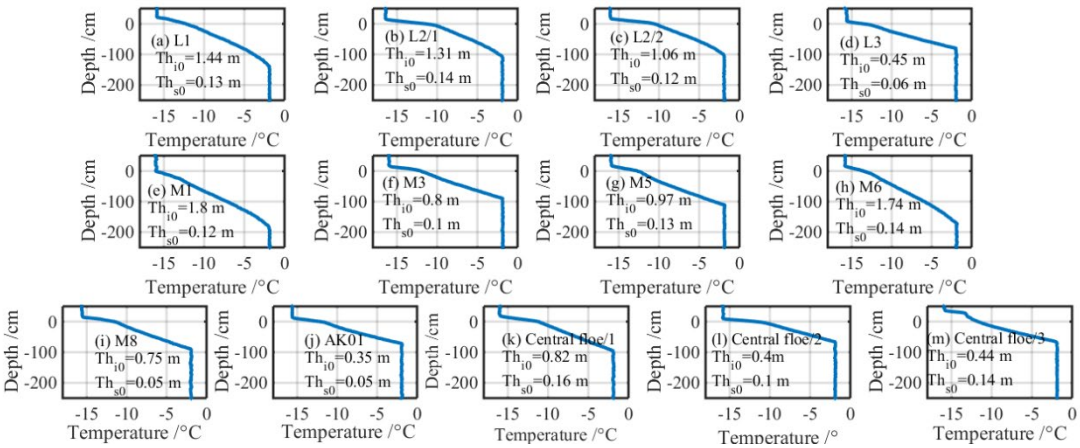

Fig.4.3.3 Temperature profile from air, through snow and ice cover, into the water measured by the SIMBA buoys at 12:00 3 December 2019; also shown are the initial thicknesses of snow (Ths0) and ice (Thi0).

Data management

All data are handled, documented, archived and published following the MOSAiC data policy (see APPENDIX). All the buoys have been added into the system of SENSOR.awi.de. The data coordination PIs of SIMBA buoys are Ruibo Lei from the PRIC, and Bin Cheng from the FMI. The coordination PI of DTC is Mario Hoppmann and that of SIMB and stake is Don Perovich from the DU. Final data products will be stored at the PANGAEA data repository (World Data Center PANGAEA Data Publisher for Earth & Environmental Science (www.pangaea.de)).

References

Jackson K, Wilkinson J, Maksym T, Meldrum D, Beckers J, Haas C, and Mackenzie D (2013) A novel and low cost sea ice mass balance buoy, Journal of atmospheric and oceanic Technology, 30(11), 13825, doi: http://dx.doi.org/10.1175/JTECH-D-13-00058.1.

Lei R, Cheng B, Heil P, Vihma T, Wang J, Ji Q, and Zhang Z (2018) Seasonal and interannual variations of sea ice mass balance from the Central Arctic to the Greenland Sea, Journal of Geophysical Research: Oceans, 123. https://doi.org/10.1002/2017JC013548.

Perovich D, Richter-Menge J, Polashenski C, Elder B, Arbetter T, and Brennick O (2014), Sea ice mass balance observations from the North Pole Environmental Observatory, Geophysical Research Letters, 41, 2019–2025, doi:10.1002/ 2014GL059356.

4.4 Transect

Stefan Hendricks[1], Marc Oggier[2], Gunnar Spreen[3], David Wagner[4]

(not on board:) Julienne Stroeve[5], Carolina Gabarró[6]

[1]DE.AWI

[2]EDU.UAF

[3]DE.UNI-Bremen

[4]CH.WSL

[5]CA.UMANITOBA

[6]ES.ICM-CSIC

Objectives

In contrast to stationary time series in the CO, measurements on the sea ice transect are designated to characterize the spatial distribution and its evolution of geophysical parameters of sea ice and its snow cover on the scale of kilometers. Among the parameters are the thickness of the sea ice and snow layers, as well as the remote sensing signature of the ice surface for active and passive microwave sensors. To understand the linkage between ice and snow thickness and the remote sensing signature, detailed observations of snow properties are necessary at selected locations that are representative for the different ice and snow conditions found along the transect.

The transects observations on MOSAiC leg 1 are part of the yearly time series with the general objectives to observe the changes of sea ice and snow properties in the CO. However, there are specific research questions since the observation period covers the late freeze-up to early winter:

How does the sea ice thickness distribution change in the early phase of the Arctic Winter driven by thermodynamic and dynamic forces?

What are the radar backscatter characteristics at Ku and Ka-Band frequencies and how are they influenced by changes in snow properties? What is the accuracy of observations of snow depth from the dual-band radar altimeter?

How does the surface emissivity at L-Band vary for the range of ice thicknesses in early winter? How does the emissivity depend on snow and ice temperature and salinity?

These objectives target local process studies, the general evaluation concept, however, specifically includes upscaling of all observations to the basin scale using satellite remote sensing.

Work at sea

The work for the transect task in response to the scientific objectives can be distributed into three segments:

- Collocated observations of sea-ice thickness and snow depth on sea ice along transect lines that are representative for ice conditions in the CO
- Towing of remote sensing sensors along segments of the transect lines with existing sea-ice thickness and snow depth information
- Snow pits and collecting of snow samples in regular intervals along the remote sensing segments of the transect lines

The transect lines themselves were established in the form or two main loops on different ice types. The loops were named for the original location in the CO.

- Northern loop: Located on thick and deformed remnant ice
- Southern loop: Initially located in an area of undeformed remnant ice, which however, was dominated by a large fraction of melted through and now refrozen melt ponds with thin ice (i.e. similar to first-year ice). Experienced significant deformation in the mid-November shear event.

The location of the two loops are illustrated in Figure 4.4.1. Observations were also made on the connecting roads between the two loops staging from the remote sensing site situated in-between. The northern loop was established first and followed by the southern loop. The latter was significantly deformed in mid-November during the shear event and not accessible for two weeks. According to the directive to observe changes in the sea-ice thickness distribution caused by deformation events, the southern loop was reconstructed as good as possible from the original markers and visible tracks on the ground.

The remote sensing (RS) segments of the transect was established on one side of the northern transect loop with variable snow and ice conditions and a surface profile allowing for towing larger sleds with sensor installations. In addition to this segment, a shorter RS transect line

was located near the remote sensing site on thinner level ice, which should be representative for the dominant ice type along the southern loop and the southern part of the floe in general.

The list of sensors used for transect work is detailed in Table 4.4.1. The three categories of transect work required three teams operating individually. The first teams consisted of sea-ice thickness and snow measurements using a combination of a broadband electromagnetic induction sensors (Geophex GEM-2) and a MagnaProbe. The GEM-2 was towed in a pulka and measuring the total (ice + snow) thickness, while the MagnaProbe measures snow depth by means of a sliding disc on a rod that stays on the top snow surface along a rod that is pushed down to the snow/ice interface. The remote sensing work consisted of two sleds, one with two pairs of radar transmitter/receiver antennas for the polarimetric Ku and Ka-Band scatterometers in nadir configuration (see section 4.9) and the side-ward looking Balamis ARIEL L-Band microwave radiometer (see section 4.9) configured for measurements at a 45-degree incidence angle. The observations of snow properties included measurements with a Snow Micro Penetrometer (SMP) to estimate the vertical profile of snow density and specific surface area (SSA), as well as in-situ observations of snow water equivalent and taking samples to measure snow salinity in the lab afterwards.

The transect lines and observation protocols were established over time and the loops were not always accessible due to limitation in visibility and ice conditions. The weekly repeat schedule for the transect work was however kept during the main observation period in leg 1, only the availability of data for the main observation groups (ice + snow, remote sensing and snow properties) varies. In total, there were 7 transect activities and the availability of data in form of device operations is listed in the Tables 4.4.2, 4.4.3 and 4.4.4.

Tab.4.4.1: Overview of sensors used on sea ice transect

Sensor	Description	Device URN	Geophysical Parameter
GEM-2	Geophex GEM-2 Broadband Electromagnetic Induction Sensor	pack_ice:ice_ps:gem2-556	Total (sea ice + snow) thickness
MagnaProbe	GPS snow depth probe	pack_ice:ice_ps:magnaprobe-kathrin	Snow depth on sea ice
KuKa Radar	Dual-Band KuKa scatterometer	pack_ice:ice_ps:kuka_radar	KuKa Band radar backscatter
Balamis	Balamis L-Band radiometer	pack_ice:ice_ps:BALAMIS_Rad	L-Band brightness temperature
SMP	Snow Micro Penetrometer	pack_ice:snowpit:SN_SMP49, pack_ice:snowpit:SN_SMP31	Snow density Specific Surface Area
SWE	Snow Water Equivalent Samples	pack_ice:snowpit:SN_SWE	Snow water equivalent
Snow Salinity	Snow Salinity Samples	pack_ice:snowpit:SN_SAMPLER	Snow salinity

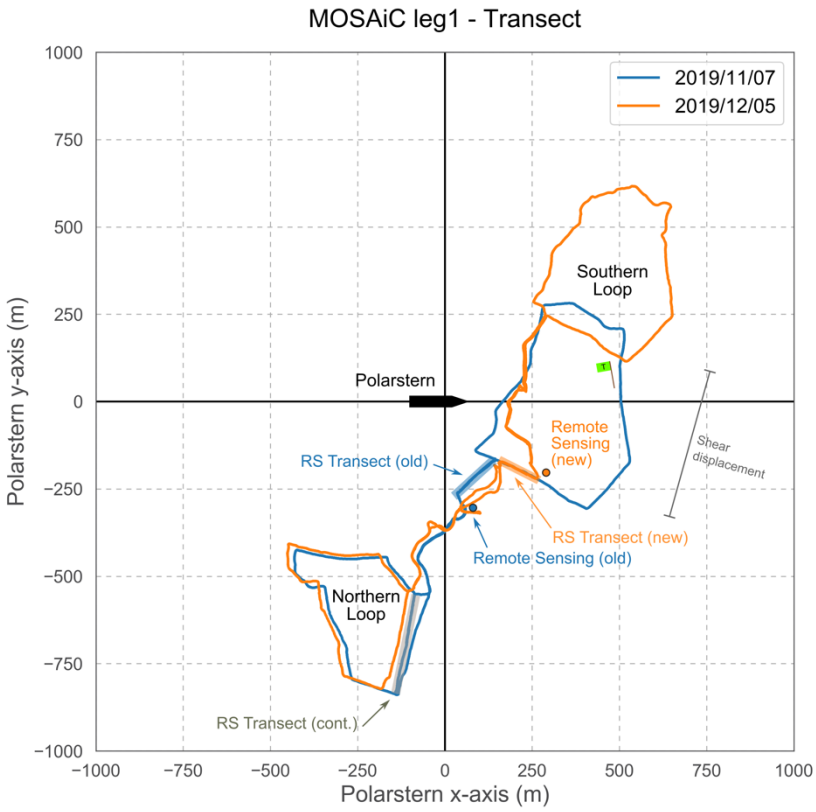

Fig.4.4.1: Location of the transect lines in the CO before (2019/11/07) and after (2019/12/05) the mid-November shear event. Coordinate reference system is defined by Polarstern location and heading.

Tab.4.4.2: Overview of device operations of the mass balance work on the sea ice transects

Transect Date	Locations	GEM-2	Magna-Probe
24.10.2019	Northern Loop	PS1 22/1_4-2 (transect) PS122/1_4-3 (cal)	PS122/1_4-1
31.10.2019	Northern Loop Southern Loop	PS122/1_5-25 (transect) PS122/1_6-26 (cal)	PS122/1_5-27
07.11.2019	Northern Loop Southern Loop	PS122/1_6-48 (transect) PS122/1_6-49 (cal)	PS122/1_6-50
14.11.2019	Northern Loop Southern Loop	PS122/1_7-60 (transect) PS122/1_7-61 (cal)	PS122/1_7-62
21.11.2019	Northern Loop	PS122/1_8-55 (transect) PS122/1_8-56 (cal thin)	PS122/1_8-58

		PS122/1_8-57 (cal thick)	
28.11.2019	Northern Loop	PS122/1_9-52 (transect) PS122/1_9-51 (cal)	PS122/1_9-54
05.12.2019	Northern Loop Remote Sensing Southern Loop	PS122/1_10-51 (transect) PS122/1_10-55 (cal)	PS122-1_10-59

Tab.4.4.3: Overview of device operations of the remote sensing work on the sea ice transects

Transect Date	Locations	KuKa-Radar	Balamis Radiometer
24.10.2019	N/A	N/A	N/A
31.10.2019	Northern Loop RS	N/A	PS122/1_5-29
07.11.2019	Northern Loop RS RS Site Segment	PS122-1_6-52	PS122-1_6-57
14.11.2019	Northern Loop RS RS Site Segment	PS122/1_7-59	PS122/1_7-57
21.11.2019	N/A	N/A	N/A
28.11.2019	N/A	N/A	N/A
05.12.2019	N/A	N/A	N/A

Tab.4.4.4: Overview of device operations of the snow properties work on the sea ice transects

Transect Date	Locations	Snow MicroPen	Snow Water Equivalent	Snow Salinity Samples
24.10.2019	N/A	N/A	N/A	N/a
31.10.2019	N/A	N/A	N/A	N/a
07.11.2019	Northern Loop RS	PS122-1_6-41, PS122-1_6-42, PS122-1_6-43, PS122-1_6-44, PS122-1_6-45, PS122-1_6-46 PS122-1_6-47	N/A	PS122-1_6-41 PS122-1_6-47
14.11.2019	Northern Loop RS RS Site Segment	PS122-1_7-68, PS122-1_7-69, PS122-1_7-70, PS122-1_7-71, PS122-1_7-72, PS122-1_7-73	PS122-1_7-68, PS122-1_7-69, PS122-1_7-70, PS122-1_7-71, PS122-1_7-72, PS122-1_7-73	PS122-1_7-68, PS122-1_7-71, PS122-1_7-72

21.11.2019	Northern Loop RS RS Site Segment	PS122-1_8-68, PS122-1_8-69, PS122-1_8-70	PS122-1_8-68, PS122-1_8-69, PS122-1_8-70	PS122-1_8-68
28.11.2019	Northern Loop RS RS Site Segment	PS122-1_9-71, PS122-1_9-111, PS122-1_9-72, PS122-1_9-73, PS122-1_9-74	PS122-1_9-71, PS122-1_9-111, PS122-1_9-72, PS122-1_9-73, PS122-1_9-74	PS122-1_9-71, PS122-1_9-72, PS122-1_9-73
05.12.2019	Northern Loop RS	PS122-1_10-50, PS122-1_10-58	PS122/1_10-50, PS122/1_10-58	PS122-1_10-50

Preliminary (expected) results

Quickview total (ice + snow) thickness from the GEM-2 results were produced after each transect activity for the purpose of quality control and initial evaluation of ice conditions. An exemplary quickview product at full sensor resolution is shown in Figure 4.4.2. The result is not corrected for different walking speeds or periods of the sensor without moving. Further processing steps for the ice and snow data is to project both the GEM-2 and MagnaProbe results to the transect lines at an equidistant spacing. This step requires transforming the geographical (time, longitude, latitude) coordinates to cartesian (x, y) coordinates of the coordinate reference system (CRS) defined by the FloeNavi base stations. The collocated GEM-2 and MagnaProbe data than will be used to convert the total ice thickness measurements of the GEM-2 to sea-ice thickness, resulting in time series of the sea-ice thickness and snow depth distribution in the CO for the entire drift of MOSAiC.

The remote sensing sensors provide (a) Ku/Ka-band radar backscatter and based on that the range distance to the main scattering horizons in the snow and ice and (b) L-band microwave brightness temperature, which are primarily related to the snow and ice microwave emissivity. The data from the instruments will be referenced to the FloeNavi CRS together with the locations of the snow pits. Analysis of the remote sensing data however requires extensive data processing, which will be done at home in cooperation with the partner institutions that have supplied the sensors.

In the context of the transect work, the snow pit data will mainly be used to interpret data from the remote sensing sensors. The results are however integrated in the wider snow task and will be used to characterize the evolution of the snow pack in the CO in general.

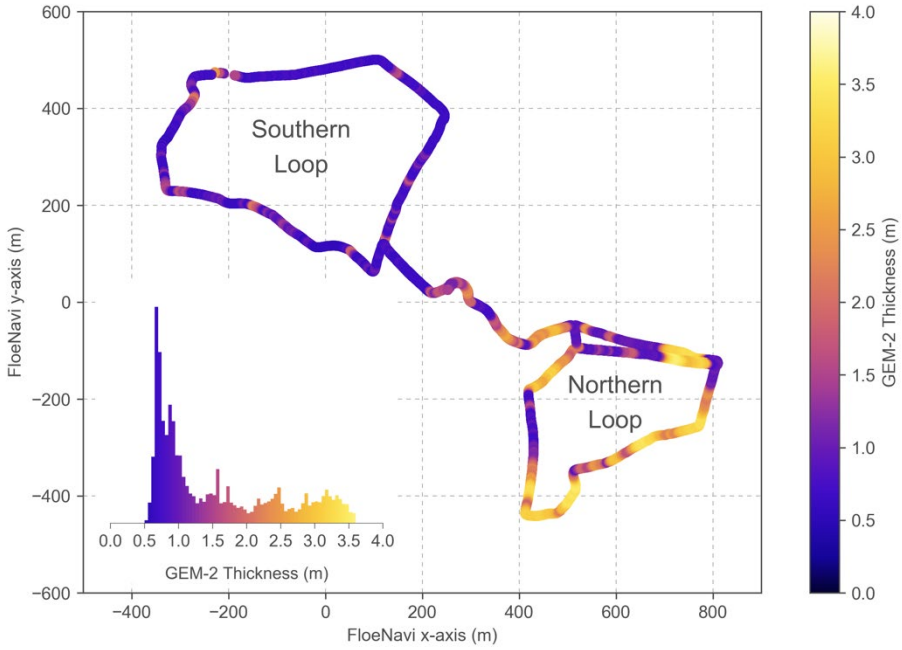

Fig.4.4.2: Exemplary total (ice + snow) thickness from GEM-2 measurements (transect activity of Nov. 14, 2019). Main figure shows geographical distribution of total thickness in the coordinate reference system of the CO (FloeNavi coordinates). Inset figure in lower left show the histogram of total thickness.

Data management

All data are handled, documented, archived and published following the MOSAiC data policy (see APPENDIX). All device operations were logged in the AWI sensorweb portal and all sensor raw data files are stored in platform section of MCS. Final geophysical parameters will be made available via the workspace section of MCS. Final data products will be stored at the PANGAEA data repository (World Data Center PANGAEA Data Publisher for Earth & Environmental Science (www.pangaea.de)).

References

No references

4.5 Ice Coring

Marc Oggier[1], Ruibo Lei[2], Nikolay Kolabutin[3], Egor Shimanchuk[3], Marcel Nicolaus[4]

(not onboard:) Mats Granskog[5], Sonke Maus[6], Martin Schneebeli[7], Sergey Kovalev[3]

[1]EDU.UAF
[2]CN.PRIC
[3]RU.AARI
[4]DE.AWI
[5]NO.NPOLAR
[6]NO.NTNU
[7]CH.WSL

Objectives

Within the general coring objectives (8.2 Objectives for General Coring.), the ICE team is responsible for the ice physics properties analysis (salinity, density, microstructure).

Work at sea

Following the general coring event, upon return from the field, the CT samples are centrifuged, and imaged using x-ray computed tomography (CT) technique within half a week. Cores for archive, backup, plastic and the upper part of the CT core are sealed in plastic sleeves and stored at -20 °C. Density is measured at -15 °C by densitometry in paraffin in the freezer lab using a Kern EMB-V scale. Salinity is then measured on the melted samples with a conductivity probe Voltcraft LWT-100 from team ICE. Within 1 day, melted salinity samples are bottled for future isotope measurement, before bulk salinity is measured on the remaining water using a conductivity probe YSI 30 from team ECO. Each week, one ice core, coming alternatively from the FYI and SYI site, was processed into horizontal and vertical thin sections. Following additional coring events, similar approach was used to process collected cores with respect to its type.

Preliminary Results

At the FYI site, ice consists of an upper layer of granular ice, about 15 to 20 cm thick, with columnar growth underneath (Figure F.SIP-IC2, top). Over 6 weeks, the ice grew from 40 to 70 cm. At the SYI, ice consists of a refrozen melt pond about 70 cm thick with a few centimeters of new ice. During the leg, columnar ice grew from 75 to 95. Figure 4.5.2 below shows the evolution of the salinity, temperature and density profiles acquired for leveled and undeformed sea-ice for the FYI and SYI site. Brine volume fraction was computing using Cox and Weeks' equation (1983), constrained with the density profiles when available. Growing FYI displays the expected C-shape salinity profiles, while the salinity value for SYI profiles mirrors the observed stratigraphy (Figure 4.5.1, bottom) with low salinity values (0-1 ppt) in the upper 70 cm, and high salinity values at the bottom (5 ppt) increase in the lowermost section (8 ppt).

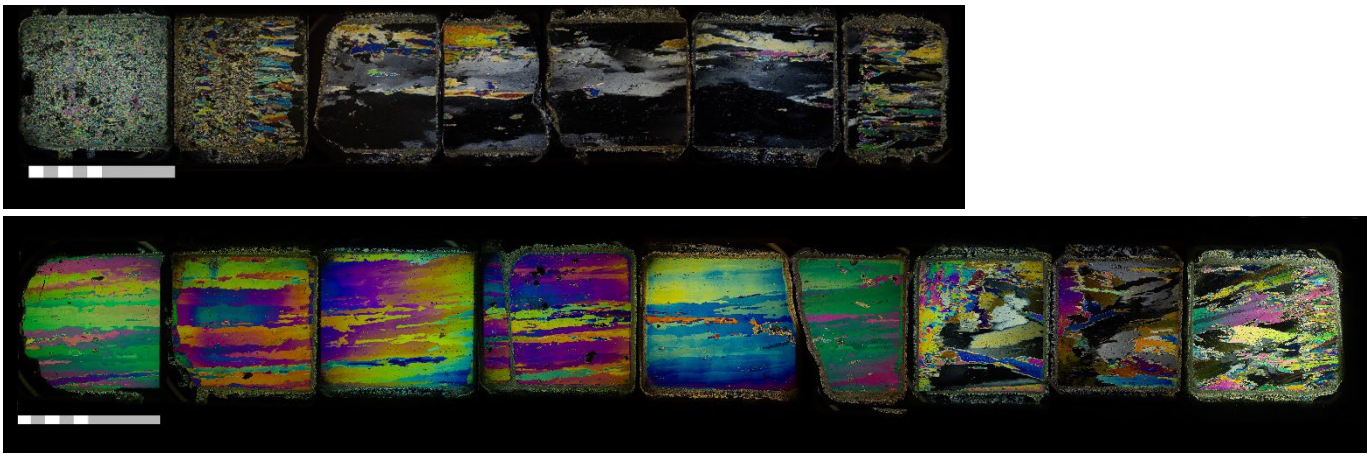

Fig.4.5.1 – Vertical thin sections for FYI (top) and SYI (bottom) core collected at the end of leg 1 (1_10). The ice surface is on the left. Scale bar is 10 cm. The stratigraphy of FYI consists of 17 cm of granular ice with columnar ice underneath. The SYI consists of 70 cm of refrozen melt pond with columnar growth underneath.

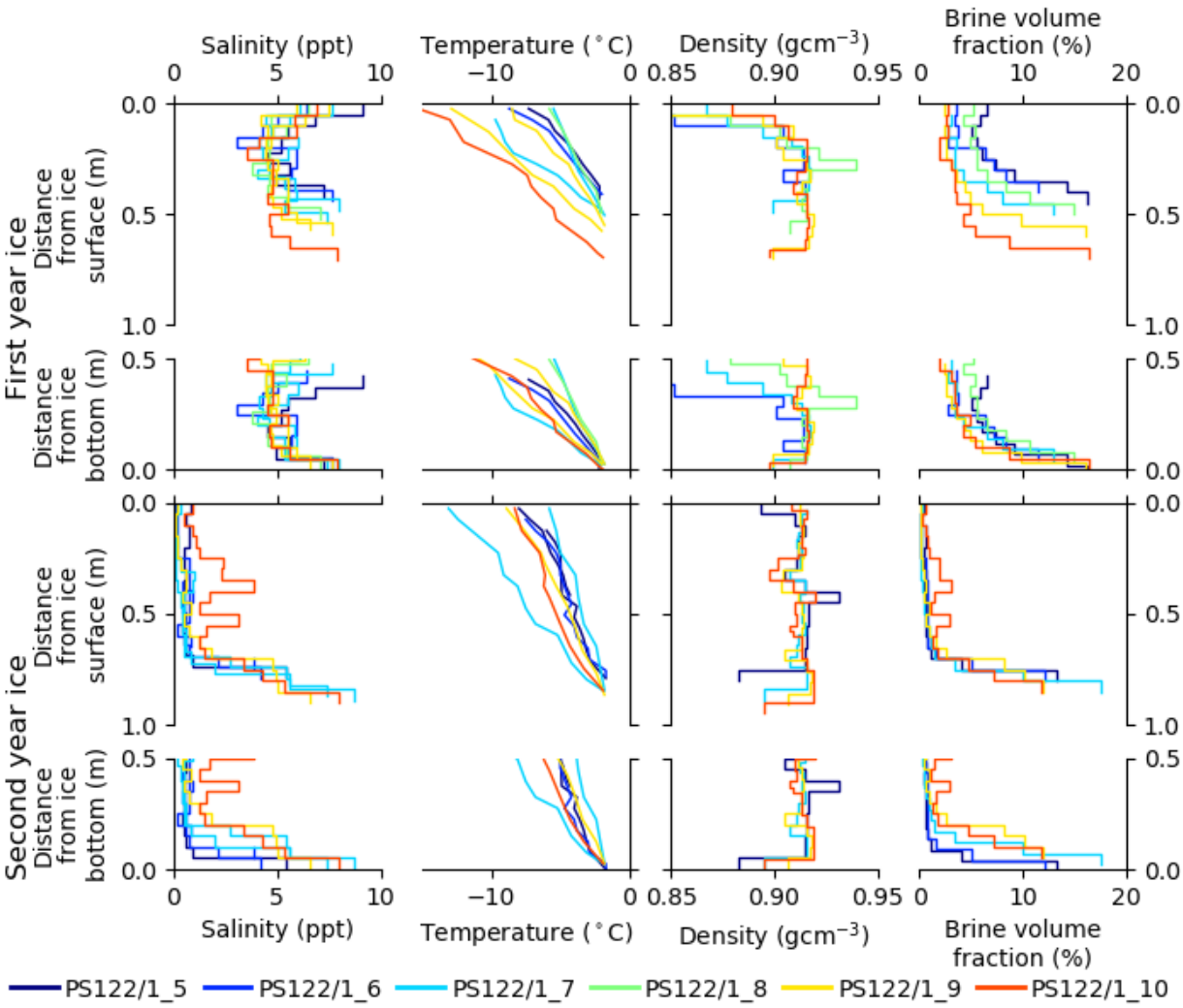

Fig.4.5.2 – Evolution of salinity, temperature and density profiles over a 6-week period for first-year ice and second-year ice. The upper panel display core data aligned at the ice surface, while the bottom panel display the same data aligned at the ice/water interface. The coldest temperature profile for SYI is associated with thinner snow.

Data Management

All data are handled, documented, archived and published following the MOSAiC data policy (see APPENDIX). All data related to a coring event are collocated on the MCS within the folder of the device operation corresponding to the deployment of the corer Kovacs Mark II, 9cm. A scanned copy of the field note and laboratory book will be uploaded. The exhaustive list includes:

Primary data for each ICE and ECO core transcribes into a spreadsheet (section depths, ice thickness, ice draft, weather, date and time…)

Salinity and density measured on board within 2 days of the coring

Vertical and horizontal thin sections photographed on board during the leg

Data of CTD cast in one of the corehole.

Tomographic imagery is available on the MCS within a separate subfolder contained in the folder of the X-ray tomographer Scanco90.

Final data products will be stored at the PANGAEA data repository (World Data Center PANGAEA Data Publisher for Earth & Environmental Science (www.pangaea.de)).

References

No references

4.6 Ice dynamics

Jari Haapala[1], Nikolay Kolabutin[2], Ruibo Lei[3], Ian Raphael[4], Egor Shimanschuk[2]

(not onboard:) Andrea Haase[5], Jennifer Hutchings[6], Phil Hwang[7], Polona Itkin[8], Mikko Lensu[1], Annu Oikkonen[1], Chris Polaschenski[4] Victor Smirnov[2]

[1]FI.FMI
[2]RU.AARI
[3]CN.PRIC
[4]EDU.DARTMOUTH
[5]DE.HSVA
[6]EDU.ORSU
[7]UK.AC.HUD
[8]NO.UIT

Objectives

On overall objective of ice dynamics research is to deepen understanding on how pack ice moves and deforms over its first year of existence. In particular, we are examining spatial and temporal scales of motion and deformation and how those vary regionally and seasonally. We also aim to establish a relationship between deformation scales and physical characteristics of pack ice.

Ice dynamics research is based on the local measurements at the Central Observatory, ice drift observations from the Distributed Network and large scale satellite products. For a collection data on local scale, we established a MOSAiC Small scale Ice Dynamics Observing System (SIDOS) on the Central Observatory. The system includes following components:

- Laser strain array (DC)
- GNSS buoys (UHud)
- Seismic stations (AARI)
- Stress gauges (DC, FMI)
- Stress panels (HSVA)
- Ice radar (FMI)

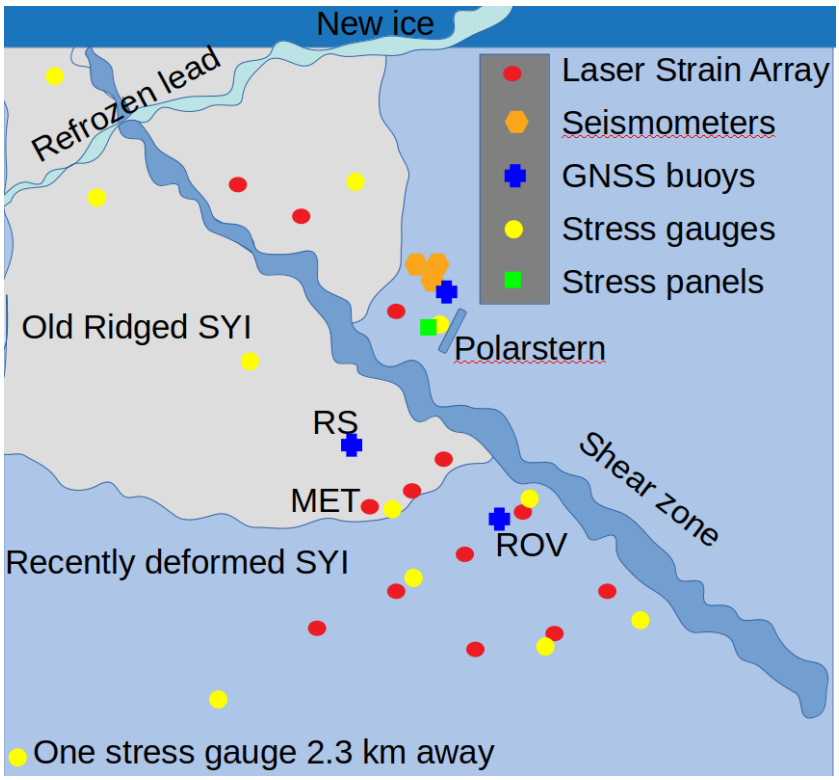

Fig.4.6.1: Schematic figure of the MOSAiC Small scale Ice Dynamics Observing System (SIDOS).

Work at sea

Laser strain array

The Laser Strain Observatory provides high-precision plastic and elastic ice strain data. The observatory is composed of an array of retroreflectors fixed very stably in the ice on metal posts, and an autonomous laser theodolite that tracks the displacement of the reflectors over time with precision on the order of 1-5mm. This displacement measurement can be used to determine strain rate and to estimate stress.

The TM50 base station is installed next to MET City. We installed ~20 reflectors throughout Leg 1, roughly in rings at ranges from 200m to 850m from the base station. After ice deformation, some reflectors were no longer in line-of-sight to the base station and we recovered them to the ship; others were lost or destroyed by ice deformation. 13 reflectors were intact and measurable at the end of Leg 1.

The base station measures continuously, and since it is accessible via the PackIce WLAN network, we could view data in real-time from *Polarstern*. During the mid-November deformation event, we could see elastic deformation in the vertical axis during the compression and following divergence of the floe. We also saw horizontal displacement preceding the brittle shearing of the floe.

GNSS buoys

The GNSS buoys to measure ice motion on high precision were deployed to three sites at the Central Observatory. The first one was deployed to the seismometers site close to the logistic area on 22 November 2019. The second one on the remote sensing site on 30 November 2019 and the third on the ROV Oasis on 5th December 2019.

Seismic stations

Objectives of the seismic observations is to obtain data on waves on ice and fracturing of the pack ice for a development of forecast methods for sea ice breaking. The seismic monitoring method has been developed in the AARI.

For continuous measurements of waves in ice, three seismic stations (Alfa, Beta, Gamma) were deployed close to the logistic area. The seismic stations have been operational since 24th October 2019. Each station includes seismometer CME 4311, tiltmeter ИН-Д3-360, autonomous recorder “Baykal-8” for logging signals, GPS-antenna, antenna for signal transmission to the base and battery for powering station. Initially all three stations were deployed at one place, then at November 8th Alfa and Beta were redeployed on the distance 30m from Gamma and from each other. Alfa and Beta were supposed to be redeployed again on the distance 600-800m from the vessel, but these works had been delayed for leg 2 because of unstable ice conditions and new large scale ice fractures.

Measurements were recorder to the “Baykal-8” datalogger with 100 Hz frequency. Data of the seismic stations were also transmitted by the wireless connection to a laptop deployed onboard the *Polarstern* for a continuous visual monitoring of seismic observations.

Seismic stations have been operationally most of the time. Together, three seismic stations have been recorded 14,9 GByte of data (4,38 GByte from Alfa, 4,96 GByte from Beta, 5,59 GByte from Gamma) during 24th October 2019 to 15th December 2019.

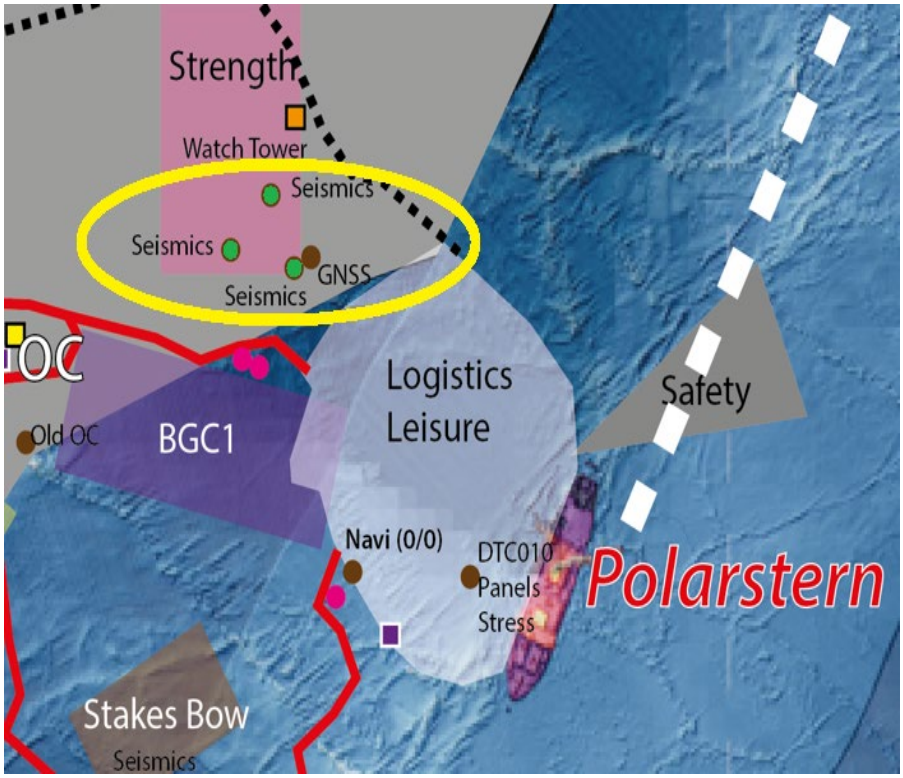

Fig.4.6.2: Seismic stations deployed on the ice at 150 m from the Polarstern.

Stress gauges

For a measurements of an internal stress of pack ice we used Geocon 4350 bi-axial stressmeters. These type of sensors have been used successfully in previous ice mechanics studies (c.f. Richter-Menge, 2002, Lensu et al, 2013). Data of the sensors were stored on the Campbell data loggers. Time interval of the Darthmount College units recordings were one minute and the FMI ones 10 minutes.

Totally 13 stress sensors were deployed during the first leg. Locations of the deployments were selected based on airborne laser scanning data and the ship radar images. At the first phase,

two sensors were deployed on the thick deformed remnant ice area (“Fortress”) and two other on the thinner undeformed remnant ice between 26th October and 2nd November 2019. In the next phase, four units were deployed inside the laser strain array measurement area on 9th - 10th November 2019. After these deployments, two cyclones passed the Central Observatory and pack ice experienced considerable deformations. Third deployments took place on 11th December when four sensors were deployed both on previous “Fortress” and “undeformed SYI” regions.

All sensors were deployed on 32 centimeters depth, i.e. that the top of gauge was on the ice surface. Hole on ice was made with a 5 cm ice auger. Due to the location near the North Pole, sensors weren’t able to oriented to the north with a compass and thus the sensors were oriented towards the *Polarstern*. After the placing devices on the ice, the hole was filled with the water. In case of the FMI sensors, with ocean water and for the Dart mount College units with fresh water.

The stress sensor sites have been visited for downloading of data around three weeks intervals. For that, a Campbell software installed on the rugged laptop was used.

The Dart001 stress sensor unit was lost during the stormy period which occurred on 15th - 20th November 2019.

Fig.4.6.3: Photos of stress buoy deployment site close to the MET city on 19 November and 8 December 2019.

Tab.4.6.1 Stress gauge deployments

Sensor name	date	h_i	h_s	fb	Description of site
FMI001	2 Nov 2019	47	2,5	2,5	Undeformed SYI about 2.3 km away from the ship.
FMI002	26 Oct 2019	40	11	2	Helicopter landing site. Undeformed patch of second year ice at the heavily deformed SYI region, close to boundary of the deformed and undeformed ice types.
FMI003	28 Oct 2019	37	7	1	Met City. Undeformed second year ice at the edge of the deformed ice region. Around 100 meters from Met City deployments towards to *Polarstern*.
FMI004	26 Oct 2019	45	10,5	2	Transect North. Undeformed second year ice, surrounded by heavily deformed second year ice. Left side of the transect line around 100

					meters ahead from the four thermistor string buoys.
FMI005					Stress panel at the logistic area. Thick SYI.
Dart001	9 Nov 2019	56	8	2	Stakes2. Undeformed second year ice in large, mostly undeformed SYI pan.
Dart002	10 Nov 2019	51	6	2	Snow5. Undeformed second year ice in large, mostly undeformed SYI pan.
Dart003	10 Nov 2019	48	8	3	Snow1. Undeformed SYI on margin of deformation zone.
Dart004	10 Nov 2019	37	8	0,5	FYI in newly refrozen lead (~2m wide). Surrounded by mostly undeformed SYI, in shear zone from major deformation event in mid October.
Dart005	11 Dec 2019	87	5	5	Southwest Snow2. Large pan of undeformed SYI surrounded by major multi year and first year deformation.
Dart006	11 Dec 2019	77	8	4	Northwest corner of Snow3. Middle of large pan of undeformed multiyear ice. Hundreds of meters from any variation in ice condition.
Dart007	11 Dec 2019	79	10	7	Between Snow2 and Helipad. 70m from newly refrozen lead, in otherwise undeformed SYI pan.
Dart008	11 Dec 2019	91	12	4	Southwest corner of original Stakes2 plot on Southern Transect loop. 100m away from recent ridging in otherwise undeformed SYI pan.

Stress panels

Stress panels were deployed to the logistic area on 6th November 2019. Panel are located 31 meters distance from the starboard side of the hull in align with the void 92.

Sea ice in that location was deformed second year ice. It's thickness was 1.65 meters. Snow thickness was 16 cm and freeboard 8 cm. Between the stress panels and hull of the ship there was a few old cracks where ice thickness was 40-60 cm.

One thermistorstring buoy (sensor id DTC16_416) was deployed within 2 meters distance from the panels on 7 November 2019. One stress buoy was deployed in the vicinity of the stress panels too on ?? December 2019.

Ice radar

In order to obtain data of local ice dynamics in high temporal and spatial scale, we used a system which digitizes the raw analogical ship radar data in a manner that echoes from the sea ice features, which normally are considered as a noise in marine applications, are digitized in high resolution. The radar signal digitizing unit, developed by the Imagesoft ltd., was connected to the antenna of the WAMOS radar. The set-up of the system is similar than used for the N-ICE2015 campaign (Oikkonen et al, 2017).

During the MOSAiC, processed images of every radar loop have been stored. Interval of those images is about 2 seconds. Digitizing area covers 20 x 20 kilometers area with 8.3 meters horizontal resolution. Continuous recordings begin on 25th October 2019.

Ice drifters

Ice drifters are part of the MOSAiC Distributed Network. Most of the drifters were deployed from *Akademik Fedorov*. Detailed description of the DN network deployments is provided in the *Akademik Fedorov* Cruise Report.

Additional 11 drifters were deployed from *Polarstern* during the Leg 1 (Table 4.6.2). Four Met-Ocean ISVP buoys, provided by the PRIC, were deployed on the way from the marginal ice zone to the region where the MOSAiC CO was established. Six Met-Ocean iSVP buoys, provided by the PRIC, and one PacificGyre Universal Tracker, provided by the OSU, were deployed within the regions with the scale of 2 km from the MOSAiC CO.

Tab.4.6.2 Deployment information of ice drifters from *Polarstern* during Leg 1

Buoy type	Deployment time (UTC)	Deployment location	Short name	IMEI number	Comments
Met-Ocean	26 Sep. 13:40	81.94ºN, 119.36ºE	P150	300234068312210	Marginal ice zone
Met-Ocean	28 Sep. 8:15	82.57ºN, 122.37ºE	P151	300234068312200	Marginal ice zone
Met-Ocean	29 Sep. 6:50	84.64ºN, 128.81ºE	P152	300234068218450	Pack ice zone
Met-Ocean	29 Sep. 1:40	84.17ºN, 129.14ºE	P153	300234068316210	At the helicopter landing site on MOSAiC floe, recovered on 29 Oct.
Met-Ocean	30 Sep. 8:53	85.11ºN, 137.62ºE	P155	300234068213470	Pack ice zone
Met-Ocean	9 Oct. 5:45	84.91ºN, 135.86ºE	P156	300234068210190	Pack ice zone
Met-Ocean	21 Oct. 5:30	85.079 ºN, 132.91ºE	P157	300234068314190	2 km from the CO
Met-Ocean	21 Oct. 5:45	85.10ºN, 132.53ºE	P158	300234068318250	2 km from the CO
Met-Ocean	21 Oct. 5:10	85.07ºN, 132.71ºE	P159	300234068215980	2 km from the CO
Met-Ocean	21 Oct. 6:10	85.088ºN, 132.78ºE	P161	300234068118580	At the first ROV city on MOSAiC floe, recovered on 15 Nov.
PacificGyre Universal Tracker	21 Oct. 4:50	85.105ºN, 132.73ºE	P183	300234066253880	2 km from the CO

Sea ice strength measurements

Aim of the ice streght measurements is to determine local strength of different ice types and and their seasonal variations. Measurements of vertical and horizontal ice strength were carried out according to a methodology developed in Ice Physics Laboratory of the AARI (patent №2348018) and described in “Methodic manual for studying physical-mechanical characteristics of ice formations as initial data for calculation of ice loading on shores, bottom and sea constructions” (SPb, AARI, 2011, p. 179).

For these measurements, a 50 meters x 50 meters area named „strength“ was reserved. The site contains level second-year ice and it‘s located around 300 meters distance away from the *Polarstern*.

Local ice strength measurements were conducted with an automatic hydro complex “ЛГК 131-01” borehole probe-indenter “ЛГЦ095.055.0050.002”.

Measurements were carried out in the following way. Firstly, point of measurements was cleaned from snow and air, snow and ice surface temperatures were measured. Then at this point a hole with diameter 250 mm is drilled throughout ice cover. After that the hole was cleaned from brash ice and probe-intenter was deployed on a tripod over the hole. After testing of the system, the probe-indenter was oriented to the seflected direction and lowered down into hole on 30 cm depth and first measurement was made. For the second measurement probe-indenter is lowered down to the 60 cm depth if the thickness of ice was larger than 75 cm.

Ice strength measurements in-situ were carried out on November 20th 2019. Four hole were made for the measurements. Ice thickness in the holes was 60, 78, 80 and 87 cm. Measurements at the 30 cm depth were made in all holes and at 60 cm depth in three holes. An average local ice strength on 30 cm depth was 24,2 MPa and on 60 cm depth it was 23,3 MPa.

For a determination of ice temperature, salinity, density and texture, a ice core was taken close to the strength measurement site.

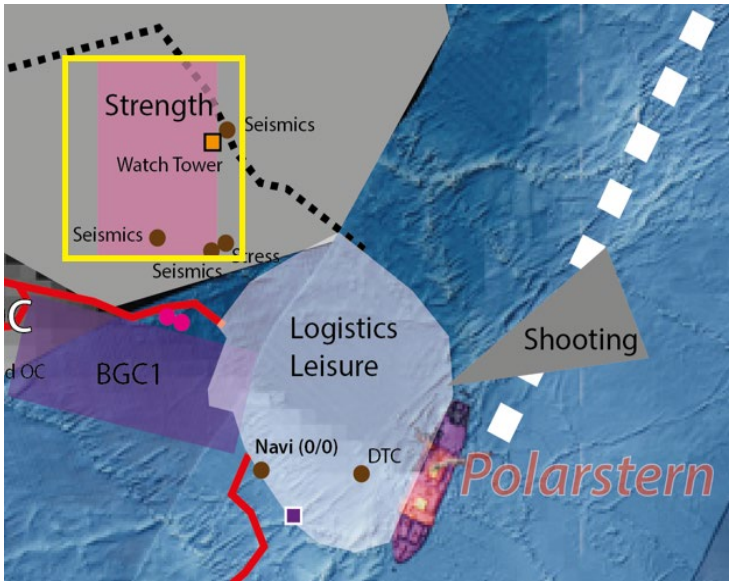

Fig.4.6.4: Location of ice strength measurements.

Tab.4.6.3 Results of ice local strength measurements 20.11.2019

Point	H_snow(cm)	H_ice(cm)	H_raft(cm)	LocStr30(MPa)	LocStr60(MPa)
t1	11	60	57	21,352	--
t2	10	80	74	28,737	25,251
t3	11	87	83	23,904	25,406
t4	12	78	74	23,081	19,403

Unaxial compressive strength measurements were conducted on December 5th 2019. The measurements were carried in a following manner. After cleaning of the surface and temperature measurements, ice cores for vertical ice strength measurements were taken with the “Kovacs” 14 cm ice corer. For the horizontal strength measurements, first a block of ice with dimension of ~ 40 cm x 50 cm x 66 cm were taken and then horizontal ice cores at 30 cm depth was taken from that block.

Usually measurements are carried out in the field but because of the strong wind and blowing snow measurements were made in ship. Ice cores were cut with the circular saw on 29-30 cm length samples before compressive strength measurements.

Ice thickness in the measurement site was 66 cm. Horizontal strength measurements were made from three samples. Two vertical strength measurements were made from surface layer (1 to 30 cm) and two other from bottom layer (30 to 60 cm). The average horizontal compressive ice strength at the surface was 3,2 MPa and 4,2 MPa at the bottom layer. The average vertical ice strength was 4,3 MPa.

Additional ice cores were taken for temperature, salinity and texture analysis.

Preliminary results

The leg1 was characterized on dynamical ice conditions. The central floe experinced tens of fracturing, shearing and ridging events which changed the icescape fundamentally (Figure 4.6.5). The most signicant deformations was caused by the two low pressure systems which occurred between 15th and 20th November 2019. Maximum wind speed during the passing of the first cyclone was ~ 20 m/s and maximum ice drift speed was ~0.4 m/s.

During the storm main floe experienced compression and shearing which resulted on cracking and fracturing of the CO. One fracture was formed between *Polarstern* and the MET-city, the Remote Sensing site and the ROV Oasis. It was well captured by seismic stations (Figure 4.6.6) The fracture was part of tens of kilometer long shearing zone. Shearing occurred in an episodic manner. Most of the time, differential motion between the two parts of the main floe was minimal but during some intensive 15-30 minutes periods shearing, opening, closing and ridge building were easily seen from the bridge. As an end result of the shearing, the other part of the CO was shifted around 600 meters.

Despite of rather cold weather conditions, deformation of the main floe has been continued until mid December. Intensity of fracturing has been surprisingly high also in the “Fortress” which consisted mainly thick ridged ice.

The MOSAiC ice dynamics program has been very successful. All the planned deployments were conducted and new data has been collected. In addition to the major fracturing during the storm on 16th - 17th November, more than 100 other ice deformation events were recorded by the seismic stations. These observations together with the ice radar, laser strain observatory, stress sensors, ice drifters and satellite data are forming an unique data set for ice dynamics research.

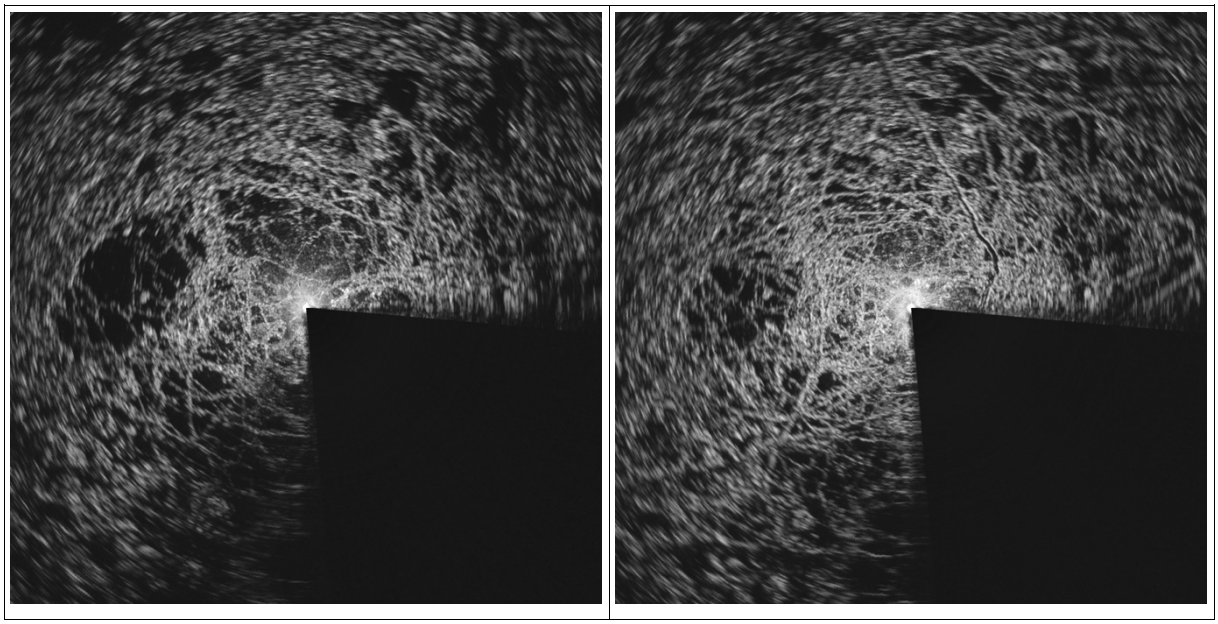

Fig.4.6.5: Ice radar images on 1 November and 7 December 2019.

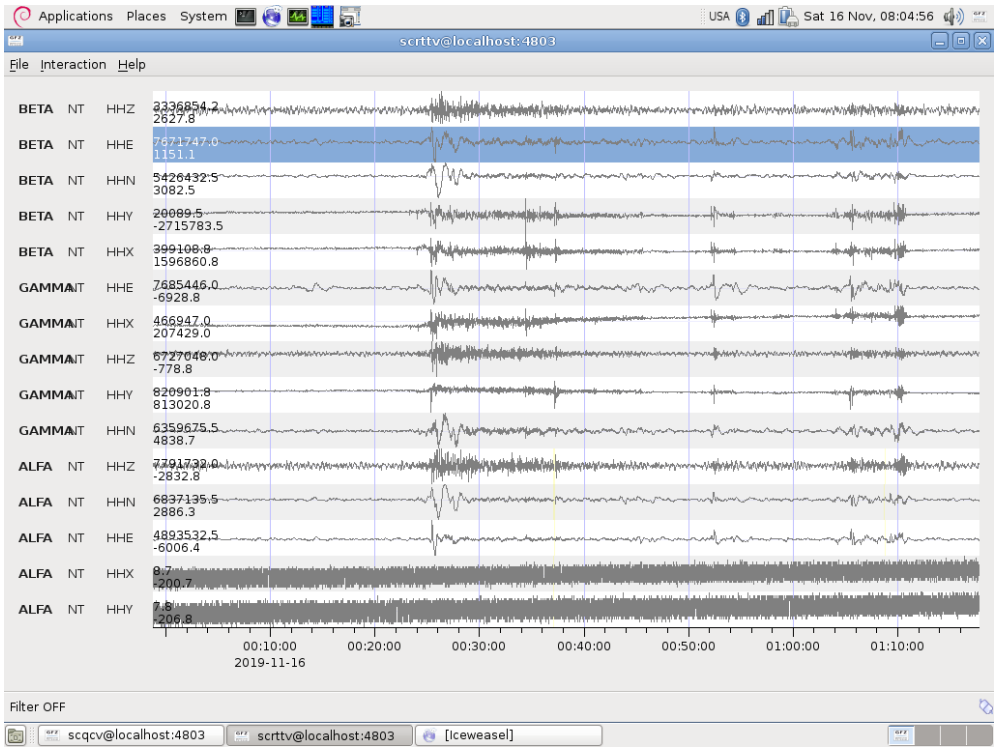

Fig.4.6.6: Example of „icequake“ during formation of a crack on 16th November 2019.

The DN network provides unique data on intermediate scale ice motions but since additional GPS drifters were deployed during the transit, the MOSAiC buoys provide also important information on how kinematic characteristics are varying from the thinner marginal ice zone to the thick pack ice region (Figure 4.6.7?). By the end of Leg 1, only three GPS buoys have been lost and position data of 72 floes are still obtained.

Size of the DN around the CO is about 100 km by 100 km (Figure. 4.6.x?). Large scale deformation has been dominated by the shearing but overall shape and positions of individual drifters of the DN has remained rather same.

Fig.4.6.7: The locations of the GPS buoys, deployed from Akademik Fedorov and Polarstern, at 12:00 3 December 2019.

Fig.4.6.8: Locations of the buoy array within the MOSAiC DN on 20 Oct. 11 Nov. and 3 Dec. 2019, respectively.

Data management

All data are handled, documented, archived and published following the MOSAiC data policy (see APPENDIX). Original ice radar, stress gauges, stress panels and seismic data have been uploaded to the MOSAiC Central Data Storage. Other collected data will be provided to the MCS later. Final processed data sets will made available via the workspace section of MCS. Final data products will further be stored at the PANGAEA data repository (World Data Center PANGAEA Data Publisher for Earth & Environmental Science (www.pangaea.de)).

References

Lensu M, Elder BC, Ricther-Menge J, Haapala J (2013), Comparison of ice stress records in terms of extreme value analysis. Annals of Glaciology, 54(62), doi:10.3189/2013AoG62A194.

Oikkonen A, Haapala J, Lensu M, Karvonen J, Itkin P (2017), Small-scale sea ice deformation during N-ICE2015: From compact pack ice to marginal ice zone, J. Geophys. Res. Oceans, 122, 5105–5120, doi:10.1002/2016JC012387.

4.7 Sea ice and water properties based on ROV surveys

Ilkka Matero[1], Marcel Nicolaus[1], Julia Regnery[1], Nicole Hildebrandt[1], Anders Svenson[2], Ian Raphael[3]

(Not on board:) Christian Katlein[1], Martin Schiller[1], Philipp Anhaus[1], Mats Granskog[4], Knut Vilhelm Høyland[5], Hauke Flores[1], Barbara Niehoff[1], Jutta Wollenburg[1]

[1]DE.AWI
[2]SE.SLU
[3]EDU.DARTMOUTH
[4]NO.NPOLAR
[5]NO.NTNU

Objectives

The research to be supported with the Remotely Operated Vehicle (ROV) as part of MOSAiC can be split into four separate parts with individual objectives. Evaluating the length scales of variability and temporal evolution of studied parameters through different seasons are common for all four. Beyond studies of the widespread level first- and second year ice, a focus of the ROV work will be on new ice, leads, and pressure ridges and their evolution through the seasons.

1. The optics research aims to improve our understanding of the spatial and temporal variability of light transmittance through the snow-covered sea ice. Another aim is to quantify the contribution of snow and ice to light attenuation as distinct layers, and as a function of depth, including contributions of different ice types and stages of melt and freezing.
2. Surveys using an upward-looking bathymetric multibeam-sonar and a high precision altimeter are used to monitor the evolution of the ice bottom topography, which in combination with surface topography from terrestrial laser scans and aerial images will allow for monitoring the evolution of co-located snow-air- and ice-ocean interfaces.
3. Through lateral and vertical profiles, the ROV provides data on the spatio-temporal variability of a variety of physical and biological parameters in the water column.
4. Towing nets under the sea ice will allow for evaluating the gypsum distribution and the evolution of the zooplankton community structure at different depths.

On PS122/1, the foci of the ROV work was on objectives 2-4 and setting up the ROV site installations. The under-ice optics measurements were of secondary importance due to limited ambient light during polar night. Studies dedicated to the evolution of pressure ridges are to commence on subsequent legs.

Work at sea

There were 10 ROV dive days during PS122-1, with scientific data collected on 4 multibeam surveys, 12 zooplankton trawls and 2 gypsum net trawls. Timing and GPS positions of all ROV dives can be found in Appendix A describing the device operations under vehicle id “BEAST”. In addition to the measuring and sampling dives, dive time was allocated for testing the ROV system and improving the LBL (Long Baseline) positioning setup. The ROV team also assisted other tasks by deploying a rope under ice to allow for an installation of a fishing net, and spent one dive day gathering footage for documentation and outreach.

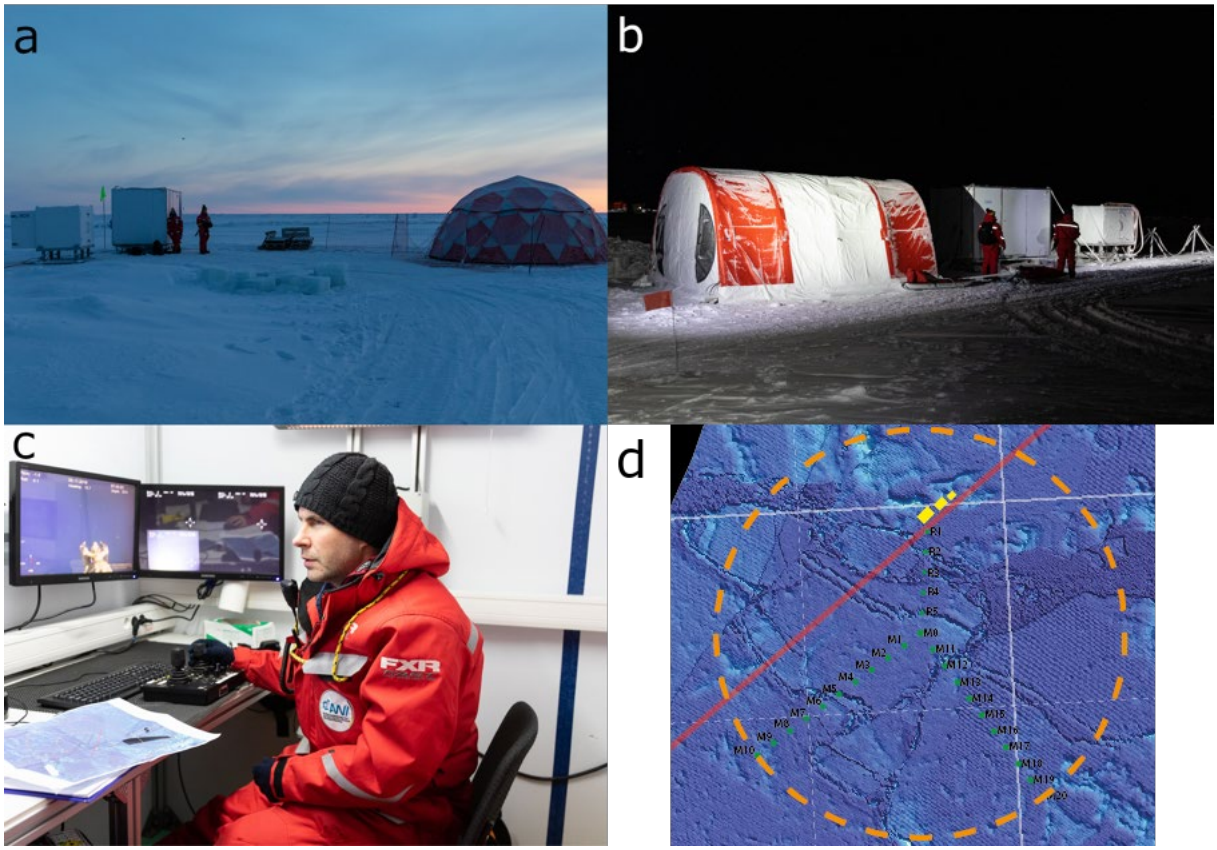

Fig.4.7.1: (a) First ROV site setup. (b) Second ROV site setup. (c) View inside the ROV control hut, with a controller using the control unit in the foreground and two of the screens with video feeds in the background. (d) Schematic of the setup at the second ROV site overlaid on a topography map based on airborne laser scanner (ALS) data. Grid marker locations are shown in green and labelled M0-M20, while locations labelled R1-R5 indicate where markers were installed to help navigation between the tent and the grid. The circled area shows a 100 m radius from the origin of the measurement grid, and the skidoo track is shown in red. The yellow rectangles denote the locations of the tent, control hut and power hub respectively from largest to smallest item. Photos and schematic by M. Nicolaus and I. Mattero, ALS topography map produced by S. Hendricks.

The first ROV site (called ROV Oasis, Figure 4.7.1a) was set up approximately 300 meters in front of bow of *Polarstern*, with the installations (Figure 4.7.1b) consisting of the ROV control hut (Figure 4.7.1c), a tent over the ice hole, a power hub and a power line. The ice hole was used to launch the vehicle (called 'Beast') and had a size of 1.5x1.5 m. The setup was finished on 18 October, but a shear event on 19 October interrupted starting scientific operations at this site. The part of the ice floe with the installations drifted approx. 600m towards to port side of *Polarstern* and underwent extensive ridging and cracking. In order to avoid loss of equipment, all the installations were retrieved after the dynamical phase ended and weather conditions stabilized.

The second ROV site (Figure 4.7.1b) was set up on a part of the ice floe that did not undergo deformation during the mid-October shear event, with the location approximately 250 m away from *Polarstern*. In addition to the first ROV site installations, a measurement grid was set up at this site after the installation of the infrastructure described in the previous paragraph. The grid consisted of 26 co-located markers on top and under ice and three transponders for the LBL positioning system. The grid installation (Figure 4.7.1d) consisted of two lines of markers at a 90 -degree angle, with 10 m spacing between the markers. In addition to the 21 markers that made up the measurement grid, 5 markers were installed between the ice hole and the origin of the measurement grid in order to aid navigation between the ice hole and the grid. Ice thickness, snow depth and freeboard measurements were done at the time of deployment at all marker locations. A second shear event on 17 and 18 November resulted in the relocation

of the ice floe with the ROV site in relation to *Polarstern*, temporarily cutting the power from the site and necessitating rebuilding the power line.

The ROV (Figure 4.7.2) is a purpose-built measurement platform based on the M500 model (Ocean Modules) [1]. A set of two RAMSES-ACC-VIS (TriOs GmbH) spectroradiometers are used for the optics measurements, with one of the sensors mounted on the ROV, and the other one set up for synchronous measurement of apparent light above the surface. A DT101 multibeam sonar (Imagenex) and a PA500 altimeter (Tritech) are used for studying the evolution of the under-ice topography. For a description of the tow nets (Figure 4.7.2b) see Section 6.2. The ROV platform also includes 3 video cameras, a still camera and a suite of sensors measuring the following parameters: radiance, conductivity, temperature, dissolved Oxygen concentration, pH, Nitrate, Chlorophyll-a, CDOM and backscatter. A full description of the measurement setup is available in Katlein *et al.*, 2017.

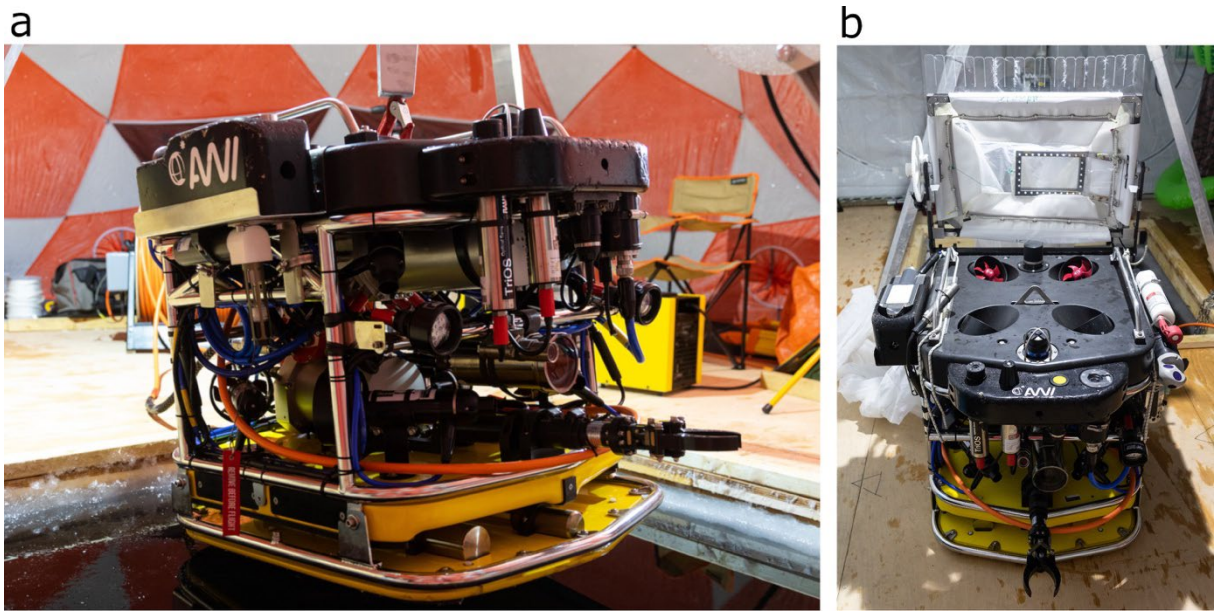

Fig.4.7.2: The M500 ROV "Beast" (Ocean Modules) (a) over the ice hole of the first ROV site; (b) with the gypsum and zooplankton nets attached. Photos by M. Nicolaus.

The ROV was operated with a team of 3 people. An additional person working as a polar bear guard completed the team and brought the total number of people on these operations to 4. During deployment and start of each dive, two team members were working in the tent, and one person inside the hut. The scientists in the tent were responsible of inspecting the ROV and e.g. potential adjustments to cameras or mounting the nets or CTD sensors. The person inside the hut took care of setting up the software and verifying ROV controls and data/video streams working as intended. During the dives one person took care of the tether inside the tent, and the two people in the hut were responsible for controlling the vehicle and scientific coordination of the dive. At the end of each dive the ROV was dived back to the ice hole, the tether wound back on its drum and the ROV was left hanging underwater. This method of storing the ROV in the water when not being operated was chosen to avoid big temperature fluctuations, which could have compromised the underwater connectors and sensors.

In general the ROV work was carried out according to the plan, but few practical issues during the leg resulted in a reduced total number of dive days. The highly dynamic sea ice proved to be a major challenge due to separating the ROV sites from power and partially burying power cables inside pressure ridges. This resulted in part of the planned dives having to be cancelled due to the time being required for re-establishing the power connection to the site. Running the ROV site is possible on generator power, and having a fixed power connection to *Polarstern* was not a strict requirement for scientific operations. Two dive days were operated

on generator power, and while possible, running the site in this fashion was inconvenient compared to the power being connected from the vessel. This was due to the need to refuel the generators and the setup being less well-equipped for dealing with spikes in power consumption. Environmental conditions were another challenge, with a total of 3 dive days cancelled due to storms and poor visibility and one due to a polar bear entering the Central Observatory.

Preliminary results

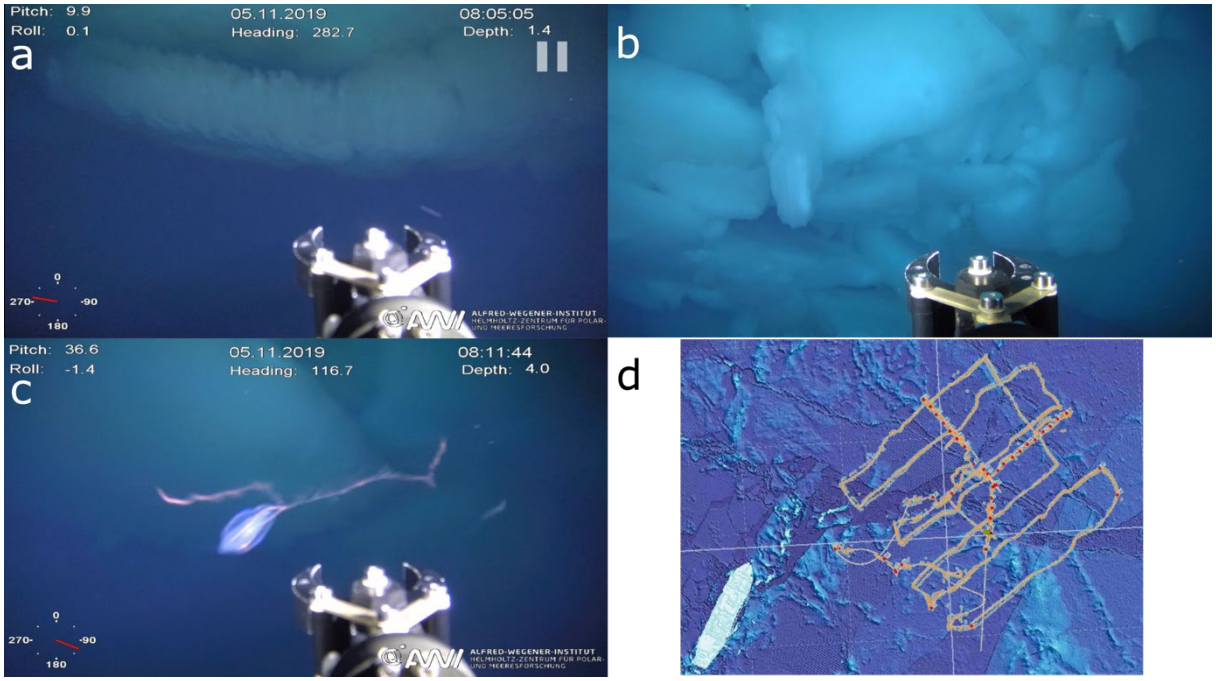

Fig.4.7.3: Dive footage from the HD video camera (panels a-c) and dive track (d) from 5 November. The manipulator arm of the ROV is visible in the foreground of panels a-c. (a) 2-layer structure commonly found on the floe that the second ROV site was set up on, with a rotten honeycomb -like ice layer underlying a denser ice layer. (b) Rafted ice blocks showing the keel of a pressure ridge. (c) Example of the fauna observed under ice, jellyfish with tentacles. (d) Dive track of a multibeam sonar survey showing a "mow-the-lawn" -pattern covering an area of roughly 200x200 m. The track is overlaid on a topography map based on Airborne Laser Scanner data by S. Hendricks, with the white shaded object in the bottom left corner indicating the position of Polarstern.

This was the first time that the ROV was used with a separate control hut, tent and power line. The hut provided a shelter for operations, allowed for more space in the tent and limited water condensation on the electronics unit and screens due to being a separate space from the dive hole. The electricity being sourced to a separate ROV site from *Polarstern* via the power line for the first time proved to be convenient due to removing the need for refuelling generators and providing a more stable power supply than the generators. The novel setup proved effective and comfortable, and is recommended for future operations when possible.

Visibility under water was good due to low amount of suspended matter and biota in the water, and individual markers with reflector tape were visible up to a distance of approx. 20 meters. Of the biota, jellyfish (Figure 4.7.3c), Arctic Cod and zooplankton were the most commonly identified specimen.

The LBL positioning system provided a reliable position when diving at depths greater than the transponder depths. The transponders were installed at a depth of 5 m, and the positioning worked up to a distance of approximately 150 m from the measurement grid. When diving in the proximity of the ice bottom, the positioning system typically did not work due to keels of

pressure ridges obstructing the signal path between the ROV and the transponders. One drawback experienced with the positioning system was that only a configuration of three transponders worked on the dives. When adding additional transponders to the setup, the software failed in providing positions, even though the number of transponders is supposedly not limited to three.

Getting a stable heading from the compass of the ROV was problematic, which is a well-known challenge when operating at latitudes close to the Magnetic Pole. This manifested as the heading randomly jumping to a new value roughly in time intervals of minutes. The way to work around this problem was to follow the changes in the position on the dive track, and using the apparent heading for calibrating the heading value.

The ice floe of second ROV site mainly comprised of ice that had survived the summer melt with other distinct ice types in reach. Two ridges were located inside the measurement grid area and newly formed ice was within reach of the ROV in a refrozen lead (dark part off the starboard side of the bow of *Polarstern* in Figure 4.7.3d). The old ice was observed to have a two-layer honeycomb structure in multiple places, with old rotten ice underneath and a younger ice layer on top (Figure 4.7.3a). The average initial ice thickness at the second ROV site was 53 cm with a standard deviation of 17 cm. This was measured at the marker locations at the time of setup (Figure 4.7.1d), excluding pressure ridges and rafted ice. The ice floe experienced deformation over time due to ice dynamics; particularly during the storm event on 16-18 November when also the part of the floe including the new ice area got deformed and consolidated into a rubble field (Figure 4.7.3b).

The average initial snow depth in the measurement grid area was 6 cm with a standard deviation of 3 cm (ridges excluded), as measured at the marker locations (Figure 4.7.1d). Significant snow accumulation with high spatial variability was observed at the ROV site over the measurement period, with an estimated increase of up to 50 cm in snow depth associated with individual snow dunes, sastrugis and close vicinity of pressure ridges. Initial plan was to use data from the terrestrial laser scanner (section 4.2) and stakes projects (section 4.3), but quantitative data of the snow accumulation at the site is not available due to the high workload related to installation and reinstallation of infrastructure limiting the availability of time for monitoring the snow conditions. Near-weekly measurements of the snow properties were however carried out approx. 200-400 m away at the nearby ‘Snow1’ site (REFERENCE TO MAP), which provide the most representative data also for the ROV site (section 4.2) as the ‘Snow1’ and ROV sites was setup on same part of the ice floe.

The following addresses the objectives 2-4 outlined in the first part of this section. The ice optics study (objective 1) is planned to commence towards the end of the polar night, when ambient light levels approach detectable levels under ice.

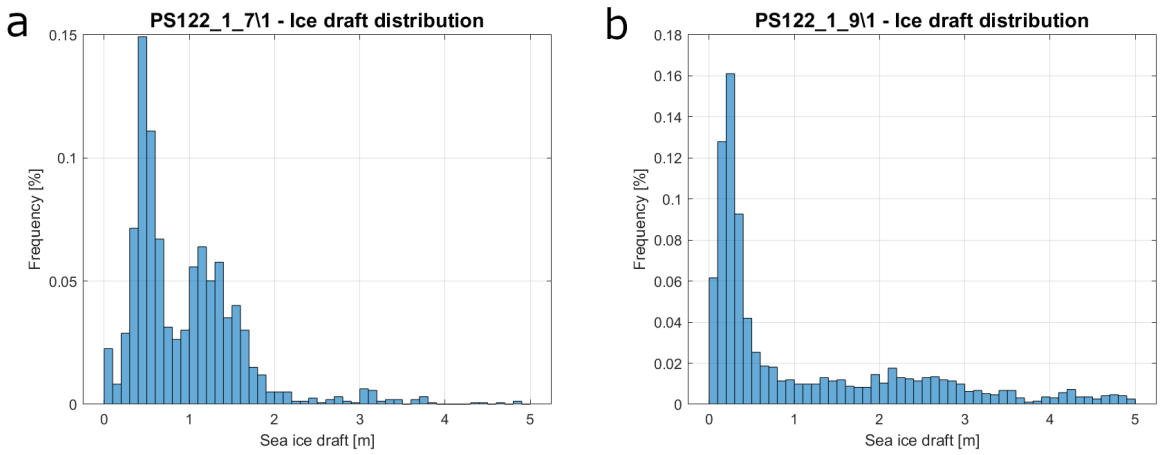

Fig.4.7.4: Altimeter -based ice draft distribution from two multibeam surveys done on (a) 12 November and (b) 26 November 2019.

The multibeam sonar data is being processed at the time of writing this report, and the preliminary results shown here (Figure 4.7.4) on the ice bottom topography evolution (objective 2) are based on altimeter data. The above histograms show ice draft (difference between ice bottom and water level), which is used here as a proxy for ice thickness. The major event of Leg 1, the mid-November storm, took place between the two dives shown here.

The data seems to indicate that the thermodynamic growth during this period would have had a smaller contribution in altering the ice thickness than ice dynamics. The fraction of ice thicker than 2 m is bigger after the dynamic event, which was an expected feature due to the ridging and rafting observed on the surface. Considering the thermodynamical growth, the modal peak is actually for thinner ice (20-30 cm) on 26 November than on 12 November (40-50 cm). This is likely a result from the altimeter data from these two dives not being directly comparable, and the ROV being under a thinner section of the floe for a larger fraction of the dive. The sensor takes point measurements of the ice that is directly above the sensor, and the variability of the dive track together with varying pitch, roll and dive velocity result in the measured points not being the same between dives.

See Section 6.2 for preliminary results from the net trawls (Objective 4).

Data management

All data are handled, documented, archived and published following the MOSAiC data policy (see APPENDIX). Data recorded on the dives on PS122/1 is stored in the Mosaic Central Storage in the “exdata” folder under the vehicle id “BEAST”. The dive data is stored in separate folders for each device operation (Appendix A).

Final data products will be stored at the PANGAEA data repository (World Data Center PANGAEA Data Publisher for Earth & Environmental Science (www.pangaea.de)).

References

Katlein C, Schiller M, Belter HJ, Coppolaro V, Wenslandt D and Nicolaus M (2017) A New Remotely Operated Sensor Platform for Interdisciplinary Observations under Sea Ice, Frontiers in Marine Science, 4(281), doi:10.3389/fmars.2017.00281

4.8 Airborne Sea Ice Surveys (HELI)

Stefan Hendricks[1], Gunnar Spreen[2] [1]DE.AWI
(not on board:) Gerit Birnbaum[1], Niels Fuchs[1] [2]DE.UNI-Bremen

Objectives

The primary objective of the airborne sea ice surveys (HELI task) is to connect the localized observations of physical sea ice properties to the regional scale within the DN. The flights serve the purposes of assessing the representativeness of observations at the CO, extend the spatial coverage of comparable in-situ observation and to measure geophysical parameters accessible only to airborne sensors. In addition, airborne surveys also deliver observations at an intermediate scale between in-situ measurements and the spatial coverage and resolution of satellite remote sensing. The helicopter observations are therefore providing ground-truth at a higher spatial resolution than achieved by satellite remote sensing to assess the impact of sub-footprint scale variability of the ice surface on the satellite retrievals. The main geophysical parameters for the satellite ground-truth are snow freeboard, the height of the air/snow surface above sea level, and the surface temperature of different ice types. At the same time, these parameters are needed to assess the surface energy budget and moment transfer in the atmosphere/ice/ocean system and relevant for corresponding process studies. Lead and ridge distributions as well as ice type information can be retrieved from the combined measurements.

Due to the fact that the main observation period of MOSAiC leg 1 is situated in polar winter with night-flight conditions, complementing observations such as surface albedo and sea-ice thickness have not been possible, except for a brief period in the beginning.

The main research questions can be summarized as:

1. What is the spatial distribution of snow freeboard and surface roughness within the DN? How does these parameters evolve with the thermodynamic and dynamic forcing in early winter?
2. What is the surface roughness downwind of the meteorological installation at the CO?
3. How does the sea ice surface deform in response to storms and other dynamic forcing?
4. How does snow precipitation and snow redistribution by wind change the snow freeboard distribution?
5. How does the surface temperature of different ice classes (classified by their snow freeboard) change during the early winter?
6. How does the lead distribution (open water and thin ice leads) change through winter?
7. What is the initial ice thickness distribution inside the DN at the start of the MOSAiC drift?
8. What is the distribution of surface albedo in the distributed network after the summer melt and during onset of the freezing season?

Work at sea

Sensors

Airborne sea ice surveys on MOSAiC leg 1 were implemented as a specific mission type with a fixed sensor installation in one (D-HARK) of the two helicopters onboard *Polarstern*. The main installation consisting of an airborne laser scanner (ALS), nadir infrared camera, distribution of power and network as well as the main data acquisition systems were located in the rear baggage compartment (Figure 4.8.1). Further downward-looking sensors (wide-

angle camera, KT19 surface temperature sensor) were located in the belly of the helicopter. All sensors were operated from the cabin with a single display and keyboard/mouse that could connect to different industrial (ebox) PC's in the baggage compartment. Two GoPros for inflight-documentation were mounted on the forward section of the skit on both sides. An overview of the sensors is provided in Table 4.8.1. All sensors were controlled by two operators during flight.

Data acquisition with the nadir-looking camera was stopped with the onset of polar night after Oct. 20, 2019. Similarly, the external GoPros were removed from the list of active sensors after it became clear that the GoPro were unable to operate in polar winter even on external power and heating. Tests of the general data acquisition system for scientific aircraft (DMS) were completed in the beginning of leg 1 to verify system readiness for later legs. After successful tests, the sensor setup for the polar winter surveys consisted of the ALS and IR-CAM only. This implicitly includes the Applanix Inertial Navigation System (INS) that constated of a gyro compass coupled with two GPS receivers of the helicopter and which was integrated into the control unit of the ALS. Data from the INS/GPS was collected during each flight and logged as specific sensor operation.

Mission Types

Two main mission modes emerged during leg 1 in response to the scientific and operational requirements for sea ice surveys during polar night:

1. Grid surveys following a mow-the-lawn pattern centered over the CO with a target side-length of 5 km.
2. Surveys using the three L-sites in the DN as waypoints including the sides and the spokes (connection between *Polarstern* and L-Site) within three triangles.

The target schedule was set to one survey per week, alternating between the two mission types. In practice, the grid surveys close to *Polarstern* were more common in response to demand for up-to-date topographic maps of the CO and limitation of the helicopter range in unstable flight conditions. The total amount of 10 flights (Table 4.8.2) in the period between September 28 and December 6, 2019 is therefore distributed to 1 test flight during the transit of *Polarstern*, 6 CO grid surveys and 3 L-site surveys.

Exemplary flight patterns are displayed in Figure 4.8.2. In practice, there was no possibility for in-flight correction of ice drift and surveys were flown either with the visual reference of *Polarstern* for the CO grid surveys, or by a mix of pre-defined waypoints from real-time buoy data and activated landing site illumination in case of the L-Site surveys. All survey lines were flown at an altitude above ground of 1000 ft due to restrictions for helicopter operations in the polar night. In a few cases, landing lights were replaced at the L-Sites on the end of a sea ice survey flight.

Preliminary (expected) results

A workflow for quick-view processing was implemented onboard for quality control of all data sets and initial scientific analysis.

Airborne Laserscanner

In the case of the ALS this required a processing of the inertial navigation data. This step usually includes differential GPS processing with the precise ephemerides of the GPS satellites in question. But since there was no practicable way to facilitate a download request from *Polarstern*, only a Kalman Filter was applied on the separate data of the INS and two GPS receivers, resulting in a joint solution for position and attitude (pitch, roll and true heading) of the aircraft. This information was used in the next step of the workflow to transform the ALS

range measurements into a point cloud of ellipsoidal surface elevations. These points clouds were projected on a space-time grid with a resolution of 25 cm in segments of 30 segments. These segments were correct with filters for biases in the GPS height of the joint INS/GPS solution. In case of the CO grid surveys the segments were merged into a full spatial grid of the entire flight delineating location of different ice types and high spatial resolution and coverage. The result was made available in geotiff and netCDF formats as well as a plotted map. Figure 4.8.3 show a subset of such a map, which has been used as a basis for selection of measurement sites and general science planning in all stages of leg 1.

The processing workflow after the cruise will include final inertial processing and elevations referenced to the instantaneous sea surface height. In case of the CO grids, sea ice drift correction will be applied on a per-points basis and the coordinates will be transformed into the ice coordinate system provided by the FloeNavi, yielding a time series of freeboard and roughness in both global and local coordinate systems.

IR-Camera

The Infratec VarioCAM HD head 680 is set to record infrared brightness temperatures (7.5–14 µm) at 2 Hz during the 1000 ft altitude survey flights. Raw data is recorded in camera specific IRB files together with simple GPS positions. After the flights these files are converted to one netCDF file per flight. Post-processing after the expedition will use the INS data to create georeferenced and viewing-geometry corrected datasets. Finally, the dataset will be brought in the same coordinate system as the ALS data to allow joint analysis of the two datasets. Figure 4.8.4 shows an example for the flight on 30 November 2019 of the infrared data converted to physical temperature assuming a constant emissivity. The images were stitched together manually and are not fully geometrically corrected yet. The fresh crack in front of *Polarstern* is visible as well as older cracks with thin ice in the surrounding. Mind that also deformation features like ridges are identifiable by the change of snow surface temperature.

Nadir Camera

The raw images from the nadir camera will corrected for distortion and vignette and the geo-referenced on a per-pixel basis. The frequency of image acquisitions allows to produce a swath of overlapping photos along the helicopter ground track. An example is shown in Figure 4.8.5. The accuracy of the resulting surface albedo information in the low-light conditions will be evaluated after the expedition.

Data management

All data are handled, documented, archived and published following the MOSAiC data policy (see APPENDIX). All device operations were logged in the AWI sensorweb portal and all sensor raw data files are stored in platform section of MCS. Final geophysical parameters will be made available via the workspace section of MCS. Final data products will further be stored at the PANGAEA data repository (World Data Center PANGAEA Data Publisher for Earth & Environmental Science (www.pangaea.de)). Data from the data acquisition system of Polar Research Aircraft (DMS) can be accessed after registration at https://dship.awi.de/exportdisplay/.

References

No references

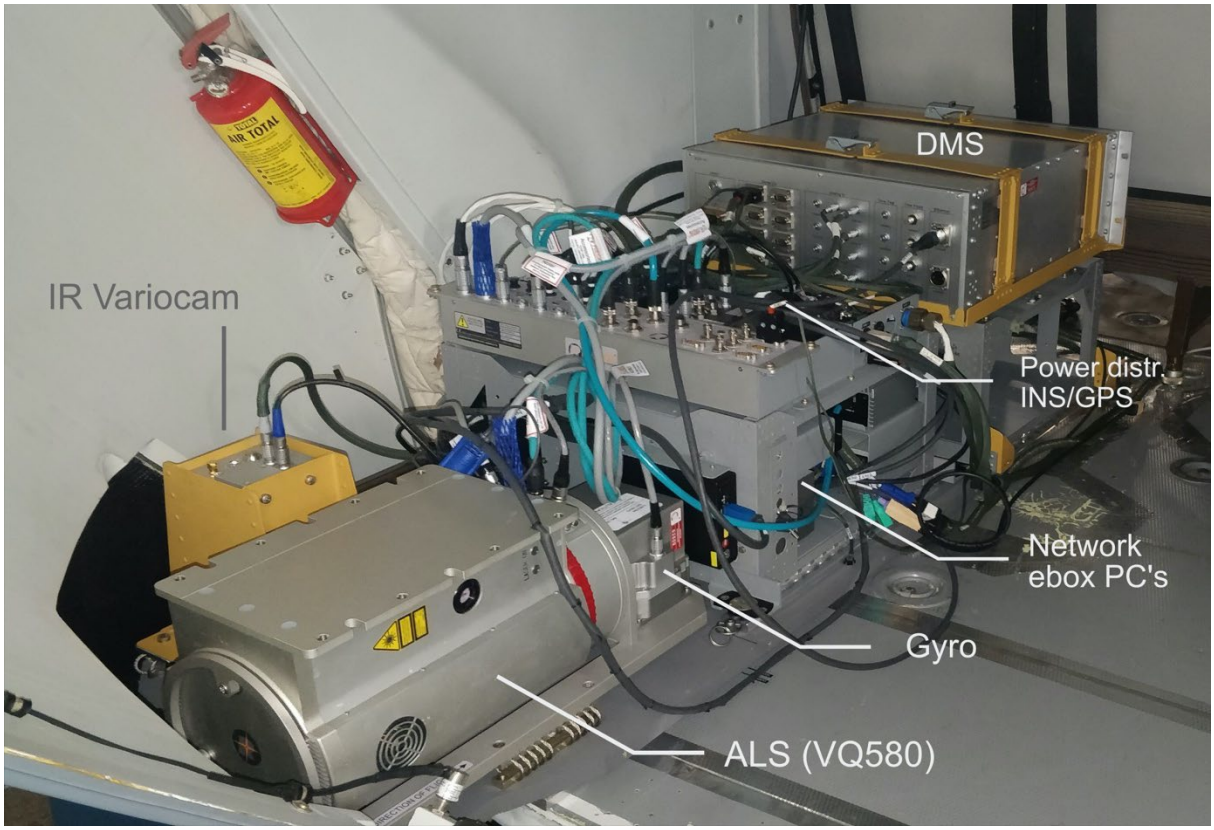

Fig.4.8.1: Sensor installation in the rear baggage compartment of the helicopter (D-HARK) housing the ALS, IR camera, power distribution, network and data acquisition systems (ebox PC's and DMS). Not on photo: GoPros (mounted on skid) and KT19, nadir camera (mounted below belly panel).

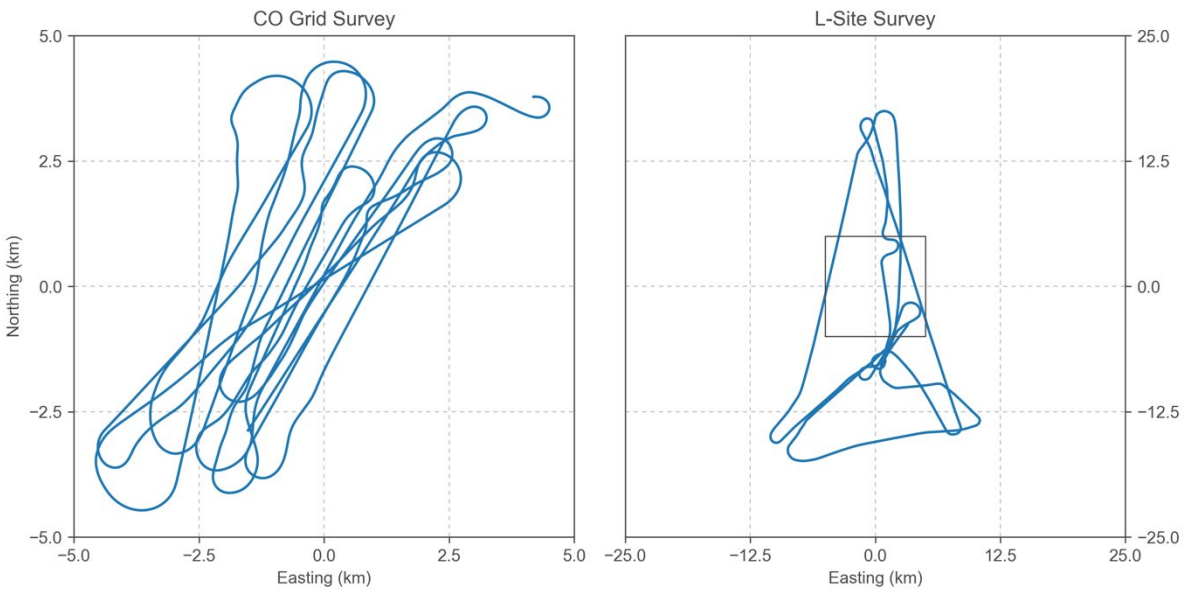

Fig.4.8.2: Example flight lines for the two main sea-ice mission types: (left) Grid survey of the CO close to Polarstern and (right) L-Site survey in the DN. Square in right panel marks the spatial extent of the panel on the left.

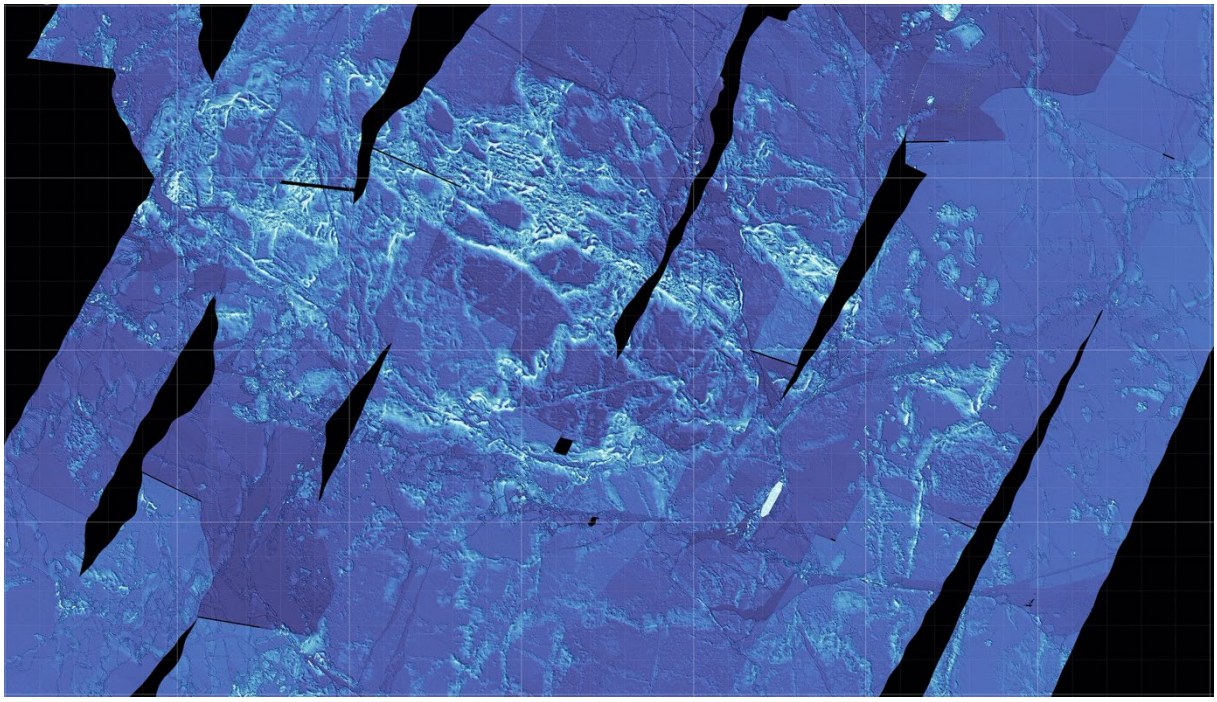

Fig.4.8.3: Gridded surface elevations from CO grid survey of Oct. 20, 2019 at a resolution of 25 cm from ALS quick-view products. The figure shows an area of 3.5km times 2km near Polarstern, which is visible in lower right of it.

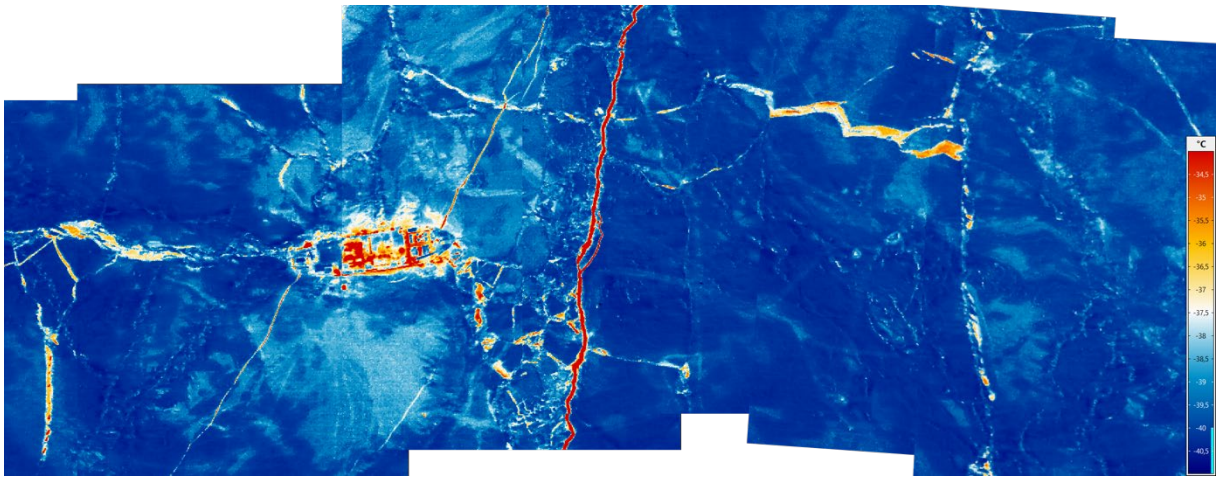

Fig.4.8.4: Sequence (down-sampled) of infrared temperature images acquired around Polarstern on 30 November 2019.

Fig.4.8.5: Example of aerial photography with wide-angle camera. Example shows Polarstern overflight on Oct. 20, 2019 stitched from three consecutive acquisitions.

Tab.4.8.1: Overview of sensors used for the airborne sea-ice surveys

Sensor	Description	Device URN	Geophysical Parameter
ALS	Airborne Laserscanner (Riegl VQ580)	aircraft:heli-ps:riegl-vq580-s9999057	Surface elevation, freeboard and roughness
IR Variocam HD head 680	Nadir Infrared-Camera	aircraft:heli-ps:ir_variocam_02	Surface temperature distribution
KT19	Heitronics Pyrometer KT19	aircraft:heli-ps:radtherm_kt19_heli	Surface temperature
WA-CAM	Wide-angle nadir camera (EOS1DMkI 14mm)	aircraft:heli-ps:rgbcam_wal_heli	Surface albedo
GoPro left	GoPro Hero 6	aircraft:heli-ps:goprolh_heli	Documentation
GoPro right	GoPro Hero 6	aircraft:heli-ps:goprorh_heli	Documentation

Tab.4.8.2: Overview of all helicopter sea ice surveys from *Polarstern* during PS122/1. (TO and LDG designate take-off and landing times in UTC respectively)

Flight ID	Device Operation	TO	LDG	Aircraft	Sensors	Mission Type
20190928_01	PS122/1_2-45	03:48	04:40	D-HARK	ALS, IR, CAM, GoPro, KT19	Test Flight
20191002_01	PS122/1_2-57	05:45	06:57	D-HARK	ALS, IR, CAM, GoPro, KT19	CO floe grid
20191020_01	PS122/1_2-167	01:02	02:20	D-HARK	ALS, IR, CAM, GoPro, KT19	CO floe grid
20191029_01	PS122/1_5-9	02:02	03:32	D-HARK	ALS, IR	L-Site survey
20191105_01	PS122/1_6-11	06:30	07:33	D-HARK	ALS, IR	CO floe grid
20191112_01	PS122/1_7-24	07:57	09:29	D-HARK	ALS, IR	L-Site survey
20191112_02	PS122/1_7-25	10:25	11:58	D-HARK	ALS, IR	CO floe grid
20191119_01	PS122/1_8-23	04:00	05:20	D-HARK	ALS, IR	CO floe grid
20191130_01	PS122/1_9-98	04:38	06:01	D-HARK	ALS, IR	CO floe grid
20191206_01	PS122/1_10-78	06:56	08:29	D-HARK	ALS, IR	L-Site survey

4.9 Remote Sensing Measurements On-ice and Onboard *Polarstern*

Gunnar Spreen[1], Oguz Demir[4], Stefan Hendricks[7], Nathan Kurtz[8], Ruibo Lei[9]

(not on board:) Estel Cardellach[2], Tania Casal[3], Claude R. Duguay[5], Friederike Fohlmeister[6], Carolina Gabarró[2], Steen Savstrup Kristensen[10], Randy K. Scharien[11], Mike Schwank[12], Maximilian Semmling[13], Julienne Stroeve[14,15], Wei Wan[16], John Yackel[17], Joel Johnson[4]

[1]DE.UNI-Bremen
[2]ES.ICM-CSIC
[3]INT.ESA
[4]EDU.OSU
[5]CA.UWaterloo
[6]DE.DLR
[7]DE.AWI
[8]GOV.NASA
[9]CN.PRIC
[10]DK.DTU
[11]CA.UVICTORIA
[12]CH.WSL
[13]DE.GFZ
[14]COM.UCL
[15]CA.UMANITOBA
[16]CN.PKU
[17]CA.UCALGAR

Objectives

Satellite remote sensing is the ideal tool to obtain Arctic-wide and long-term observation of the sea ice cover, ocean, and the atmosphere above. Remote sensing datasets can be used to extend the local MOSAiC observations to a larger scale and set them in context with preceding environmental conditions, like the history of the ice floes MOSAiC will be established on.

MOSAiC provides ideal conditions for validation of satellite remote sensing observations: (a) it is a rare case to observe the complete seasonal cycle. Especially winter observations from the central Arctic are basically absent. (b) The MOSAiC concept to not only have one central measurement site but a distributed grid of measurements that cover the typical satellite footprint scales make meaningful comparisons feasible. (c) Furthermore, the combined MOSAiC airborne campaigns will allow to bridge the gap between in situ and satellite observations.

One scientific goal of MOSAiC for remote sensing is the ground validation of satellite products and to develop new method to retrieve improved sea ice parameters from satellites. Research questions for leg 1 are:

- How well do satellite algorithms perform in the Central Arctic for parameters such as sea ice thickness distribution, snow depth, ice type, floe sizes, ice concentration, and ice drift and deformation?
- Can co-located ground-based sea ice/snow and microwave measurements help to develop improved satellite retrieval methods for ice area, thickness, type, and snow depth?
- What is the prospect to retrieve additional physical parameters with satellite remote sensing to expand the observational capability of processes at the ice/atmosphere interface like surface roughness?

Most observed changes of the Arctic climate system are based on results from satellite remote sensing, which is one of the most important and reliable tools for Arctic monitoring. However, most satellites do not directly measure the geophysical parameters that are needed for research and monitoring. Sea ice concentrations, for example, are typically derived from passive microwave brightness temperatures or high-resolution radar images. Both methods make use of the characteristic difference between surface properties of open water and sea ice, which can be complicated by a variety of seasonal and conditional factors. Sea ice thickness is derived from microwave brightness temperature (thin ice) or from altimeters. Altimeters measure the ice or snow freeboard, which is then converted to ice thickness based on critical assumptions on snow depth and snow/ice densities. Continuous development of methods and algorithms to analyze satellite measurements is necessary to improve observational capabilities, reduce uncertainties, and ensure consistency of satellite data sets.

Work at sea

Several remote sensing (RS) instruments were operated on the ice and from the ship in the Central Observatory. Table 4.9.1 gives an overview about all instruments and the responsible PI on land and during leg 1. Many more people are involved with the measurements.

Measurements are used for satellite remote sensing validation and the development of new remote sensing methods. All measurements will be taken either quasi-continuously or with at least weekly repetition to fully cover the complete seasonal cycle from winter, spring, to summer. Two remote sensing sites were established during leg 1. A log of all activities at the two remote sensing sites can be found in Table 4.9.15 at the end of this section.

Tab.4.9.1: List of remote sensing instruments in the Central Observatory

Instrument	Details	PI	Institution	Leg 1 responsible
On the ice				
Ku/Ka-band radar	Dual-frequency scanning radar: 12-18 GHz (Ku) and 30-40 GHz (Ka)	J. Stroeve	U Manitoba	S. Hendricks

L-band Scatterometer	1.26 GHz scanning radar	R. Scharien	U. Victoria	G. Spreen
C-band Scatterometer	C-band (~5 GHz) scanning radar	J. Yackel	U Calgary	G. Spreen
X-band Scatterometer	9.6 GHz scanning radar	C. Duguay	U Waterloo	G. Spreen
MW Radiometer UWBRAD	Ultra-wideband 0.5 – 2 GHz radiometer (P to L-band)	J. Johnson	Ohio State University	O. Demir
MW Radiometer ELBARA	1.4 GHz (L-band)	M. Schwank/ T. Casal	WSL/ESA	G. Spreen
MW Radiometer 19-37-89-GHz	19, 37, 89 GHz (K, Ka, W-band)	J. Stroeve	U Manitoba	G. Spreen
MW Radiometer Balamis ARIEL	1.4 GHz (L-band)	C. Gabarro	ICM-CSIC	G. Spreen
GNSS-R	reflected GNSS signals from snow/ice	E. Cardellach/ T. Casal	ICE-CSIC/ESA	G. Spreen
Infrared Camera	Surface temperature	G. Spreen	U Bremen	G. Spreen
Video Camera	Visual overview of RS site	G. Spreen	U Bremen	G. Spreen
On *Polarstern*				
GNSS-R	reflected GNSS signals from snow/ice	W. Wan	Peking U.	R. Lei
GNSS-R & atmosphere	reflected GNSS signals from snow/ice and GNSS for atmospheric water vapor	M. Semmling	GFZ	G. Spreen
GNSS Ionosphere	Ionospheric scintillations for GNSS measurements	F. Fohlmeister	DLR	G. Spreen
MW Radiometer EMIRAD2	1.4 GHz (L-band)	S. Savstrup Kristensen/ T. Casal	DTU/ESA	G. Spreen

Remote Sensing Site 1 (18.10. to 16.11.2019)

Measurements at Remote Sensing Site 1 started on 18 October 2019 with the installation of the Ku/Ka radar. More and more instruments were then installed in the following days and weeks. See the tables in the Instruments subsection for a list of measurement durations for each instrument. Figure 4.9.1 shows the layout of the site on 10 November 2019 with the surface topography from airborne laser scanning (ALS, Section 4.8) in the background. The photos in Figure 4.9.2 give an overview of the RS1 site. All instruments look at a homogenous ice area with similar properties typical for the southern part of the floe at that time: second year (or remnant) ice with a dominant fraction (>60%) of melted-through melt ponds. The new ice in the melt pond areas have in most cases first-year ice properties (subsection Ice Cores) and

will be referred to as FYI here. Typical ice thickness at the beginning of November for the dominant level ice in the footprints of remote sensing instruments was 60±5 cm. However, some thicker remnant ice could also be present. The thicker ridges/rafted areas, the instruments were deployed on, had a thickness of about 2 m. Snow depth was 10±5 cm for the level ice areas (all measurements from thermistor chain deployments). On 16 November 2019 cracks appeared at the site and parts of the ice got depressed. All measurements (beside IR/web camera) stopped and instruments were retreated closer to the remote sensing hut. In the following days more and more cracks appeared, which later partly ridged, and this part of the floe got sheared away about 500 m towards the port side of *Polarstern*. The former measurement area got first flooded and later completely destroyed. On 23 November opportunistic ARIEL L-band radiometer, Ku/Ka-band radar, and IR camera measurements were taken at one of the cracks covered with thin ice and frost flowers. On 26 November all instruments and the hut were moved to the new Remote Sensing Site 2.

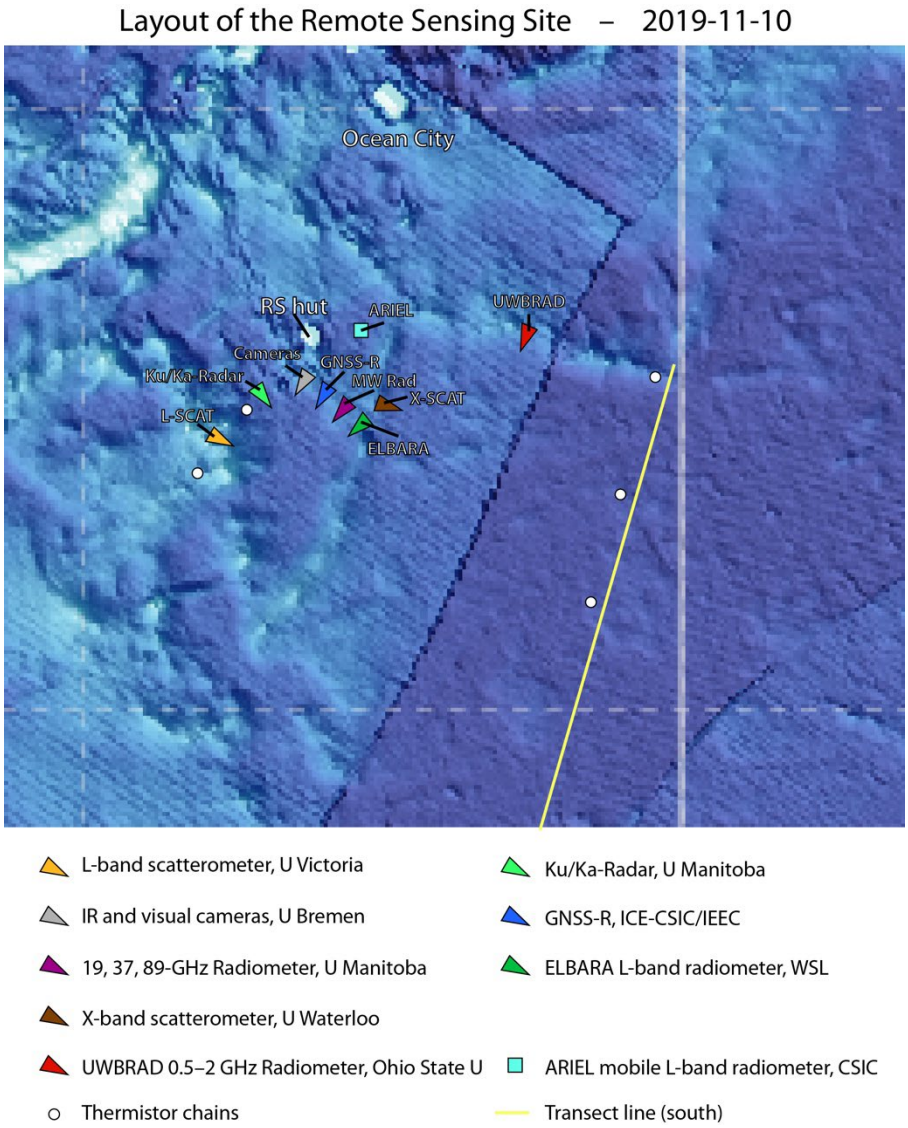

Fig.4.9.1: The map shows the status of the Remote Sensing Site 1 on 10 November 2019 with the ALS surface topography map from 20 October 2019 as background.

Fig.4.9.2: Remote Sensing Site on 2. November 2019. Left image from left to right: a) ELBARA L-band microwave radiometer (WSL), b) 19-37-89-GHz microwave radiometer (U Manitoba), c) GNSS-R (ICE-CSIC/IEEC), Infrared and visual cameras (U Bremen), d) Ku/Ka-band radar (U Manitoba), e) L-band scatterometer (U Victoria). The sled for the mobile ARIEL L-band radiometer can be seen on the right side of the remote sensing hut. The right image shows the same instruments from the opposite point of view. In the back the UWBRAD 0.5–2 GHz radiometer (Ohio State U) can be seen (photos: Stefan Hendricks).

Remote Sensing Site 2 (start: 29.11.2019)

After the relocation of the RS hut and all instruments on 26 November and re-establishing power on 28 November the first measurements at the Remote Sensing Site 2 started on 29 November. The full set of instruments (besides X-SCAT) was operational again on 10 December 2019. This includes now the UWBRAD radiometer in addition to the ELBARA, 19-37-89 GHz, and ARIEL (for transects) radiometers, the L-band, C-band, and Ku/Ka-band radars, the GNSS-R instrument and the IR/web cameras. Figure 4.9.3 shows a map of the site on 12 December 2019 with the ALS surface topography from 6 December in the background, the photo in Figure 4.9.4 gives an overview of the site layout.

The ice and snow properties at RS2 site are similar to the ones at RS1 site. Because of the vicinity of more ridges the snow depth was slightly higher. The ice thickness of the level ice was 70–80 cm at the beginning of December (from initial drillings and thermistor chain deployments). Snow depth was about 9±5 cm for the level ice. However, increased snow fall and wind in the first week of December caused snow dunes to build up behind some of the instruments. They can be seen in Figure 4.9.3. Luckily the south-western wind deposited most of the snow outside the measurement field. Still this event increased snow depth for the snow dune areas while the snow depth on the level ice even slightly (~2 cm) decreased. This results in a mean snow depth of 18±9 cm along the RS instruments on 10 December 2019 (all from ruler stick measurements and thermistor chain deployments).

On Friday the 13 December, the day of the arrival of Kapitan Dranitsyn, again cracks appeared at the remote sensing site. By 14 December all instruments (besides the IR/web cameras) were retreated to the RS hut and measurements stopped. On 15 December the site was handed over to leg 2. By then the cracks started to freeze over and a small ridge build up at one of them. If the situation stayed stable as this leg 2 personnel planned to continue the measurements at Remote Sensing Site 2.

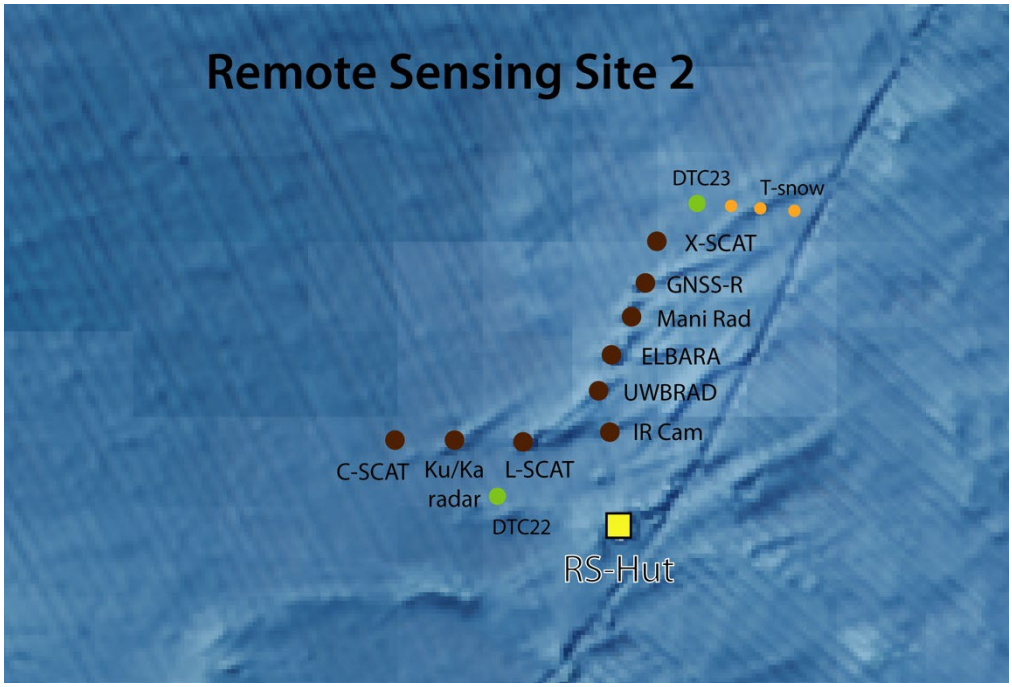

Fig.4.9.3: Map with the layout of the Remote Sensing Site 2 on 12 December 2019 with the ALS topography map from 6 December 2019 in the background.

Fig.4.9.4: Overview of the Remote Sensing Site 2 on 8 December 2019. From left to right: X-SCAT, GNSS-R, 19-37-89 GHz radiometer, IR/web cameras (in back), ELBARA, UWBRAD, L-SCAT, Ku/Ka radar, C-SCAT (photo: Stefan Hendricks).

Onboard Polarstern

All instruments onboard *Polarstern* were installed on the port side of upper and lower Peil deck, the highest deck of *Polarstern*. Figure 4.9.5 gives an overview of the installations. Processing and data recording units were installed in the observation alley in front of the meteorologist's office.

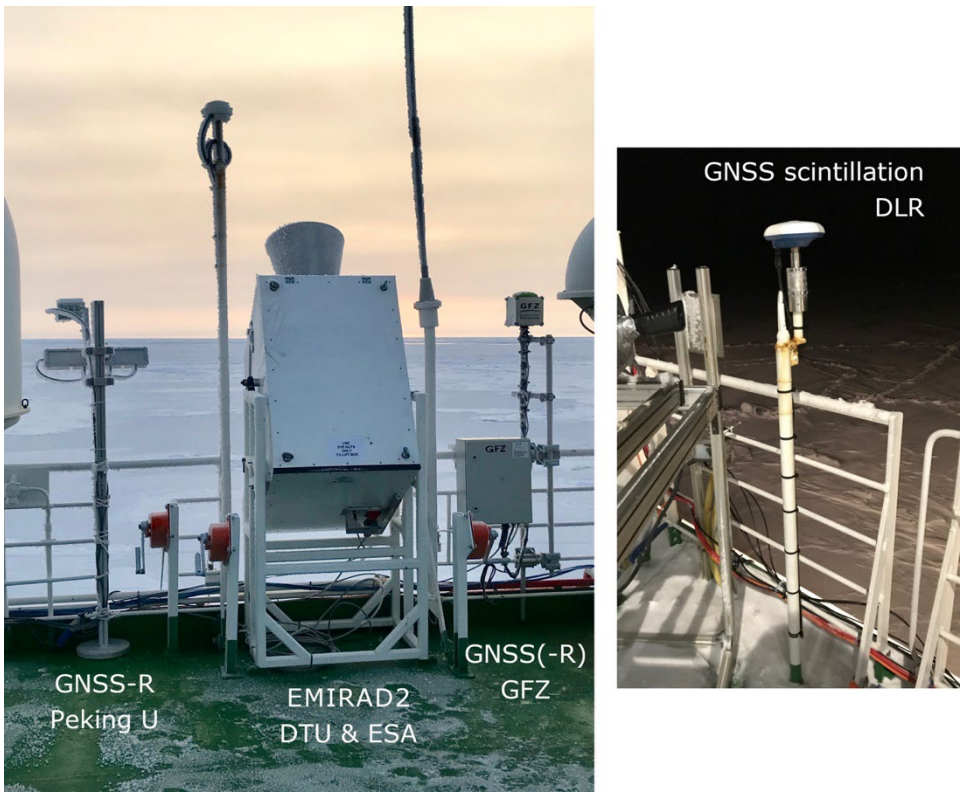

Fig.4.9.5: Remote sensing installations on the port side of Peil deck onboard Polarstern.

Instruments and measurement periods

In total 14 different instruments were operated as part of the Remote Sensing task, 10 on the ice and 4 onboard. Here we give a brief overview of the instruments and their measurement periods during leg 1. A complete list of device operations can be found in Appendix XXX.

Radar Ku/Ka-band

- List of measurement periods in Table 4.9.2
- Ku- (12–18 GHz) and Ka-band (30–40 GHz) radar
- Nadir view for altimetry application; elevation and azimuth scanning as scatterometer
- Has additional sledge to be towed along transect in nadir configuration
- DSHIP/SensorWeb: Radar dual Ka- and Ku-band altimeter (KuKa_Radar)
- University of Manitoba
- Projects: U Manitoba internal, NERC MOSAiC funding, and ESA MOSAiC remote sensing
- Corresponding satellite observations: CryoSat-2, Sentinel-3, AltiKa, ERS-1/2, Envisat, and future CRYSTAL altimeters; QuikSCAT, OSCAT, CFOSAT scatterometers

The instrument was operated in a permanent scanning mode stationary at the RS sites (typical ±45° azimuth, 0–50° elevation) with a break of 30 minutes between the scans. For the Transect Task (Section 4.4) the two radars were mounted on a smaller and more lightweight sledge in a nadir configuration.

Scientific Objectives:

1. Better understanding of radar interface and volume backscatter in the snow layer and corresponding range biases as a function of seasonally varying snow pack properties;
2. Validation and algorithm development of satellite retrieval of snow depth on sea ice with dual-band altimetry;
3. Better characterization of the uncertainty of freeboard retrieval in regions and periods where no validation data is currently available.

Research questions:

1. What is the seasonal evolution of snow backscatter at Ku/Ka-Band, especially in mid-Winter? What is the impact of snow accumulation and changes of snow properties?
2. What is the lateral variability of snow backscatter within the footprint of a satellite radar altimeter?
   a. Can potential changes in snow backscatter in both bands be constrained by auxiliary information (e.g. reanalysis data)?
   b. What is the impact of salinity on Ku and Ka-band backscatter?

Output from measurements:

- Co-located Ku- and Ka-band backscatter at cm-scale range resolution
- Tracked range distance for primary scattering horizon in nadir mode. Difference between Ku (snow-ice interface) and Ka (air-snow interface) frequency could be indicative for snow depth.

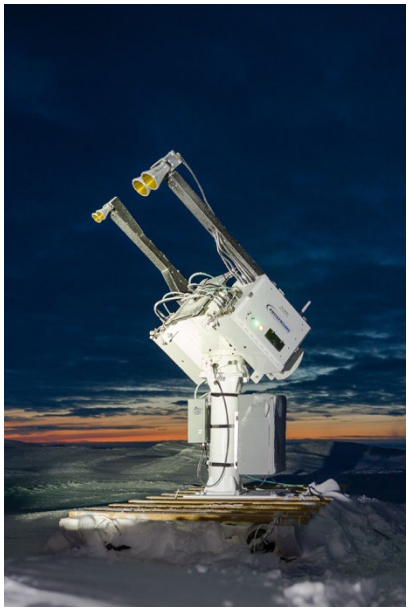

Fig.4.9.6: Ku/Ka-band radar (photo: Stefan Hendricks)

Tab.4.9.2: List of measurement periods of the Ku/Ka-band radar.

Activity - Device Operation	*Timestamp*	*Action*	*Comment*
PS122/1_1-102 KuKa_Radar	18.10.19 02:02	recording start	
PS122/1_1-102 KuKa_Radar	18.10.19 02:51	recording end	end time is approximated
PS122/1_1-103 KuKa_Radar	19.10.19 04:53	recording start	Target scan settings: azimuth: -45deg -> 45deg; elevation: 0 deg -> 50 deg; scan speed: 2 deg/sec sleep between scans: 30 min
PS122/1_1-103 KuKa_Radar	20.10.19 05:35	recording end	
PS122/1_1-104 KuKa_Radar	20.10.19 05:38	recording start	
PS122/1_1-104 KuKa_Radar	20.10.19 13:42	recording end	
PS122/1_1-105 KuKa_Radar	20.10.19 14:04	recording start	
PS122/1_1-105 KuKa_Radar	22.10.19 06:50	recording end	

PS122/1_1-106 KuKa_Radar	22.10.19 07:43	recording start	
PS122/1_1-106 KuKa_Radar	22.10.19 07:46	information	Scan Settings: Az Begin: -45deg, Az End: -45deg, El Begin: 0deg, El End: 50deg, El Delta: 5deg, Scan Velocity 2 deg/sec
PS122/1_1-106 KuKa_Radar	26.10.19 04:00	recording end	End time is approximated
PS122/1_1-107 KuKa_Radar	26.10.19 11:26	recording start	
PS122/1_1-107 KuKa_Radar	26.10.19 12:33	recording end	
PS122/1_1-108 KuKa_Radar	26.10.19 12:36	recording start	
PS122/1_1-108 KuKa_Radar	31.10.19 06:07	recording end	Device switched off for converting into transect configuration
PS122/1_1-109 KuKa_Radar	02.11.19 06:51	recording start	Restart with default scanning settings
PS122/1_1-109 KuKa_Radar	07.11.19 00:39	recording end	
PS122/1_6-52 KuKa_Radar - Transect	07.11.19 07:01	recording start	
PS122/1_6-52 KuKa_Radar - Transect	07.11.19 08:03	recording end	
PS122/1_1-110 KuKa_Radar	07.11.19 08:51	recording start	
PS122/1_1-110 KuKa_Radar	14.11.19 01:22	recording end	Stopped recording in preparation for transect work
PS122/1_7-59 KuKa_Radar - Transect	14.11.19 08:16	recording start	at start of northern RS transect line
PS122/1_7-59 KuKa_Radar - Transect	14.11.19 08:27	recording end	at end of northern RS transect close to Balloon Town
PS122/1_7-59 KuKa_Radar - Transect	14.11.19 08:58	recording start	at UWBRAD -> start of transect to ROV road along RS site and snow1
PS122/1_7-59 KuKa_Radar - Transect	14.11.19 09:18	recording end	end of transect (back at UWBRAD)
PS122/1_1-131 KuKa_Radar	14.11.19 09:58	profile start	Restart of standard scan after transect
PS122/1_1-131 KuKa_Radar	16.11.19 02:00	information	The last scan of this device operation have been made over slushy snow
PS122/1_1-131 KuKa_Radar	16.11.19 02:40	recording end	Recording stopped due to instrument evacuation from site
PS122/1_8-107 KuKa_Radar - Thin Ice	23.11.19 10:03	recording end	
PS122/1_8-107 KuKa_Radar - Thin Ice	23.11.19 10:07	recording start	not yet correct

PS122/1_1-245 KuKa_Radar	29.11.19 11:41	recording start	Distance Ka-Antenna underside to top snow surface: 151 cm, Snow Depth: 7 cm (measured at sleeping position -> 45deg azimuth, 0deg elevation)
PS122/1_1-245 KuKa_Radar	05.12.19 04:02	recording end	Switched off for transect task
PS122/1_1-245 KuKa_Radar	06.12.19 10:43	recording start	Scanning restarted after transect day
PS122/1_1-245 KuKa_Radar	10.12.19 15:00	information	Distance of Ku-Antenna to snow surface: 1.47 m in sleeping position (azimuth 45 deg). Ka-Antenna over snow drift with significant topography

Scatterometer L-band

- List of measurement periods in Table 4.9.3
- L-band (1.26 GHz), full-polarimetric (HH, VV, HV, VH) scatterometer
- Bandwidth: 500 MHz, range resolution 0.3 m
- Antenna beamwidth: 14°
- Transmit power: -13.5 dBm
- DSHIP/SensorWeb: Scatterometer L-band (Scat-L)
- University of Victoria
- Project: CanScat supported by Canadian Space Agency and EUMETSAT
- Corresponding satellite observations: L-band SAR: ALOS/PALSAR-1, -2, and -3; SAOCOM; NISAR

The instrument was operated in a permanent scanning mode stationary at the RS sites (typical 180° azimuth scan, 15–66° elevation) with a break of 30 minutes between the scans.

Scientific Objectives:

- Evaluation of current and future satellite missions with ground-based measurements.
- Investigation of the temporal evolution of radar backscatter and its changes caused by environmental conditions like snow accumulation and metamorphism, temperature changes, ice growth and melting, desalination, ice crusts and wind-packed snow formation, etc. for an entire annual sea ice cycle.
- Improving forward models of radiative transfer in snow and sea ice like the Snow Microwave Radiative Transfer Model (SMRT) and Microwave Emission Model of Layered Snow-packs (MEMLS) with the goal to develop new satellite retrievals.

Output from measurements:

- Calibrated polarimetric radar backscatter data at L-band frequency

Fig.4.9.7: L-band scatterometer (photo: Gunnar Spreen)

Tab.4.9.3: List of measurement periods of the L-band scatterometer.

Activity - Device Operation	*Timestamp*	*Action*	*Comment*
PS122/1_1-97 Scat-L	21.10.19 12:55	recording start	L-SCAT installed on 21.10.2019. Start of first official scan. Azimuth -140 to 140, elevation 15° to 66°, elevation delta 3°, sleep 30 minutes, scan vel 5°/sec, with this azimuth and elevation other instruments will be in the FOV.
PS122/1_1-97 Scat-L	23.10.19 06:12	recording end	
PS122/1_1-98 Scat-L	23.10.19 07:10	recording start	scan setup 2: azimuth -50 deg till +140deg, elevation 15deg - 66deg
PS122/1_1-98 Scat-L	15.11.19 19:55	recording end	L-SCAT measurements ended after RS site lost power after the floe break up.
PS122/1_1-246 Scat-L RS site 2	30.11.19 22:46	recording start	Start of measurement at 2nd RS site.

Scatterometer C-band

- List of measurement periods in Table 4.9.4
- C-band, dual-polarisation (H+V) scatterometer
- Manufacturer: ProSensing
- Kipp & Zonen positioner
- build 2002
- DSHIP/SensorWeb: Scatterometer C-band (Scat-C)
- University of Calgary
- Project: CanScat supported by Canadian Space Agency and EUMETSAT
- Corresponding satellite observations: C-band SAR: Sentinel-1 a/b, Radarsat-1/2, Radarsat Constellation Mission; ASCAT scatterometers

The C-SCAT offers azimuth and elevation scan but now programing of scan times. Typically, scans with 90° azimuth variation and changing elevation from 30° to 60° in 3° steps were activated for periods of a few hours. In addition, longer measurements at a fixed incidence angle of 45° were performed. However, to avoid potential RFI for the radiometers C-SCAT was kept turned off for periods on a regular basis. The data acquisition program “scatd” running on the C-SCAT server stopped working and crashed after a few hours on a regular basis. No data is lost. Measurements had then to be restarted, which can be done via network also from the ship.

Scientific Objectives:

- see under “Scatterometer L-band”

Output from measurements:

- Calibrated polarimetric radar backscatter data at C-band frequency

Fig.4.9.8: C-band scatterometer (photo: Gunnar Spreen)

Tab.4.9.4: List of measurement periods of the C-band scatterometer.

Activity - Device Operation	*Timestamp*	*Action*	*Comment*
PS122/1_10-133 Scat-C_stare45	07.12.19 16:25	recording start	first test measurement of C-SCAT
PS122/1_10-133 Scat-C_stare45	07.12.19 21:47	recording end	
PS122/1_10-131 Scat-C	08.12.19 11:24	recording start	
PS122/1_10-131 Scat-C	08.12.19 12:15	recording end	stopped because scatd on C-SCAT server crashed.
PS122/1_10-132 Scat-C	08.12.19 13:26	recording start	
PS122/1_10-132 Scat-C	08.12.19 15:12	recording end	
PS122/1_11-21 Scat-C	10.12.19 13:12	recording start	
PS122/1_11-21 Scat-C	10.12.19 16:32	recording end	
PS122/1_1-289 Scat-C	11.12.19 08:32	recording start	scan azimuth 60° to 150°, elevation 30° to 60°, step 3°
PS122/1_1-289 Scat-C	11.12.19 11:25	recording end	end scan
PS122/1_1-289 Scat-C	11.12.19 11:31	recording start	stare measurement at azimuth 100° and elevation 45°
PS122/1_1-289 Scat-C	11.12.19 11:41	recording end	scatd crashed and measurement ended

Scatterometer X-band

- X-band (9.6 GHz), dual-polarisation (H+V) scatterometer
- Bandwidth: 500 MHz, range resolution 0.3 m, sensitivity -50 dB m2/m2 at 15 m range
- Antenna beamwidth: 4.3° (narrow) to 5.8° (flood)
- Transmitted power: -9.5 dBm (flood) to -11.8 dBm (narrow)
- Manufacturer: ProSensing
- Kipp & Zonen 2AP positioner
- DSHIP/SensorWeb: Scatterometer Ku- and X-band (Scat-Ku_X)
- University of Waterloo
- Project: CanScat supported by Canadian Space Agency and EUMETSAT
- Corresponding satellite observations: TerraSAR-X, PAZ, COSMO-Skymed

The X-SCAT was assembled and tested in wet lab 2. It was fully functional. It was deployed at RS1 and RS2 sites on 10 November and 8 December 2019, respectively. Connection to the instrument was established but no backscatter was measured (flat signal). This likely could be a cable connection problem. However, until the end of leg 1 this never was resolved due to missing time and the relocation of instruments between RS1 and RS2 sites. No usable X-SCAT measurements were recorded.

Scientific Objectives:

- see under “Scatterometer L-band”

Output from measurements:

- Calibrated polarimetric radar backscatter data at X-band frequency

Fig.4.9.9: X-band scatterometer (photo: Gunnar Spreen)

Microwave Radiometer UWBRAD

- List of measurement periods in Table 4.9.5
- 0.5 to 2 GHz in four channels (540, 900, 1380 and 1740 MHz)
- 125 MHz bandwidth resolved in 512 sub-channels per each of the four channel
- DSHIP/SensorWeb: Ultra-Wideband Software-defined Microwave Radiometer (0.5-2GHZ) (UWBRAD)
- Ohio State University
- Project: “Ultra Wide Band Radiometer Measurements of Sea Ice” supported by NSF
- Corresponding satellite observations: SMOS, SMAP, Aquarius

The UWBRAD (Ultra-Wide Band Microwave Radiometer) is a novel instrument designed to observe sea ice microwave emissions at four different channels (540, 900, 1380 and 1740 MHz) over the spectrum range 0.5–2 GHz in real-time. Each channel occupies 125 MHz bandwidth resolved into 512 sub-channels, and the medium rate data samples are generated approximately every four seconds after integration over 100 ms acquisition. The lowest channel of UWBRAD is more sensitive to the emissions from deeper layers of the ice compared to the space-borne radiometers operating at L-band, so it will contribute to the estimations of thicker ice floes. In addition, its advanced sampling features allow the instrument to detect the spectral and temporal changes of ice properties with a high precision. The UWBRAD also performs an advanced RFI mitigation algorithm over each channel to clear the acquired data from unwanted signals which allows it to operate at a large bandwidth.

Output from measurements:

- Integrated brightness magnitudes for both the ice surface and the sky before the calibrations and RFI mitigations.

Fig.4.9.10: UWBRAD microwave radiometer (photo: Gunnar Spreen)

Tab.4.9.5: List of measurement periods of the UWBRAD microwave radiometer.

Activity - Device Operation	*Timestamp*	*Action*	*Comment*
	02.11.19	recording start	RS1 site; 40° incidence angle; 2 m height
	04.11.19	recording end	
	07.11.19	calibration	RS1 site; calibration at 180° incidence angle; 2 m height
	10.11.19	recording start	RS1 site; test measurement at 180° incidence angle; 2 m height
	15.11.19	recording end	
PS122/1_1-265 UWBRAD	04.12.19 07:57	recording start	Setup at new Remote Sensing 2 Site; 45° incidence angle; 2 m height
	06.12.19	recording start	RS2 site; 40° incidence angle; 3 m height
	07.12.19	recording start	RS2 site; 35° incidence angle; 4 m height
	13.12.19	recording end	

Microwave radiometer ELBARA

- List of measurement periods in Table 4.9.6
- L-band (1.4 GHz)
- Swiss Federal Institute WSL
- DSHIP/SensorWeb: Microwave Radiometer ELBARA L-band (ELBARA)
- Project: ESA MOSAiC remote sensing
- Corresponding satellite observations: SMOS, SMAP, Aquarius

ELBARA was operated continuously at a constant incidence of 40°. Once per week a sky calibration at 130° incidence angle was performed.

Scientific Objectives:

- The large penetration depth of electromagnetic waves at L-band provides good sensitivity to thickness of ice up to approximately one meter.
- The long observation wavelength allows to simplify physical emission models of snow and sea ice by neglecting e.g. volume scattering at snow grains, brine inclusions and air bubbles.
- Coincident measurements of L-band microwave emission and in-situ sea ice profiles of e.g. dielectric properties are used for the development and improvement of sea ice microwave emission models and corresponding retrieval schemes.
- Better understanding of the emissivity for improved satellite retrieval of sea ice parameters or assimilation of brightness temperatures in ocean-ice forecast models.

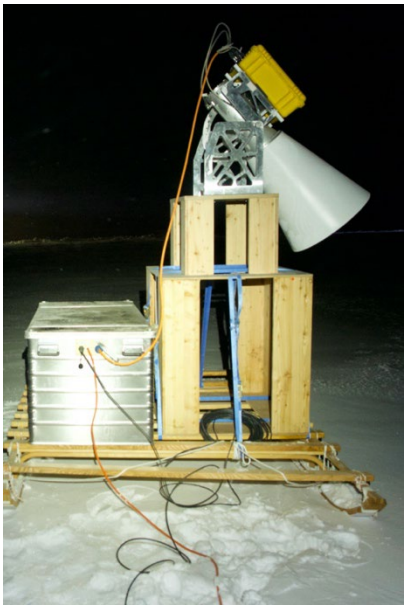

Output from measurements:

- Calibrated microwave brightness temperature data at L-band frequency

Fig.4.9.11: UWBRAD microwave radiometer (photo: Gunnar Spreen)

Tab.4.9.6: List of measurement periods of the ELBARA microwave radiometer.

Activity - Device Operation	*Timestamp*	*Action*	*Comment*
PS122/1_1-101 ELBARA	29.10.19 06:50	recording start	Measurement at 40° incidence angle (scale -50°).
PS122/1_1-101 ELBARA	29.10.19 06:55	recording end	end of first measurement to do sky calibration.
PS122/1_1-101 ELBARA	29.10.19 07:06	calibration	Sky calibration at 130° (scale +40°)
PS122/1_1-101 ELBARA	29.10.19 07:15	recording start	restart measurement at 40° incidence angle (scale -50) after sky measurement.
PS122/1_1-101 ELBARA	04.11.19 06:24	recording end	stop before sky calibration
PS122/1_1-101 ELBARA	04.11.19 06:40	calibration	sky calibration at 130° (+40 scale)
PS122/1_1-101 ELBARA	04.11.19 06:48	recording start	restarted measurements at 40° incidence angle (scale -50)
PS122/1_1-101 ELBARA	10.11.19 08:00	information	Observed alarm at UPS. System was shut down. While trying to get it started again the UPS display broke of. This was repaired on 11.11. at 8-tish and measurement should be available again.
PS122/1_1-101 ELBARA	11.11.19 09:02	recording end	stopped 40 degree incidence angle measurement. However, the system shut down for unknown reason and not all data were recorded.
PS122/1_1-101 ELBARA	11.11.19 09:09	calibration	Sky calibration at 130 degree incidence angle (+50).
PS122/1_1-101 ELBARA	11.11.19 09:14	recording start	Start of regular measurements at 40 degree (-50) incidence angle
PS122/1_1-101 ELBARA	16.11.19 04:35	recording end	End of ELBARA measurements at Remote Sensing Site 1 (after power loss and floe break-up).
PS122/1_1-257 ELBARA	02.12.19 07:00	recording start	Continuous measurements at 40° incidence angle (scale at 50).
PS122/1_1-257 ELBARA	08.12.19 12:14	recording end	stopped for calibration
PS122/1_1-257 ELBARA	08.12.19 12:18	calibration	Sky calibration at 130° elevation (scale 40)
PS122/1_1-257 ELBARA	08.12.19 12:23	recording start	restarted after sky calibration at 40° elevation (scale -50)

Microwave radiometer 19-37-89-GHz

- List of measurement periods in Table 4.9.7
- Dual-polarization microwave radiometers
- 19 GHz, 1 GHz bandpass, 0.04 K sensitivity for 1 second delta T, direct detection (AC1900)
- 37 GHz, 2 GHz bandpass, 0.03 K sensitivity for 1 second delta T, direct detection (AC3700)
- 89 GHz, 4 GHz bandpass, 0.08 K sensitivity for 1 second delta T, double-sideband downconvert (AC8900)
- Manufacturer: Radiometrics Corporation
- Kipp & Zonen 2AP positioner
- DSHIP/SensorWeb: Microwave Radiometer 19, 37, 89 GHz (SSMI type) (SSMI_radiometer_SN002)
- University of Manitoba
- Projects: U Manitoba internal and NERC MOSAiC funding
- Corresponding satellite observations: AMSR-E/2, SSM/I, SSMIS, CIMR, MWR

Scans with the 19-37-89-GHz radiometer were obtained at least weekly for a duration of several scan cycles. For the periods between the radiometer was set to a fixed incidence angle, usually 45°, for continuous measurements. In addition to the three radiometers a visual camera obtains pictures of the observed surface in regular time intervals. No calibrations were performed during leg 1. This should be followed up during leg 2 and following legs.

Scientific Objectives:

- Evaluation of satellite microwave radiometers with ground-based measurements. While the point-measurements do not fully cover the footprint of the satellite observations, they will allow investigation of the temporal evolution of signals caused by environmental changes like snow accumulation and metamorphism, temperature changes, ice growth and melting, desalination, ice crusts and wind-packed snow formation, etc. These environmental changes are effective on a satellite footprint scale, which will allow to compare the temporal evolution of the ground-based and with current satellite radiometers like AMSR2 and SSMIS measurements.

- Develop a better understanding of the electromagnetic wave interaction with snow and sea-ice and thus the brightness temperature measured by satellite radiometers. To develop retrieval methods of snow and ice properties from these measurements, improved forward models of the radiative transfer in the snow and sea ice are needed. To develop and validate such models joint ground-based microwave radiometer measurements with in-situ measurements of all relevant variables are needed.
- The measurements at 19, 37, and 89 GHz will be analyzed in conjunction with the lower frequency microwave radiometer measurements by ELBARA, EMIRAD2, Balamis ARIEL, and UWBRAD. Together the full frequency range from P to W-band will be covered.

Output from measurements:

- Calibrated microwave brightness temperature data at frequencies 19, 37, and 89 GHz.
- Photographs of the field of view of the radiometers in regular intervals

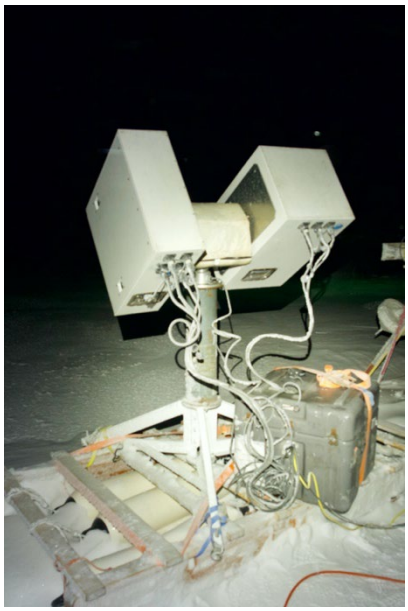

Fig.4.9.12: 19-37-89-GHz microwave radiometer (photo: Gunnar Spreen)

Tab.4.9.7: List of measurement periods of the 19-37-89-GHz microwave radiometer.

Activity - Device Operation	*Timestamp*	*Action*	*Comment*
PS122/1_4-23 SSMI_radiometer_SN002	26.10.19 08:00	recording start	first measurement, 30° to 60° incidence angle, about 3 cycles (lat/lon is for end of measurement)
PS122/1_4-23 SSMI_radiometer_SN002	26.10.19 08:13	recording end	end of first measurement
PS122/1_5-76 SSMI_radiometer_SN002	29.10.19 07:39	recording start	
PS122/1_5-76 SSMI_radiometer_SN002	29.10.19 07:57	recording end	
PS122/1_5-77 SSMI_radiometer_SN002	29.10.19 08:05	recording start	
PS122/1_5-63 SSMI_radiometer_SN002	02.11.19 06:30	recording start	20191102_scan: scan 30 to 60
PS122/1_5-66 SSMI_radiometer_SN002	02.11.19 07:43	recording start	20191102_stare45: continues measurements at 45
PS122/1_6-1 SSMI_radiometer_SN002	04.11.19 07:10	recording start	scan 30 to 60 degree incidence angle.
PS122/1_6-1 SSMI_radiometer_SN002	04.11.19 08:46	recording end	

PS122/1_6-2 SSMI_radiometer_SN002	04.11.19 08:52	recording start	start constant stare measurement at 45 degree
PS122/1_6-2 SSMI_radiometer_SN002	07.11.19 08:10	recording end	end of 45° stare measurement
PS122/1_6-127 SSMI_radiometer_SN002	07.11.19 08:31	recording start	
PS122/1_6-127 SSMI_radiometer_SN002	07.11.19 08:57	recording end	
PS122/1_6-128 SSMI_radiometer_SN002	07.11.19 08:58	recording start	stare measurement at 45°
PS122/1_6-128 SSMI_radiometer_SN002	10.11.19 09:38	recording end	stare measurement at 45° end
PS122/1_7-1 SSMI_radiometer_SN002	11.11.19 07:15	recording start	
PS122/1_7-1 SSMI_radiometer_SN002	11.11.19 09:32	recording end	
PS122/1_7-7 SSMI_radiometer_SN002	11.11.19 09:42	recording start	
PS122/1_7-7 SSMI_radiometer_SN002	13.11.19 05:43	information	From the data file it looks like only data from this date onward was recorded. It also indicates an incidence angle of 55° (instead of 45°).
PS122/1_7-7 SSMI_radiometer_SN002	14.11.19 10:20	recording end	end of stare measurements at 45°
PS122/1_10-79 SSMI_radiometer_SN002	06.12.19 12:54	recording start	time stamp some time after instrument was turned on but from here on measurements should be nominal. The lower incidence angles could have the sledge in the field of view.
PS122/1_10-79 SSMI_radiometer_SN002	07.12.19 11:20	recording end	Stopped scan after about 24 hours
PS122/1_10-130 SSMI_radiometer_SN002_stare	07.12.19 12:03	recording start	
PS122/1_10-130 SSMI_radiometer_SN002_stare	08.12.19 08:14	recording end	measurement stopped for unknown reason
PS122/1_1-303 SSMI_radiometer_SN002	12.12.19 08:00	recording start	continuous scan 30° to 60° elevation in 5° steps

Microwave radiometer Balamis ARIEL

- List of measurement periods in Table 4.9.8
- L-band (1.413 GHz), dual-polarisation (H+V)
- Bandwidth 20 MHz, 0.7 K radiometric accuracy at 1 Hz

- Beamwidth: 37° (correct?)
- Manufacturer: Balamis
- Operated on a sledge to be pulled along transects; sledge parked at remote sensing site
- Institut de Ciències del Mar - CSIC
- DSHIP/SensorWeb: BALAMIS_Radiometer (BALAMIS_Rad)
- Project: “Improving emission models for sea ice low-frequency microwaves” supported by Spanish MOSAiC funding (MINECO)
- Corresponding satellite observations: SMOS, SMAP, Aquarius

The Balamis ARIEL radiometer was only operated during transects. See description in Section 4.4.

Scientific Objectives:

- Measurements of brightness temperatures at L-band frequencies for snow covered ice across a long period of time under varying environmental conditions.
- Spatial and temporal variability of 1.4 GHz brightness temperatures by combining measurements from two radiometers, i.e. ARIEL and ELBARA, and comparison against satellite measurements.
- Validation of microwave emission models across frequencies using collocated remote sensing and in-situ measurements.
- The data collected will be the basis for improved sea ice emission / radiative transfer models, for improved retrieval algorithms of key sea ice parameters

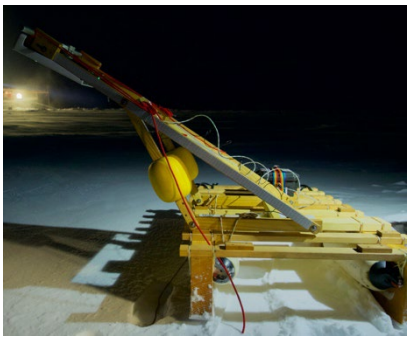

Output from measurements:

- Calibrated microwave brightness temperature data at L-band frequency.

Fig.4.9.13: Balamis ARIEL microwave radiometer (photo: Gunnar Spreen)

Tab.4.9.8: List of measurement periods of the Balamis ARIEL microwave radiometer.

Activity - Device Operation	*Timestamp*	*Action*	*Comment*
PS122/1_2-198 BALAMIS_Rad	23.10.19 07:32	calibration	calibration: calibration with absorber at remote sensing site; temperature: -8°C absorber calibration start: 07:44:00 absorber calibration stop: 07:46
PS122/1_2-198 BALAMIS_Rad	23.10.19 08:01	recording start	obs: test measurements over night at remote sensing site file: data_20191023_075634.log
PS122/1_5-29 BALAMIS_Rad	31.10.19 06:47	calibration	calibration absorber until 06:52 temperature: -17°C (warming up started at 06:10)
PS122/1_5-29 BALAMIS_Rad	31.10.19 06:54	calibration	calibration sky until 06:58

PS122/1_5-29 BALAMIS_Rad	31.10.19 07:42	recording start	remote sensing transect leg in northern transect loop. GEM and Magnaprobe done shortly before. Some snow pits.
PS122/1_5-29 BALAMIS_Rad	31.10.19 08:50	deployed	transect1: t1 (recorded by floe navi; meaning not clear anymore; time seems to be strange)
PS122/1_6-57 BALAMIS_Rad_transect	07.11.19 06:15	calibration	absorber calibration until 06:16:30 calibration was repeated because Garmin GPS was laying on top of radiometer -> possible RFI (?); temperature: -19°C
PS122/1_6-57 BALAMIS_Rad_transect	07.11.19 06:18	calibration	absorber calibration until 06:19:15 temperature: -19°C
PS122/1_6-57 BALAMIS_Rad_transect	07.11.19 06:20	calibration	sky calibration until 06:21:50
PS122/1_6-57 BALAMIS_Rad_transect	07.11.19 07:02	recording start	start of northern transect with thicker ice
PS122/1_6-57 BALAMIS_Rad_transect	07.11.19 07:23	recording end	end of transect at Ballon Town (actual transect line ends a bit earlier).
PS122/1_6-57 BALAMIS_Rad_transect	07.11.19 07:51	recording start	start of southern transect line (RS site to ROV road)
PS122/1_6-57 BALAMIS_Rad_transect	07.11.19 08:00	recording end	end of southern RS transect line
PS122/1_7-103 BALAMIS_Rad_transect	14.11.19 07:00	information	equalisation before calibration
PS122/1_7-103 BALAMIS_Rad_transect	14.11.19 07:16	calibration	black body calibration
PS122/1_7-103 BALAMIS_Rad_transect	14.11.19 07:21	calibration	sky calibration
PS122/1_7-103 BALAMIS_Rad_transect	14.11.19 08:14	recording start	start of northern RS transect line
PS122/1_7-103 BALAMIS_Rad_transect	14.11.19 08:26	recording end	end of northern RS transect line
PS122/1_7-103 BALAMIS_Rad_transect	14.11.19 08:56	recording start	Start at UWBRAD for southern RS transect line towards ROV road
PS122/1_7-103 BALAMIS_Rad_transect	14.11.19 09:14	recording end	end of southern RS transect line (walked forth and back)
PS122/1_8-104 BALAMIS_Rad	23.11.19 09:20	calibration	20191123 b_cal: blackbody calibration until 9:27 Temperature -16°C
PS122/1_8-104 BALAMIS_Rad	23.11.19 09:29	calibration	sky cal: sky calibration until 09:31

PS122/1_8-104 BALAMIS_Rad	23.11.19 09:47	recording start	thin ice measurement: thin ice with frost flowers at the crack until 10:26; thin ice thickness 9 cm; salinity under the ice: 31.6 psu

Microwave radiometer EMIRAD2 (ONBOARD)

- Picture in Figure 4.9.5
- List of measurement periods in Table 4.9.9
- Location: upper Peil deck, port side
- L-band (1.400–1427 GHz)
- Full polarimetric
- Retrieved geophysical variables: ice thickness up to 1 m
- Technical University of Denmark
- DSHIP/SensorWeb: Microwave Radiometer L-band EMIRAD2 (EMIRAD2)
- Project: ESA MOSAiC remote sensing
- Corresponding satellite observations: SMOS, SMAP, Aquarius

EMIRAD was operated continuously at 45° incidence angle from the time we left the Russian EEZ. Twice per week a sky calibration at 150° and additional measurements at 35° and 55° were performed. During the transit to the ice floe multiple different ice situations at the port side of the ship were observed. After *Polarstern* anchored to the floe the ice situation on port side stayed variable with several events of ice dynamics with cracks opening and refreezing and ice shear. The PANOMAX 360-degree camera (Section 4.1) can provide some information about the measured surface type and its changes. In addition, photographs were taken during the twice weekly calibration measurements. However, no other in-situ data were obtained close to the EMIRAD2 footprint during leg 1.

Scientific Objectives:

- see under “Microwave radiometer ELBARA”

Output from measurements:

- Calibrated microwave brightness temperature data at L-band frequency

Tab.4.9.9: List of measurement periods of the EMIRAD2 microwave radiometer.

Activity - Device Operation	*Timestamp*	*Action*	*Comment*
PS122/1_1-19 EMIRAD2	22.09.19 06:00	recording start	
PS122/1_1-19 EMIRAD2	22.09.19 13:00	recording end	
PS122/1_1-27 EMIRAD2	27.09.19 00:00	recording start	start of continuous EMIRAD measurements
PS122/1_1-27 EMIRAD2	27.09.19 08:40	calibration	calibration at 150°, measurement at 55° and 35° incidence angle for 3 min.
PS122/1_1-27 EMIRAD2	05.10.19 01:04	calibration	calibration at 150°, measurement at 55° and 35° incidence angle for 3 min.
PS122/1_1-27 EMIRAD2	10.10.19 03:47	calibration	calibration at 150°, measurement at 55° and 35° incidence angle for 3 min.

PS122/1_1-27 EMIRAD2	13.10.19 10:25	calibration	calibration at 150°, measurement at 55° and 35° incidence angle for 3 min.
PS122/1_1-27 EMIRAD2	17.10.19 09:24	calibration	calibration at 150°, measurement at 55° and 35° incidence angle for 3 min.
PS122/1_1-27 EMIRAD2	21.10.19 10:52	calibration	calibration at 150°, measurement at 55° and 35° incidence angle for 3 min.
PS122/1_1-27 EMIRAD2	24.10.19 04:35	calibration	calibration at 150°, measurement at 55° and 35° incidence angle for 3 min.
PS122/1_1-27 EMIRAD2	27.10.19 05:06	calibration	calibration at 150°, measurement at 55° and 35° incidence angle for 3 min.
PS122/1_1-27 EMIRAD2	30.10.19 09:15	calibration	calibration at 150°, measurement at 55° and 35° incidence angle for 3 min.
PS122/1_1-27 EMIRAD2	04.11.19 11:15	calibration	calibration at 150°, measurement at 55° and 35° incidence angle for 3 min.
PS122/1_1-27 EMIRAD2	07.11.19 10:10	calibration	calibration at 150°, measurement at 55° and 35° incidence angle for 3 min.
PS122/1_1-27 EMIRAD2	11.11.19 11:12	calibration	calibration at 150°, measurement at 55° and 35° incidence angle for 3 min.
PS122/1_1-27 EMIRAD2	15.11.19 11:11	calibration	calibration at 150°, measurement at 55° and 35° incidence angle for 3 min.
PS122/1_1-27 EMIRAD2	19.11.19 07:34	calibration	calibration at 150°, measurement at 55° and 35° incidence angle for 3 min.
PS122/1_1-27 EMIRAD2	21.11.19 11:02	calibration	calibration at 150°, measurement at 55° and 35° incidence angle for 3 min.
PS122/1_1-27 EMIRAD2	24.11.19 11:48	calibration	calibration at 150°, measurement at 55° and 35° incidence angle for 3 min.
PS122/1_1-27 EMIRAD2	03.12.19 08:58	calibration	calibration at 150°, measurement at 55° and 35° incidence angle for 3 min.
PS122/1_1-27 EMIRAD2	08.12.19 09:32	calibration	calibration at 150°, measurement at 55° and 35° incidence angle for 3 min.

GNSS reflectometry on ice

- List of measurement periods in Table 4.9.10
- DSHIP/SensorWeb: GNSS Reflectometry equipment on MOSAiC Sea Ice Floe (GNSS-R_IceFloe)
- Sub-device: GNSS Reflectometer at dual linear polarizations on MOSAiC sea ice floe (GNSS-R_LinPol)

- Sub-device: GNSS Reflectometry receiver on the sea ice floe at two circular polarizations (GNSS-R_CircPol)
- Instituto de Ciencias del Espacio (ICE-CSIC/IEEC)
- Project: ESA MOSAiC remote sensing
- Corresponding satellite observations: UK TDS-1, future: ESA PRETTY, China FY-3E and Taiwan FS-7R

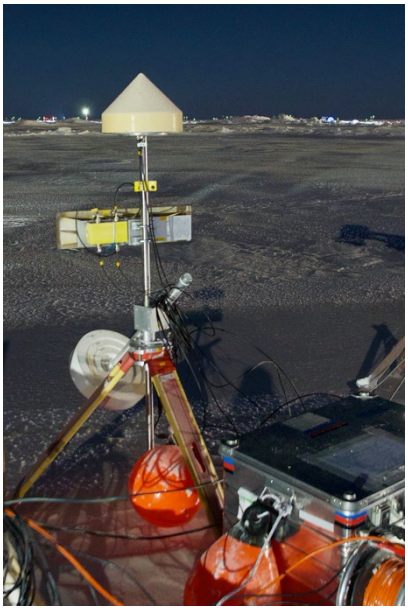

The three GNSS antennas are installed on a tripod and are controlled by the GNSS receivers and instrumentation in a Zarges box located close by. The setup is quite mobile and can be carried by two persons. The installation is meant for continuous operation. However, the powering and recharging of the internal battery did not work during leg 1. Therefore, measurement periods were limited to the length the battery could power the instrument (typically 1-2 days). The batteries were exchanged during each visit to the RS sites.

Scientific Objectives:

- GNSS signals reflect off the sea ice
- The delay, amplitude and polarization of the reflected signals can provide information about:
  - Sea Ice thickness
  - Sea Ice concentration
  - Snow layer on the Sea Ice
  - Sea Ice age

Fig.4.9.14: GNSS reflectometry instrument (photo: Gunnar Spreen)

Tab.4.9.10: List of measurement periods of the GNSS-R on ice instrument.

Activity - Device Operation	*Timestamp*	*Action*	*Comment*
PS122/1_11-27 GNSS-R_IceFloe	12.12.19 12:30	recording end	The reset of charger was not successful. The instrument stopped at an unknown time before 12:30. Reason not known.
PS122/1_11-27 GNSS-R_IceFloe	12.12.19 07:00	recording start	restarted GNSS-R measurements by restarting charger. Confirmed that battery was charging and instruments recording.
PS122/1_11-27 GNSS-R_IceFloe	11.12.19 12:00	recording end	battery ran out and recording stopped. Exact time not known.
PS122/1_11-27 GNSS-R_IceFloe	10.12.19 07:45	recording start	Start of measurements. The problem that the battery is not recharged was not resolved yet.
PS122/1_7-16 GNSS-R_IceFloe	15.11.19 20:03	recording end	stopped after battery ran out. The day after the RS site got a crack and was retreated.
PS122/1_7-16 GNSS-R_IceFloe	14.11.19 06:50	recording start	restarted after battery exchange

PS122/1_7-16 GNSS-R_IceFloe	13.11.19 20:14	recording end	battery ran out
PS122/1_7-16 GNSS-R_IceFloe	11.11.19 06:37	recording start	
PS122/1_6-51 GNSS-R_IceFloe	08.11.19 12:00	recording end	system ran out of power again (despite plugging it in and out on 10.11.). Data ends somewhen on 8.11.
PS122/1_6-51 GNSS-R_IceFloe	07.11.19 06:09	recording start	
PS122/1_5-64 GNSS-R_IceFloe	04.11.19 12:00	recording end	exact time when recording ended not known
PS122/1_5-64 GNSS-R_IceFloe	02.11.19 07:25	recording start	20191102: restarted instrument after device shutdown
PS122/1_5-85 GNSS-R_IceFloe	01.11.19 12:00	recording end	exact time when recording stopped is not known
PS122/1_5-85 GNSS-R_IceFloe	29.10.19 07:08	recording start	Restarted GNSS-R after device shutdown on 25.10.2019. It looks like data was recorded until 01.11.2019.
PS122/1_4-11 GNSS-R_IceFloe	24.10.19 08:06	deployed	20191024_1:1st deployment next to IR camera
PS122/1_4-11 GNSS-R_IceFloe	24.10.19 08:06	information	Data recording stopped on 25.10.2019 due to empty battery.

GNSS sea ice reflectrometry (ONBOARD)

- Picture in Figure 4.9.5
- List of measurement periods in Table 4.9.11
- Location: upper Peil deck, port side
- Retrieved geophysical variables: snow depth, thin ice thickness
- Peking University
- Project: Chinese contribution to MOSAiC
- Corresponding satellite observations: UK TDS-1, future: ESA PRETTY, China FY-3E and Taiwan FS-7R

This GNSS system is used to observe the reflected GNSS signals from the snow and ice. No user interaction is needed. Only a regular daily check if the data is recorded was performed. When the software is interrupted, we have to restart the software. There are some temporary interruption (~several hours) for the recording program occurring on 28 Oct., 1 Nov., 7 Nov., 16 Nov., 27 Nov., 1 Dec., and 13 Dec. By the end of Leg 1, this system is handed over to Hailong Liu (Ocean Team).

Scientific Objectives:

- GNSS signals reflect off the sea ice
- The delay, amplitude and polarization of the reflected signals can provide information about:
    - Sea Ice thickness of thin ice
    - Snow depth

- Moisture of snow layer over the ice

Output from measurements:

- Reflected GNSS data from the sea ice in four polarizations of LHCP, RHCP, Vertical, and Horizontal.

Tab.4.9.11: List of measurement periods of the GNSS-R onboard instrument.

Activity - Device Operation	*Timestamp*	*Action*	*Comment*
PS122/1_1-60 GNSSR_FPOL	18.10.19 12:00	recording start	Continuous measurements with some temporary interruptions

GNSS atmosphere and sea ice reflectrometry (ONBOARD)

- Picture in Figure 4.9.5
- List of measurement periods in Table 4.9.12
- Location: upper Peil deck, port side
- Retrieved geophysical variables: atmospheric water vapour, sea ice properties like thin ice thickness
- Helmholtz Centre Potsdam GFZ, German Research Centre for Geosciences
- DSHIP/SensorWeb:
- GNSS-receiver for multi-GNSS observations (GNSS-receiver-TINY)
- GNSS-receiver for Occultation Reflectometry and Scatterometry measurements (GNSS-receiver-GORS)
- Corresponding satellite observations: UK TDS-1, future: ESA PRETTY, China FY-3E and Taiwan FS-7R

The GNSS system to observe reflected GNSS signals from the snow and ice and measure atmospheric water vapor from GNSS delay is a fully automatic system. No user interaction is needed. Only a regular weekly check if the data is recorded was performed. The system daily sends an email with a data report back to GFZ on land.

Scientific Objectives:

- The refractive delay of GNSS signals can be measured to estimate atmospheric parameters, for example, the atmospheric water vapor content.
- Reflected GNSS signals can be used to sense surface parameters including, for example, water or ice surface heights or the permittivity or amount of sea ice.
- Collect data of GNSS reflections over the Arctic ocean and sea ice. Delay and amplitude of these signals are used to investigate L-band reflectivity and penetration depth for different sea ice conditions. Dependencies on sea ice thickness, conductivity (brine content) and concentration will be in focus.

Output from measurements:

- Precipitable water vapor with accuracy of about 1 mm
- Reflected GNSS data from the sea ice

Tab.4.9.12: List of measurement periods of the onboard atmosphere and sea ice GNSS.

Activity - Device Operation	*Timestamp*	*Action*	*Comment*

PS122/1_1-21 GNSS-receiver-GORS	22.09.19 06:00	profile start
PS122/1_1-20 GNSS-receiver-TINY	22.09.19 06:00	profile start
PS122/1_1-21 GNSS-receiver-GORS	22.09.19 13:00	profile end
PS122/1_1-20 GNSS-receiver-TINY	22.09.19 13:00	profile end
PS122/1_1-29 GNSS-receiver-GORS	27.09.19 00:00	profile start
PS122/1_1-28 GNSS-receiver-TINY	27.09.19 00:00	profile start

GNSS ionospheric scintillation (ONBOARD)

- Picture in Figure 4.9.5
- List of measurement periods in Table 4.9.13
- Location antenna: lower Peil deck, port side
- Location processing unit: observation alley, in front of meteorologist's office
- Global Satellite Navigation Systems (GNSS) recording
- DLR, Germany
- DSHIP/SensorWeb:
- GNSS_NTlab_FE (GNSS_NTlab_FE)
- GNSS_navX_MBANT (GNSS_navX_MBANT)

The GNSS ionospheric scintillation installation is an autonomous instrument that does not require operator interaction. The operation and data acquisition were checked on a weekly basis. Some instrument problems lead to small manual changes of the data processing and acquisition software running on the instrument server, which was accomplished by the instructions from. The system daily sends an email with a data report back to DLR on land.

Scientific Objectives:

- Different distortions can severely degrade the GNSS accuracy and availability. One of these distortions are ionospheric scintillations, which occur mainly in equatorial and polar regions.
- The goal of this research is to record pre- and post-correlation samples of polar ionospheric scintillations to evaluate the impact of scintillations on GNSS and to develop new signal processing algorithms to mitigate scintillation from the received signal.

Tab.4.9.13: List of measurement periods of the ionospheric scintillation GNSS.

Activity - Device Operation	*Timestamp*	*Action*	*Comment*
PS122/1_1-5 GNSS_NTlab_FE	22.09.19 06:00	profile start	
PS122/1_1-4 GNSS_navX_MBANT	22.09.19 06:00	profile start	
PS122/1_1-3 GNSS_JAVADd3	22.09.19 06:00	profile start	
PS122/1_1-4 GNSS_navX_MBANT	22.09.19 13:00	profile end	
PS122/1_1-5 GNSS_NTlab_FE	22.09.19 13:00	profile end	
PS122/1_1-3 GNSS_JAVADd3	22.09.19 13:00	profile end	

PS122/1_1-30 GNSS_JAVADd3	27.09.19 00:00	profile start
PS122/1_1-31 GNSS_navX_MBANT	27.09.19 00:00	profile start
PS122/1_1-32 GNSS_NTlab_FE	27.09.19 00:00	profile start

Infrared thermography system and visual camera

- List of measurement periods in Table 4.9.14
- VarioCAM HDx head 625
- Manufacturer: Infratec
- 7.5-14 µm, 640x480 pixel
- In addition to the IR camera a visual camera is installed for monitoring purposes
- DSHIP/SensorWeb: Infrared VarioCAM HDx head 625 (IR_VarioCAM_01)
- DSHIP/SensorWeb: Camera VIS_INFRALAN_01 (VIS_INFRALAN_01)
- University of Bremen
- Project: Satellite Remote Sensing – Germany and MOSAiCmicrowaveRS supported by DFG

The infrared and visual cameras are installed together on one tripod, which is accompanied by one Peli case with a battery and an ebox PC for operation. Thus the system is mobile and can be moved to different sites. During leg 1 the system monitored the instruments field of view at RS 1 and RS2 sites. The time between the break-up of the RS1 site and the repositioning at RS2, the IR camera was setup at two different cracks with thin ice. Sampling was set to 10 minutes for the IR and 5 minutes for the visual camera.

Scientific Objectives:

- Monitor the surface temperature of snow and thin sea ice in dependence of environmental parameters like incoming longwave radiation, air temperature, water temperature, snow depth, and ice thickness.
- Provide a support dataset for the microwave radiometer and scatterometer measurements about the surface temperature variability at the remote sensing sites. The visual images will in addition support the interpretation of the microwave data.
- Derive the thickness of thin ice at leads and cracks from the surface temperature measurements.

Output from measurements:

- Time series of infrared brightness temperatures (every 10 minutes) and visual images (every 5 minutes) of the RS sites and two cracks

Fig.4.9.15: Infrared and visual camera systems (photo: Gunnar Spreen)

Tab.4.9.14: List of measurement periods of the infrared camera system. The measurement periods of the visual camera are similar.

Activity - Device Operation	*Timestamp*	*Action*	*Comment*
PS122/1_1-99 IR_VarioCAM_01	20.10.19 07:57	recording start	First recording of IR camera at remote sensing site. incidence angle 40°; facing southerly (exact heading to be determined); about 2.5m height (exact height to be determined)
PS122/1_1-99 IR_VarioCAM_01	18.11.19 13:17	recording end	End of recording after battery ran out after ice break-up on 16.11.
PS122/1_8-108 IR_VarioCAM_01	23.11.19 10:09	recording start	thin ice: thin ice at crack; 30° incidence angle; height 225 cm; heading NNW thin ice thickness 9 cm; salinity under the ice: 31.6 psu
PS122/1_8-108 IR_VarioCAM_01	25.11.19 09:10	recording end	end of 1. recording when battery ran out.
PS122/1_8-108 IR_VarioCAM_01	26.11.19 05:57	recording start	2nd recording at thin ice crack after battery exchange.
PS122/1_8-108 IR_VarioCAM_01	27.11.19 12:16	recording end	End of 2nd recording after battery ran out
PS122/1_1-258 IR_VarioCAM_01	02.12.19 06:28	deployed	started recording for testing at lower height of tripod
PS122/1_1-258 IR_VarioCAM_01	02.12.19 11:30	recording start	Start of regular measurements. Height of IR camera: 230 cm; heading 295°; elevation angle: 75° (15° on scale)
PS122/1_1-258 IR_VarioCAM_01	04.12.19 05:56	recording end	short break of measurements due to network problems.
PS122/1_1-258 IR_VarioCAM_01	04.12.19 07:12	recording start	restart of measurements after network problem
PS122/1_1-258 IR_VarioCAM_01	06.12.19 10:36	recording end	ebox PC shut down for unknown reason
PS122/1_1-258 IR_VarioCAM_01	10.12.19 11:56	recording start	restart after ebox PC failure; now with working network connection

Supporting snow and ice measurements

The measurements listed in Table 4.9.1 will be combined with detailed measurements of the snow and sea ice close to the remote sensing validation site (e.g., thickness, densities, SSA, temperature, salinity, ice stratigraphy). Within the snow task (Section 4.2) “A” snow pits were performed on comparable snow and ice conditions to RS1 and RS2 at the respective “snow1” and “snow2” sampling sites. During the transects (Section 4.4) with the mobile Balamis ARIEL radiometer and Ku/Ka-band radar systems, “C” snow pits with additional salinity measurements were taken. For continues ice and snow thickness measurements at the RS1 site five thermistor chains (Section 4.3) were deployed at the locations indicated in Figure 4.9.1. At RS2 site two thermistor chains were deployed. One of them was extended with three snow temperature probes (Section 4.3) to form a transect over a snow dune. In addition to these activities described in the respective task sections, snow depth measurements were taken along the RS instruments. With the help of the BGC team salinity

ice cores with a higher vertical resolution of 3 cm in the upper part were taken at the BGC1 site. BGC1 neighbored the RS1 site and had similar ice properties. These ice properties should also be representative for the RS2 site. In addition, the salinity cores (5 cm sections) from the "dark site" can be used. The additional snow and ice measurements performed within the remote sensing task are listed in Table 4.9.14. Many measurements from the ICE and other teams are relevant for interpreting the RS measurements. Here a none exclusive list of supplementary measurements:

Important supplementary measurements for the remote sensing program

- Meteorological data acquired on the ship and at MET city (Chapter 3)
- Helicopter (Section 4.8): laser scanning and thermal imaging for characterizing the snow, ridge, lead, over-frozen melt pond, and thin ice distributions of the CO and for regional upscaling for, e.g., comparison to satellite data.
- Terrestrial laser scanning (Section 4.2): snow distribution and redistribution by wind for the RS sites and CO
- Snow (Section 4.2): snow depth, density, grain size, moisture, salinity, presence of special structures (snow crust, superimposed ice), snow structure CT
- Ice cores (Section 4.5): density & salinity sections; thick, thin sections, and CT for air bubble, brine channel distributions and ice structure
- Autonomous observation in the CO and DN (Section 4.3): snow and IMB buoys, thermistor chains (CO), and snow temperature profilers (CO)
- Ice dynamics (Section 4.6): position data from all buoys of the distributed network; ice stress measurements (direct and laser array)

Tab.4.9.14: List of additional snow and ice measurements taken in addition to the ones described in Sections 4.2, 4.3, 4.4, 4.5.

Activity - Device Operation	*Timestamp*	*Comment*
PS122/1_4-29 si_corer_9cm	2019-10-24	Salinity ice core (3 cm sections) at BGC1 site
PS122/1_6-28 snow-stick	2019-11-04	Snow depth measurements along instruments
PS122-1_7-57 snow-stick	2019-11-14	Snow depth measurements along instruments
PS122-1_7-78 si_corer_9cm	2019-11-14	Salinity ice core (3 cm sections) at BGC1 site
PS122/1_8-22 si_corer_9cm	2019-11-19	Salinity ice core (3 cm sections) at BGC1 site
PS122-1_8-126 sali_ubremen_1	2019-11-23	Salinity measurements of thin ice and frost flowers
PS122/1_8-132	2019-11-23	Ice thickness of thin ice
PS122/1_10-39 si_corer_9cm	2019-12-04	Salinity ice core (3 cm sections) at BGC1 site
PS122/1_11-37 snow-stick	2019-12-10	Snow depth measurements along instruments

Preliminary (expected) results

All RS instruments (Table 4.9.1) will provide a time series of the seasonal development of their measured parameters, i.e., microwave brightness temperature and backscatter at different frequencies, reflected GNSS signals, infrared temperatures and visual images. Their variability and changes will depend on the atmospheric conditions, e.g., temperature and snow accumulation. The combination of on-ice remote sensing measurements together with the comprehensive snow and ice measurements will allow to improve microwave emission and scattering models of snow and ice, which in turn will lead to improved satellite remote sensing datasets.

Data recorded and stored in the MCS during leg 1 are primarily raw, uncalibrated measurements like backscatter power from the radars and voltages from the radiometers. We here show a few exemplary early results.

19-37-89-GHz Radiometer

Figure 4.9.16 shows as an example the uncalibrated microwave brightness temperatures (TB) measured by the 19-37-89-GHz radiometer on 2 November 2019 during an about one hour period from 06:34 to 07:30 UTC. During that time period the radiometer was scanning in elevation from 30° to 65° incidence angle. These scan cycles clearly can be seen in the time series in the upper plot. The lower plot shows the TBs versus the incidence angle. A TB change with incidence angle can be observed, however, not necessarily as expected with an increase of TB. This likely is due to the at the moment missing calibration. In addition, for low incidence angles at 30° the deviation might be due to the sled and the instrument itself come in the field of view and thus altering the measurements.

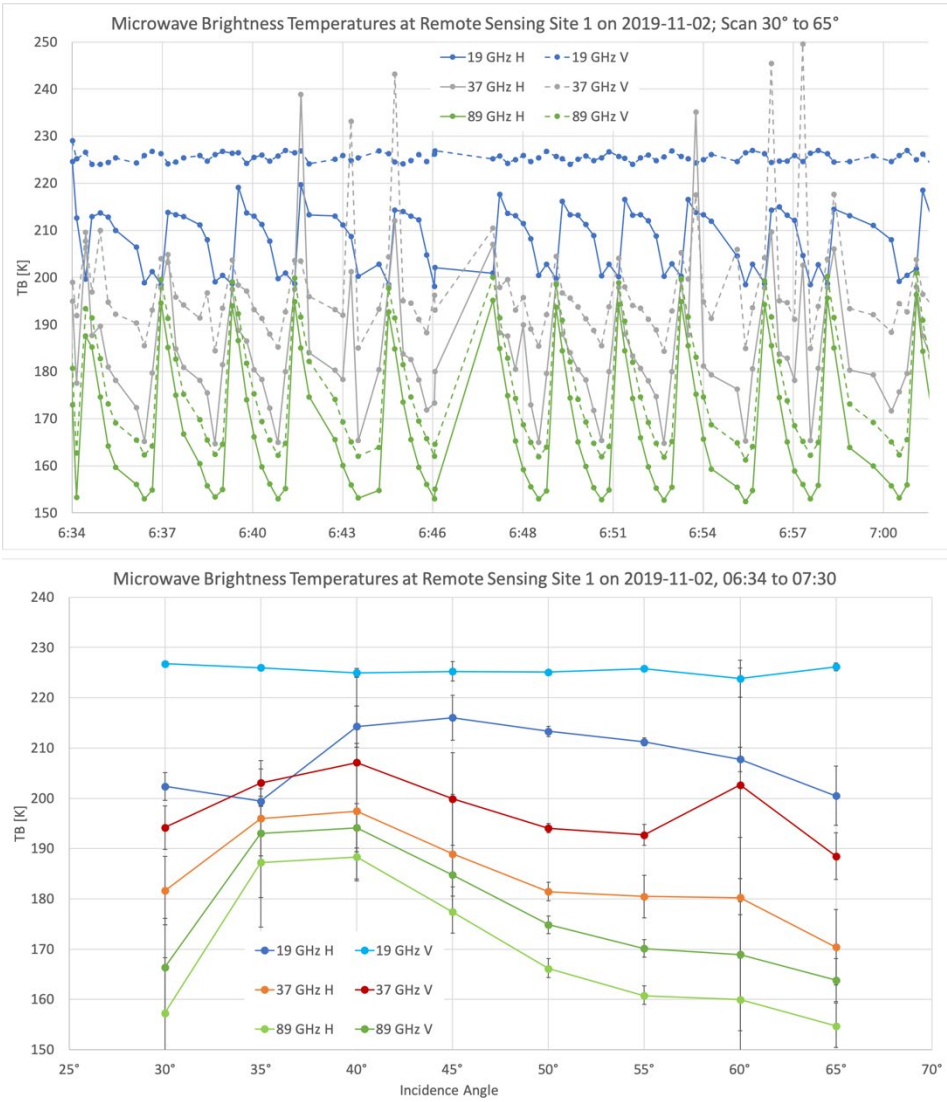

Fig.4.9.16: Exemplary, uncalibrated microwave brightness temperatures (TB) from the 19-37-89-GHz radiometer measured during about one hour on 2 November 2019 at RS1 site. Top: time series during several scan cycles from 30° to 65° incidence angle. Bottom: TB vs. incidence angle including standard deviations (error bars) for that about one hour long scan.

UWBRAD

The UWBRAD processes raw data, and generates Level1 products every hour for preliminary observations. The measured power from the entire spectrum for one hour of operation is illustrated in Figure 4.9.17. All four channel powers drop significantly every 10 minutes due to the sky calibrations. Some portions of the spectrogram are polluted with internal or external RFI sources (the spots with extreme power levels, especially at channel 540 MHz). These will be discarded during calibration and post-processing in order to derive the true brightness temperatures of the monitored scene.

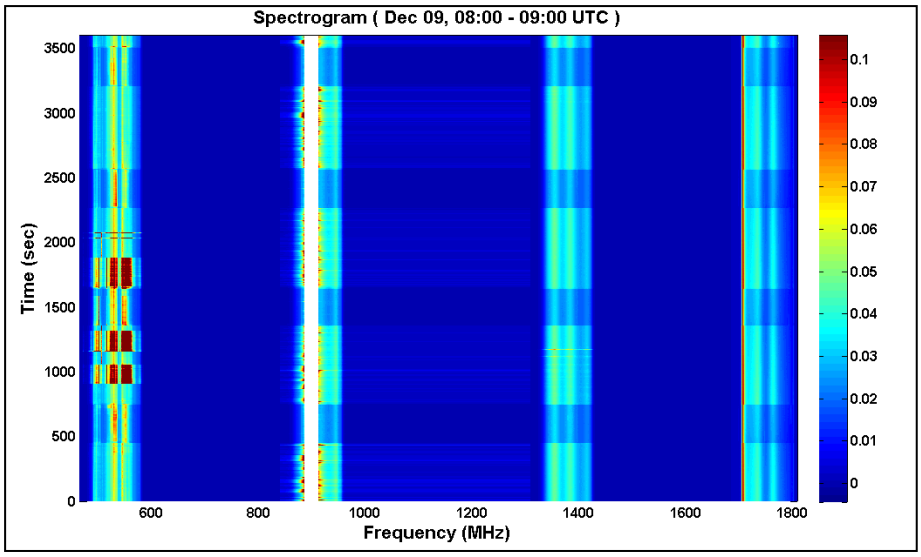

Fig.4.9.17: Entire power spectrum for the four UWBRAD channels at 540, 900, 1380 and 1740 MHz measured during one hour (y-axis). For this uncalibrated data the power has an arbitrary unit.

Infrared camera

The infrared thermography system measures the surface temperature at the remote sensing site, which is influenced by the incoming longwave radiation, atmosphere and ocean temperatures, and snow and ice thickness. Figure 4.9.18 shows to example images from the IR camera looking at thin ice in a crack. The initially with frost flowers covered surface got snowed over and sea water leaked in forming slush. Such measurements are available continuously for both remote sensing sites.

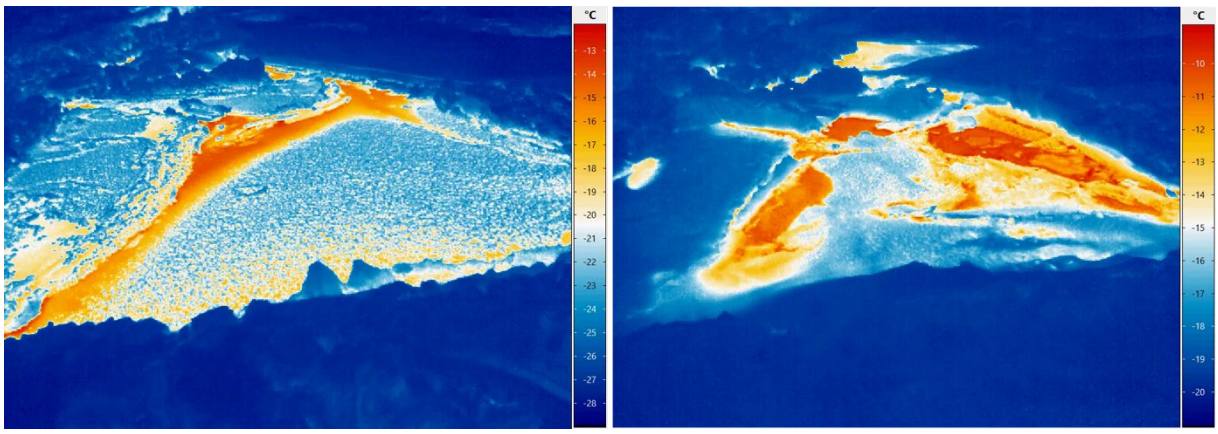

Fig.4.9.18: Crack with thin ice and frost flowers observed by the infrared camera on 23 November 2019 (left image). The right image shows the same scene one day later, when snow covered parts of the crack and frost flowers and sea water leaked in through a crack forming slush. Mind the different temperature scales.

Salinity ice cores

The salinity ice cores (Table 4.9.14) taken at the BGC1 site show a typical C-shaped profile for newly formed sea ice. This ice likely was formed in one of the melted through melt ponds, which dominated the ice cover (>60%) in the southern part of the floe where BGC1 was located before the deformation events or the BGC1, and thus should be representative for the two RS sites, which were located on a similar ice cover.

Figure 4.9.19 shows the salinity profiles of the four extra cores taken at the BGC1 site with higher vertical resolution (3 cm) for the top 15 cm. All profiles show high similarity with an average salinity of 5±2 psu and the c-shaped profile indicative for newly grown ice within this

winter season. The top layer salinity decreases with time as can be expected when more brine gets expulsed and wicked up by the snow on top. Only the much thicker core of 102 cm from 4 December show a slightly different behaviour and due to its thickness either is older (not supported by the salinity) or got rafted.

Salinity cores were taken at many more occasions at the BGC1 site and can be used to further constrain the salinity profile and evolution. However, they only have a vertical resolution of 10 cm. Salinity cores from the weekly ice coring at the “dark site” have a vertical resolution of 5 cm.

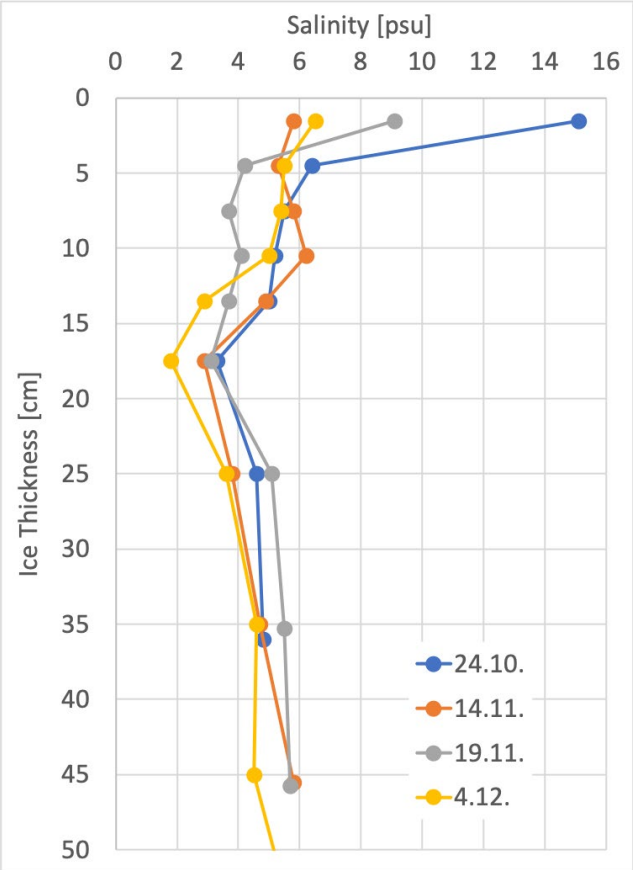

Fig.4.9.19: Salinity profiles of the four extra “remote sensing” cores taken at the BGC1 site. 0 is at the ice top. For better visibility the 102 cm of the core from 4 December 2019 are not fully shown.

Data management

All data are handled, documented, archived and published following the MOSAiC data policy (see APPENDIX). All final data of all on-ice and onboard remote sensing instruments will be stored at the MOSAiC Central Storage (MCS) and at PANGAEA (World Data Center PANGAEA Data Publisher for Earth & Environmental Science (www.pangaea.de)) after post-processing and quality checks.

Tab.4.9.15: Log of the activities at the two remote sensing sites during leg1

Date	*Activity*	*Device Operation*
2019-10-12	Remote sensing hut installed (using Argo)	
2019-10-18	Ku/Ka-radar installed and first test measurement	PS122/1_1-102
2019-10-20	IR and webcam installed and measurement start	PS122/1_1-99
2019-10-21	L-SCAT installed and measurement start	PS122/1_1-97

2019-10-23	L-SCAT start of continuous measurements	PS122/1_1-98
2019-10-23	ARIEL Balamis radiometer test	
2019-10-24	Ice core salinity at BGC1 site, i.e., close to RS (+BGC cores)	PS122/1_4-29
2019-10-24	GNSS-R installed and measurement start	PS122/1_4-11
2019-10-26	19, 37, 89 GHz radiometer installed and test measurement	PS122/1_4-23
2019-10-28	ELBARA installed but no measurements	
2019-10-29	ELBARA measurement start	PS122/1_1-101
2019-10-29	19, 37, 89 GHz radiometer start continuous measurements	PS122/1_5-77
2019-10-31	Transect: GEM, MagnaProbe, ARIEL Balamis	
2019-11-01	UWBRAD deployed and first tests	
2019-11-04	Snow depth measurements	PS122/1_6-28
2019-11-05	Thermistor chains deployed 3x	PS122/1_6-19, PS122/1_6-20, PS122/1_6-21
2019-11-07	Thermistor chains deployed 2x	PS122/1_6-39, PS122/1_6-40
2019-11-07	Transect: GEM, MagnaProbe, KuKa-radar, ARIEL Balamis	,PS122/1_6-57
2019-11-10	Deployed X-SCAT; on power but no measurements started	
2019-11-11	ELBARA (192.168.3.176) not responding to ping; last access 9.11.. Repaired display of UPS and restarted ELBARA; did sky calibration; started measurement at 40°	PS122/1_1-101
2019-11-11	Connection to X-SCAT established; backscatter looks okay; no movement of the leveller -> no scan	
2019-11-11	Restarted GNSS-R measurement after battery ran out	PS122/1_7-16
2019-11-14	RS transect with ARIEL and Ku/Ka-Radar (plus GEM, snow)	PS122-1_7-103, PS122-1_7-59
2019-11-14	Snow depth measurements along instruments	PS122-1_7-57
2019-11-14	Exchanged GNSS-R battery	
2019-11-14	Ice core salinity at BGC1 site, i.e., close to RS (+BGC cores)	PS122-1_7-78
2019-11-16	Crack between RS site and OC; depression of parts of the RS site; puddles with water in measurement area: retreat of all instruments behind the hut closer to the ridge, only IR and web camera kept out	
2019-11-17	Movement along crack during the night; loss of power at RS site at about 14:00 on 1019-11-16; opening of crack in the morning (10-20 m); power cable to RS site got disconnected and pulled in to OC	
2019-11-18	Moved RS hut out of slush area; cleaned up site	
2019-11-19	Ice core salinity at BGC1 site, i.e., close to RS1 (+BGC cores)	PS122/1_8-22
2019-11-20	The site has moved about 500 m to the port side of the ship. More cracks in the RS area. Pulled the instruments and hut to higher location on a ridge.	
2019-11-21	Not successful attempt to exchange battery for IR/webcam → computer was not starting. Brough back on the ship.	
2019-11-23	Thin ice (9 cm) with frost flowers measurements close to 1st RS site: Ku/Ka-Radar, ARIEL Balamis L-band radiometer, Infrared/web camera; probing of thin ice and frost flowers/slush	PS122/1_8-104, PS122/1_8-107, PS122/1_8-108, PS122/1_8-126, PS122/1_8-132

2019-11-26	Relocation of RS instruments and hut to new site: Remote Sensing 2; ~80 cm ice thickness	PS122/1_9-49
2019-11-28	Build road and deploy power cable between RS hut and MET city	
2019-11-29	Power back at RS2 site	
2019-11-30	Start of L-SCAT and Ku/Ka-radar measurements at RS2	PS122/1_1-246, PS122/1_1-245
2019-12-02	Start of ELBARA and IR/web camera measurements at RS2. Network connection back using radio LAN (~1 MB/s).	PS122/1_1-257, PS122/1_1-258
2019-12-04	UWBRAD gets in operational measurement mode the first time. Storm with a lot of snow caused snow dune to develop around some instruments.	PS122/1_1-265
2019-12-04	Ice core salinity at BGC1 site, i.e., close to old RS1 site (+BGC cores). Decided to continue that ice core time series for RS because ice at BGC1 is also most similar to the ice at RS2 site (compared to BGC2 and BGC3).	PS122/1_10-39
2019-12-05	Preparation for RS transect measurements with Ku/Ka-radar and ARIEL radiometer → cancelled due to bad weather; just when calibration of ARIEL was finished	
2019-12-06	U Manitoba 19, 37, 89 GHz radiometer starts measuring	PS122/1_10-79, PS122/1_10-130
2019-12-07	C-SCAT installed and starts measuring	PS122/1_10-131, PS122/1_10-132, PS122/1_10-133, PS122/1_11-21
2019-12-08	X-SCAT setup but not measuring yet → needs cable check	
2019-12-08	Thermistor chain for ice and snow thickness installed	PS122/1_1-268
2019-12-10	GNSS-R starts measuring again; IR/Web-camera starts measuring again; thermistor chain for ice and snow thickness installed; 3 snow thermistors and pingers installed; snow depth measurements by snow ruler	PS122/1_11-27, PS122/1_1-258, PS122/1_1-301, PS122/1_1-302, PS122/1_11-37
2019-12-11	Changed C-SCAT to continuous science activity to keep everything in one MCS directory	PS122/1_1-289
2019-12-12	Restarted charging of dead GNSS-R battery; collected 19, 37, 89 GHz radiometer data and started new scan (30-60°) as continuous device operation	PS122/1_11-27, PS122/1_1-303
2019-12-13	Cracks in the ice at RS2 site. One under UWBRAD and one under GNSS-R. All instruments but L-SCAT and IR camera retreated close to the RS hut. Arrival of Kapitan Dranitsyn.	
2019-12-14	Handover at RS site to leg 2; retreat of L-SCAT because of more cracks close to the instrument	
2019-12-15	Handover at RS site to leg 2	

References

No references